Colloidal Mineral Liquid Crystals

Formation & Manipulation

Anke Leferink op Reinink

ISBN: 978-94-6108-595-5
Printed by: Gildeprint Drukkerijen

Colloidal Mineral Liquid Crystals
Formation & Manipulation

Vloeibare kristallen van minerale colloïden
Formatie & Manipulatie

(met een samenvatting in het Nederlands)

Proefschrift

ter verkrijging van de graad van doctor aan de Universiteit Utrecht op gezag van de rector magnificus, prof. dr. G.J. van der Zwaan, ingevolge het besluit van het college voor promoties in het openbaar te verdedigen op woensdag 19 maart 2014 des middags te 2.30 uur.

door

Anke Brigitta Geertruida Maria Leferink op Reinink

geboren op 27 december 1985 te Weerselo

Promotor: Prof. dr. H.N.W. Lekkerkerker

Co-promotoren: Dr. G.J. Vroege
Dr. A.V. Petukhov

This work is part of the research program of the 'Stichting voor Fundamenteel Onderzoek der Materie' (FOM), which is financially supported by the 'Nederlandse Organisatie voor Wetenschappelijk Onderzoek' (NWO). Support by the 'Deutsche Forschungsgemeinschaft' (DFG) through the 'Sonderforschungsbereich Transregio 6' (SFB TR6) is acknowledged.

Contents

List of Publications

This thesis is based on the following publications:

• A. B. G. M. Leferink op Reinink, E. van den Pol, A. V. Petukhov, G. J. Vroege, and H. N. W. Lekkerkerker, *Phase behaviour of lyotropic liquid crystals in external fields and confinement,* Eur. Phys. J. Spec. Top. **222** (2013) 3053-3069 (Chapter 1)

• A. B. G. M. Leferink op Reinink, E. van den Pol, D. V. Byelov, A. V. Petukhov and G. J. Vroege, *Ageing in a system of polydisperse goethite boardlike particles showing rich phase behaviour*, J. Phys.: Condens. Matter **24** (2012) 464127 (Chapter 2)

• A. B. G. M. Leferink op Reinink, S. Belli, R. van Roij, M. Dijkstra, A. V. Petukhov and G. J. Vroege, *Tuning biaxiality of nematic phases of board-like colloids by an external magnetic field*, Soft Matter **10** (2014) 446-456 (Chapter 4)

• A. B. G. M. Leferink op Reinink, J. M. Meijer, D. Kleshchanok, D. V. Byelov, G. J. Vroege, A. V. Petukhov and H. N. W. Lekkerkerker, *3D structure of nematic and columnar phases of hard colloidal platelets*, J. Phys.: Condens. Matter **23** (2011) 194110 (Chapter 6)

Manuscripts in preparation:

• A. B. G. M. Leferink op Reinink, H.N. W. Lekkerkerker, A. V. Petukhov and G. J. Vroege, *Phase behaviour in suspensions of goethite board-like colloids and small spheres,* to be submitted. (Chapter 3)

• A. B. G. M. Leferink op Reinink, E. van den Pol, G. J. Vroege and A. V. Petukhov, A*lignment pathway of the goethite columnar liquid crystal phase studied by SAXS*, submitted. (Chapter 5)

• A. B. G. M. Leferink op Reinink, E. J. van Harten, G. J. Vroege, A. V. Petukhov and H. N. W. Lekkerkerker, *Gibbsite systems for confocal microscopy studies*, to be submitted. (Chapter 7)

Other publications by the author:

• A. Zych, A. B. G. M. Leferink op Reinink, K. van der Eerden, C. de Mello Donega and A. Meijerink, *Luminescence properties of lanthanide doped alkaline earth chlorides under (V)UV and x-ray excitation*, J. Alloy. Compd. **509** (2011) 4445

• D. V. Byelov, J. Hilhorst, A. B. G. M. Leferink op Reinink, I. Snigireva, A. Snigirev, G. B. M. Vaughan, G. Portale and A. V. Petukhov, *Diffuse scattering in random-stacking hexagonal close-packed crystals of colloidal hard spheres,* Phase Transit. **83** (2010) 107

1

Introduction

The central topic of this thesis is the formation and characterization of liquid crystals (LC) [1, 2]. The key feature in this research is how we can influence the formation of liquid crystals and tune the liquid crystalline structures formed. Liquid crystals have a wide range of possible applications including lasers, photovoltaics and field-effect transistors [3]. They are, however, mostly known for their application in liquid crystal displays (LCD) [4].

The work in this thesis focuses on *colloidal* liquid crystals. A colloid is a particle with a dimension roughly between a few nanometers and a few micrometers [5]. Although colloids are considerably larger than atoms and molecules, their behaviour is very similar, only on a much slower timescale. Their larger size combined with the slower dynamics makes it significantly easier to study them. In addition, the inter-particle interactions can be tuned. Colloidal particles are therefore frequently used a 'model' system for more complex atoms and molecular systems. Additionally, colloids are highly susceptible to external electric and magnetic fields.

The systems studied in this thesis are *goethite* and *gibbsite*. They consist of colloidal mineral particles. Also these systems function as model systems. They will, most likely, not be directly suitable for applications but the fundamental knowledge obtained on the formation and behaviour of the liquid crystals is not limited to these systems and can be applied to more complex systems.

This introduction aims to give a background of the work described in this thesis. We will first describe and explain what colloidal liquid crystals are and how they are formed (section 1.1). In section 1.2 various methods that can be used to influence liquid crystal phase behaviour -the earth gravitational field, an external magnetic field and spatial confinement- will be described. Then we will introduce the colloidal mineral systems studied in this work, goethite and

gibbsite (section 1.3). Additionally we will give a short introduction of the two techniques that were predominantly used to characterize the liquid crystals (section 1.4). Finally the outline of this thesis is given in section 1.5.

1.1 Colloidal liquid crystals

Colloidal liquid crystals consist of ordered anisotropic colloidal particles, like rods and platelets [6-8]. When these particles are brought in suspension, i.e. dispersed in a liquid medium, they have the ability to self-organize into various liquid crystalline structures including isotropic (*I*), nematic (*N*), smectic (*S*) and columnar (*C*) phases. In the *I* phase the particles do not possess any long-range order. In the *N* phase the particles are aligned and thus possess orientational order, but lack positional order. In the *S* phase orientationally ordered particles are stacked in layers and thus have in addition positional order in one dimension. In the *C* phase the oriented particles stack into columns, which form a periodic structure in two dimensions. The spontaneous formation of colloidal liquid crystals is an entropy-driven process. Already in the 1940s Onsager explained in his seminal work [9] the *I* - *N* phase transition for rod-like particles on the basis of the particle shape alone: at sufficiently high concentration the loss in orientational entropy is smaller than the gain in excluded volume entropy, i.e. translational entropy. As a result the particles favour nematic alignment. Later Frenkel and co-workers predicted the formation of *N*, *S* and *C* phases of hard anisotropic particles using computer simulations [10-13]. Generally, more highly ordered phases (*S*, *C*) are found for higher particle volume fractions.

The first observation of a colloidal liquid crystal was of the *N* phase, which was found in a suspension of ribbon-like vanadium pentoxide (V_2O_5) particles [14]. Later the *N* phase was also found in suspensions of rod-like tobacco-mosaic-virus (TMV) particles [15, 16] and plate-like bentonite, a natural clay [17]. The nematic phase found in systems of rod-like particles (which align their long axis) is often referred to as prolate nematic (N_+), while plate-like particles display oblate nematic ordering (N_-), in which the short particle axes are aligned. For particles with a shape exactly in between rod- and plate-like the rare biaxial nematic phase (N_B) is predicted [18-20]. In the N_B phase both particle axes are aligned [21]. Nowadays a rich variety of different liquid crystalline phases has been observed in suspensions of anisotropic mineral particles, which has been extensively reviewed in the papers by Davidson & Gabriel [6, 7] and Lekkerkerker & Vroege [8].

1.2 Influencing liquid crystal phase behaviour

Colloidal liquid crystals are highly susceptible to external fields. External fields are therefore prime candidates for influencing liquid crystal phase behaviour. We discuss two external fields that are frequently used: the earth gravitational field (of course always present) and a magnetic field. Additionally, the influence of spatial

confinement on LC phase formation will be discussed.

Gravitational field

Generally, the influence of the gravitational field on the formation of mineral liquid crystal phases is very important. At low volume fractions a colloidal dispersion builds up a barometric concentration profile [22, 23] proportional to $\exp(-z/l_g)$ where z is the vertical height and l_g the gravitational length. The gravitational length is inversely proportional to the mass density difference $\Delta\rho$ (between the particles and the solvent) and the particle volume $V_{particle}$

$$l_g = \frac{k_B T}{g \Delta\rho V_{particle}}, \tag{1.1}$$

where g is the gravitational acceleration and $k_B T$ the thermal energy. The gravitational length of colloidal mineral particles can easily be 1 mm or less. The sedimentation profile for more concentrated dispersions may contain different coexisting liquid crystal phases. However, it should be borne in mind that in a sedimented multiphase system the osmotic pressure at each interface between different phases is different so that Gibbs' phase rule predicting the maximum number of coexisting phases does not necessarily hold for a macroscopic sample in a gravitational field (even for the monodisperse case). For a polydisperse system, like colloidal mineral particles, the chemical potential for each component must be equal at each interface and also the typical gravitational length (Eq. (1.1)) can strongly vary for components with different particle volumes. Since this effect couples to the fractionation or partitioning of particles over the different phases, sedimented colloidal systems may display very rich phase behaviour. For the N phase, e.g., the tendency that long rods order first due to their larger excluded volume [24, 25] is reinforced by sedimentation and leads to additional fractionation. Generally, in sedimentation-induced phase-separated samples the more highly ordered phases are formed below the less ordered and disordered phases. Liquid crystalline phases with partial positional order (S, C) may be more difficult to form since inherent polydispersity may prevent particles to fit within the positionally ordered structures. Hence, low polydispersity rods form layer-like smectic [26, 27] phases while the smectic phase destabilizes at higher length polydispersity favouring the nematic phase at low density and the columnar phase at higher density [28-30]. If sedimentation takes place sufficiently slowly, Brownian motion may permit particles to keep re-arranging [31] and fractionating.

Sedimentation and fractionation are therefore of significant importance in the mineral liquid crystal formation process; it enables systems to locally reduce the polydispersity, which is inherent for colloidal mineral particles. This stimulates the formation of positionally ordered phases which enriches the liquid crystal phase behaviour.

External magnetic field

When a (colloidal) particle is submitted to an external magnetic field, a magnetic moment is induced in the particle. Anisotropic colloidal particles often have an anisotropic magnetic susceptibility tensor and hence the induced moment results in alignment of a specific axis, generally the long axis, in the field. The strength of the induced magnetic moment depends on the strength of the magnetic field.

For low particle volume fractions the field-induced alignment breaks the symmetry of the isotropic phase and an orientationally ordered *para*-nematic (*pN*) phase is formed. The degree of the induced order is expressed in the nematic order parameter, which under certain restrictive conditions, i.e. field strength, can take values of true nematic phases. This is supported by Khokhlov and Semenov [32] who constructed theoretical phase diagrams for several types of rod-like particles in an external field of various field strengths. Also Fraden and co-workers studied the field-induced alignment of colloidal anisotropic particles. They determined the alignment of rod-like virus particles, TMV-virus and fd-virus respectively, as a function of concentration, polydispersity and ionic strength in the entire isotropic range [33-35].

Usually, for colloids consisting of magnetically anisotropic material it is energetically most favourable to align their long axis parallel to the magnetic field [36], as is the case for the examples described above. However, various colloids do not display this behaviour due to the material they are composed of and/or the specific crystal structure. Examples are plate-like beidellite [37] and Co-doped ZnO nanowires [38] which were found to align their long axis perpendicular to the field due to their magnetocrystalline anisotropy.

Apart from aligning particles in the *I* phase, an external magnetic field can additionally be utilized to realign spontaneously formed liquid crystals. Liquid crystals often consist of several small domains with different orientations. By applying an external field the different domains will realign and fuse to form a large *single* domain. The bulk of research on this topic is devoted to *nematic* phases, and has been studied in various dispersions of anisotropic colloidal particles. For example, in a relatively dilute *N* phase of V_2O_5-ribbons it was found that the magnetic field removes the topological defects and produces a completely aligned single nematic domain [39]. More recently similar behaviour was found in a nematic phase of $GdPO_4$ nanorods [40]. The field-induced formation of single nematic domains was also found in suspensions of lath-shaped nontronite [41] and disk-shaped beidellite [37, 42], both natural clays.

Confinement

Anisometric colloids have, due to particle-wall interactions, a favourable orientation near a wall or a surface. For example plate-like particles prefer to align their normal perpendicular to a flat wall (homeotropic anchoring), whereas rod-like particles often align their longest axis parallel to a flat wall (homogenous anchoring).

For bulk samples the effect of the wall-induced alignment decays away from the wall and can often be neglected. For sufficiently confined samples though, the wall anchoring can have a significant influence on the liquid crystal phase behaviour. Theoretical work on suspensions of rod- [43] and plate-like [44] particles confined between two planar parallel walls (i.e. slit-pore confinement) revealed that sufficiently strong confinement lowers the $I - N$ binodal; alignment imposed by the walls induces formation of the N phase which is now found at volume fractions for which the bulk is isotropic. This phenomenon, known a capillary nematization, vanishes again below a critical wall separation distance of some particle lengths.

Regarding *positionally* ordered phases in confinement, capillary smectization was theoretically predicted for specific wall separation distances [45-47]. These studies additionally predicted that confinement can induce $S - S$ demixing in a binary mixture of rods with identical diameters but dissimilar lengths.

Little experimental work has been published on positionally ordered liquid crystals of hard rod/plate-like particles in confinement. One of the few experimental studies was performed by Dammone and co-workers who studied the director fields of nematic liquid crystals of fd-virus rod-like particles in channels with wedge-structured walls for various wedge angles [48]. They found a splay-to-bend transition with increasing wedge angle. Interestingly, the defect formed where splay configuration meets bend configuration could be observed with confocal laser scanning microscopy (CLSM).

In general, the effects of several types of confinement on suspensions of anisotropic particles have been studied extensively *theoretically*. Experimental research has also been performed, but not to the same extent and it mainly focused on nematic liquid crystals. Barely any experimental research has been performed on confined *positionally* ordered liquid crystals of (hard) colloidal particles. The challenge lies in the characterization techniques, e.g. small angle x-ray scattering (SAXS) is an excellent technique to characterize positionally ordered liquid crystals, but since confinement samples are often micrometer sized the scattered intensity is (too) low. Difficulty also lies in characterizing the structures locally. However, colloids are on the verge of becoming accessible with the improved optical techniques. Lettinga and Grelet e.g., were able to directly visualize *single* particle transport between smectic layers of fd-virus using CLSM [31]. Recently also a smectic phase formed in a system of fluorescent rod-like silica particles could be observed at the single particle level with CLSM [49].

1.3 Colloidal systems in this thesis

In this thesis two different systems of anisometric mineral particles are studied: board-like goethite and plate-like gibbsite. Mineral particles have several advantages: they are electron rich and therefore highly susceptible to external fields. Additionally, they have a high thermal stability and therefore the LCs are stable over a

wide range of temperatures.

Goethite

Goethite (α-FeOOH) is a naturally occurring iron-oxide that has been used as a pigment since prehistoric times. Colloidal goethite particles can be synthesized via hydrolysis of iron-nitrate [50, 51]. The resulting board-like particles (Fig. 1.1(a)) are characterized by their three distinct axes: the length (L) > width (W) > thickness (T). The particles have an inherent polydispersity which can, depending on the synthesis method, be as high as 55%. Therefore sedimentation and fractionation in the earth gravitational field has proven extremely important for the goethite LC phase behaviour. This was already suspected from the observation of a smectic phase within a 55% polydisperse batch [52], which is far above the terminal polydispersity of 18% for the smectic phase of spherocylinders [29]. Careful analysis of the size distributions of coexisting I, N, S and C phases [53] showed an almost threefold increase of particle length over 5 cm sample height, a strongly reduced polydispersity (<28%) in the S phase and the exclusive presence of the longest particles in the C phase, which acts as a waste disposal for particles that do not fit the smectic periodicity. In contrast, a similar system with an overall polydispersity of 17% only displayed a gradual shift of 10% in the length distribution without changing its form while a C phase was completely absent.

Goethite also has outstanding magnetic properties. This was presumably already discovered in ill-defined iron oxide dispersions in the early 1900s by Majorana, Cotton and Mouton, who observed a magnetic field-induced positive birefringence in weak fields, which decreased to reach even negative values above a certain field strength [54-56]. This behaviour was not understood until a century later, when Davidson, Lemaire and co-workers found that this behaviour could be attributed to anti-ferromagnetic goethite particles bearing a permanent magnetic moment along L, while the magnetic easy axis is perpendicular to the L-axis [57]. The particles therefore align their L-axis parallel to a weak magnetic field, but reorient to align their T-axis parallel to fields above a certain critical magnetic field strength (B^*) [50, 58, 59].

Magnetic fields have therefore frequently been used to study and influence the phase behaviour. A weak magnetic field was e.g. used to align macrodomains of *spontaneously* formed *biaxial* liquid crystal phases formed in a batch with a shape almost exactly in between rod- and plate-like ($L/W \approx W/T$) [60]. The crystal structures were characterized by SAXS and the field was applied in different directions to reveal the full 3D structures. SAXS revealed a N_B phase on top of a biaxial smectic phase. Although their L/W ratio was slightly larger than their W/T ratio, biaxial phases could still be formed due to a rather high particle polydispersity (25%), which stabilizes the biaxial phases [61].

Apart from aligning LC domains, magnetic fields were also found to induce phase transitions in dispersions of goethite. For example, a stable N_B phase is formed

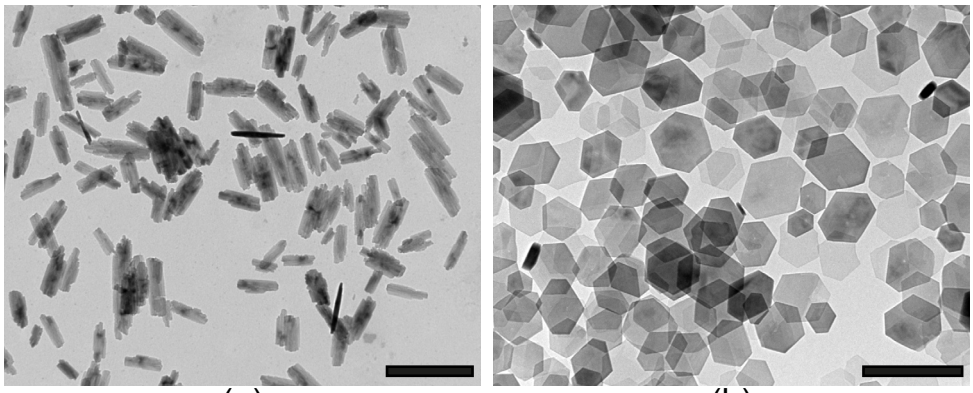

Fig. 1.1 Transmission electron microscopy images of (a) goethite and (b) gibbsite. The black bars denote 500 nm.

when a strong (above B^*) magnetic field is applied to a N_+ phase [57-59, 62]. Van den Pol *et al*. found that this property, in combination with the system's inherent polydispersity, can be utilized to induce $N_B - N_+$ phase separation in a dispersion of slightly elongated goethite boards [63, 64]. The strength of the induced magnetic moment scales with particle volume, thus for larger goethite particles the critical magnetic field (B^*) is slightly lower. Applying a magnetic field with a carefully chosen field strength to the N_+ phase induces a N_B phase for part of the particles. The created excluded volume between the differently oriented particles is sufficient to cause macroscopic phase separation.

Particle alignment in dense suspensions in a strong magnetic field is a complicated process which can lead to the formation of positionally ordered phases. It was e.g. found that applying a strong magnetic field to a dense nematic phase can trigger the $N \longrightarrow$ C phase transition [65]. Also the S phase was found to transform into a C phase in a strong magnetic field [52]. This transition was found only in systems with a high polydispersity, in which the C phase was also spontaneously formed. In systems with a low polydispersity, which displayed $I - N - S$ phase separation, the S phase remains smectic in a strong magnetic field [66]. Dispersions of chromium-modified goethite form two different C phases: the centred rectangular (R_C) and the simple rectangular (R_S) columnar phase. In dispersions of these particles a strong magnetic field was found to induce the $R_S \longrightarrow R_C$ phase transition [67].

In this thesis we study the effect of the earth gravitational field on a chromium-modified goethite dispersion, which displays $I - N - S - R_S - R_C$ phase separation, over a time span of five years (Chapter 2). Additionally, we study the influence of a magnetic field with various field strengths, all smaller than B^*, on the biaxiality of the nematic phase (Chapter 4) and the reorientation process of the C phase in a strong magnetic field (Chapter 5). In Chapter 3 we take a different approach

to influence goethite LC phase behaviour. Instead of applying an external field, we change the inter-particle interactions from soft-repulsive to attractive by introducing a depletant into the dispersion.

Gibbsite

Gibbsite (γ-$Al(OH)_3$) is an intermediate in the Bayer process for aluminium production [8] in the form of agglomerates of small crystals. Synthetic colloidal gibbsite can be conveniently obtained by hydrolysis of a mixture of aluminium hydroxides at 85˚C [68]. The particles typically have a diameter D of ~200 nm and a high aspect ratio (Fig. 1.1(b)). Gibbsite suspensions are a unique plate-like system as they display a well-defined $I - N - C$ phase separation [69]. Also for this system the earth gravitational field plays a significant role in the liquid crystal phase formation. For example a polydispersity of 25% in the platelet diameter does not preclude the C phase from forming [8]. Interestingly, for polydisperse platelets a density inversion for the $I - N$ phase was found [70], which could be explained by fractionation effects [71]. Thicker platelets sediment faster but they remain, due to their smaller aspect ratio, in the isotropic phase for volume fractions at which the thinner platelets already form the nematic phase. The importance of sedimentation speed is also apparent from a study in which the sedimentation process was sped up by centrifugation. Whereas slow sedimentation can lead to the formation of a *single* columnar phase [69, 72], fast sedimentation at 900g led to the formation of many small columnar liquid crystals [73]. Additionally, under osmotic compression exerted by a free polymer a single hexatic domain was formed, which lacks long-range positional order [74].

Gibbsite is colourless and is therefore a prime candidate for optical studies. Polarized light microscopy, e.g., was used to study the shape and director field of gibbsite particles confined in tactoids (nematic droplets formed in the I phase). There is a competition between the particles preferring homeotropic anchoring and the elastic energy favouring a homogenous director field. Small tactoids were therefore found to have a homogenous director field, but are deformed and have an oblate shape, whereas larger tactoids remain spherical with a radial director field with a point-defect in the centre [75]. Gibbsite particles will align in a magnetic field [76, 77], which can therefore be used to change the director field and shape of a tactoid [78, 79].

Gibbsite can easily be grown to larger sizes via a seeded-growth method [80, 81], and can additionally be fluorescently labelled [81]. Gibbsite is therefore a candidate for CLSM experiments. However, by increasing the particle size the sedimentation speed will increase and inherently the formation of well-ordered liquid crystals can be hindered. E.g. for large gibbsite platelets it was found that phase separation only took place after the main part of the sample had sedimented into an amorphous phase [82]. In another system of large platelets the hexagonal columnar phase was found, although SAXS revealed the presence of orientational fluctuations in the co-

lumnar structure; the average platelet orientation was decoupled from the column axis. These effects could be ascribed to gravitational compaction [83].

In this thesis we focus on *large* gibbsite platelets. These larger particles are challenging for x-ray scattering experiments. Due to their short sedimentation length the liquid crystalline structures formed are less ordered. Additionally, resolution becomes an issue since their larger size requires smaller scattering angles. However, the recent development of a micro-radian x-ray scattering set up [84] enables SAXS experiments for larger colloids. In Chapter 6 we develop a '3D-SAXS' method, in which the samples are studied with different orientations to obtain more information about the 3D liquid crystal structure. In Chapter 7 we describe several methods to adjust the gibbsite system such that the particles can be used for confocal microscopy. Additionally we study the LC structures formed locally, at the particle level and in real-space with CLSM.

1.4 Characterization

In this thesis various techniques are used to study and characterize the liquid crystals. Here we give a short introduction of the technique that was predominantly used: small angle x-ray scattering. Additionally confocal laser scanning microscopy, the technique that is crucial in Chapter 7, is introduced.

Small angle x-ray scattering

SAXS is a scattering method in which high energy x-rays are used to determine the structure of particle systems in terms of averaged particle sizes or shapes [85]. Fig. 1.2(a) shows the basic principle of SAXS. X-rays are sent through the sample and every particle scatters the incoming beam. The scattered signal is collected by a 2D detector, often a CCD camera, which results in a scattering pattern. This pattern is typically represented as a function of the scattering vector Q, which is the vector connecting the wave vectors of the direct beam (k_0) and the scattered beam (k_1), as illustrated in Fig. 1.2(b). The length of the scattering vector Q is defined as

$$Q = \frac{4\pi}{\lambda}\sin(\theta), \tag{1.2}$$

where 2θ is the angle between the scattered and incident beam. Since colloids are relatively large (nm-mm) compared to the wavelength of the x-rays ($\sim$ 1Å) the scattering angles are extremely small, hence the name *small angle* x-ray scattering.

The scattering intensity is determined by the scattering of single particles in the suspension and the interference of their contributions. For anisometric particles, however, the separation of the scattering intensity into the form (P(Q)) and structure (S(Q)) factors is ambiguous because of the coupling of orientational and positional degrees of freedom. In densely packed periodically ordered structures pro-

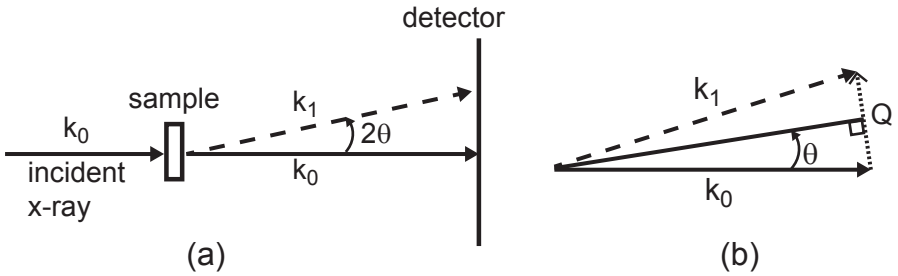

Fig. 1.2 Schematic representations of (a) small angle x-ray scattering where k_0 is the wave vector of the incident beam, k_1 the wave vector of the scattered beam and 2θ the angle between the incident beam and the observation direction and (b) the scattering vector Q.

nounced Bragg peaks develop in the structure factor. The positions of its maxima (Q_{peak}) indicate the average characteristic distances (d) between the aligned particles by

$$d = \frac{2\pi}{Q_{peak}}. \tag{1.3}$$

For positionally ordered systems these peaks are found at well-defined angles indicative for the crystal structure. The ratio between the Q-values of the peak positions reveal the crystal symmetry. Smectic peaks, e.g., have ratios 1, 2, 3, 4, 5. whereas for (perfect) hexagonal symmetry the peaks have ratios 1, $\sqrt{3}$, 2, $\sqrt{7}$, 3 [85]. For orientationally ordered systems (N phases) the sharp Bragg peaks are replaced by diffuse reflections that peak at certain azimuthal angles, which reveal the particle alignment. Because all particles in the bulk scatter, the average structure of all illuminated particles is measured.

Confocal laser scanning microscopy

While SAXS is an excellent technique to reveal average liquid crystal structures of large areas of the sample at once, it does not give information on the local structure. An excellent technique to study colloidal particles in real time and space is CLSM. CLSM is an optical imaging technique. The basic principle is sketched in Fig. 1.3. A single spot in the sample is illuminated through the use of an objective lens and an illumination pinhole. The emitted light is subsequently focused by an identical lens onto the second emission pinhole, which is positioned exactly at the focal plane conjugate to the imaged spot. Therefore the bulk of light emitted from elsewhere in the sample, i.e. the out-of-focus light, does not pass through this pinhole. The light generally is detected by a photo-multiplier tube and a 2D image of the sample is obtained. Because the out-of-focus light is eliminated, a 3D image can be obtained by scanning through the sample in the lateral and axial directions. The use of pinholes, eliminating the out-of-focus light, results in CLSM having an increased contrast and resolution compared to regular optical techniques.

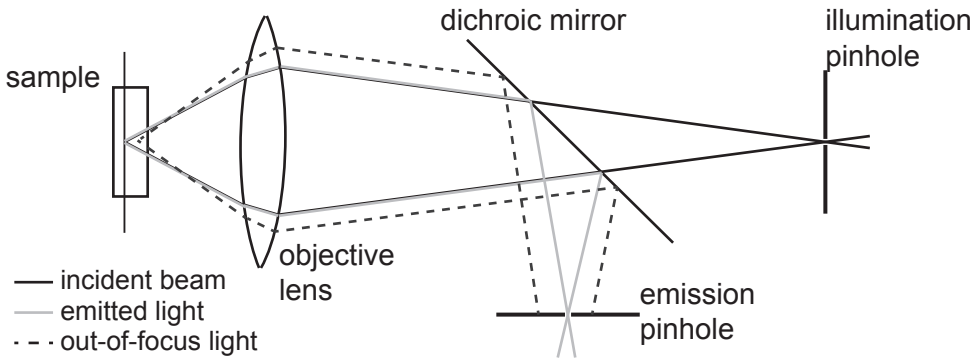

Fig. 1.3 Schematic drawing of the principle of a confocal microscopy. By using two emission pinholes, all out-of-focus light (dashed lines) is filtered out, which severely improves the resolution and contrast.

CLSM exhibits best results in fluorescence mode and the particles therefore need to be fluorescently labelled. The anisometric mineral particles used in this thesis, goethite and gibbsite, are not fluorescent and additionally have dimensions below the resolution of the microscope. Goethite is a coloured pigment and is therefore not suitable for CLSM. Gibbsite on the other hand, is colourless, can be grown to larger sizes and can be fluorescently labelled. In the final chapter of this thesis we therefore focus on imaging gibbsite liquid crystals in real-time and space using confocal laser scanning microscopy.

1.5 Outline of this thesis

This thesis focuses on the liquid crystal phase behaviour and characterization of liquid crystals of colloidal mineral particles. Small angle x-ray scattering is the characterization technique that is predominantly used throughout this work. Additionally, we also take steps towards enabling CLSM for liquid crystal characterization, which might enable future research on confinement studies of positionally ordered colloidal liquid crystals.

This thesis is split into two parts. Part 1 describes the goethite system, in which the focus is on influencing liquid crystal phase formation, partly by using external fields. In Chapter 2 we follow a sample of polydisperse (30%) chromium-modified goethite colloids, that spontaneously form *I*, *N*, *S* and two types of columnar phases, that is slowly sedimenting in the earth gravitational field over a time span of five years. In Chapter 3 a different approach is taken. Instead of using an external field, we introduce a depletant, which changes the interaction between the particles, and study its effect on goethite phase behaviour. We investigated two different goethite-depletant systems with similar particle dimensions but different polydispersities. Furthermore, we make use of external magnetic fields aiming in Chapter 4 to tune

the biaxiality of the *N* phase by varying the field strength, and in Chapter 5 to study the reorientation process of the columnar liquid crystal phase in a high magnetic field

In part 2 we focus on liquid crystal formation of *large* gibbsite platelets. Due to their high sedimentation velocity they often form less ordered phases. In Chapter 6 we therefore develop a '3D'-SAXS method to enable better characterization of distorted positionally ordered structures. Chapter 7 describes different methods to modify the platelets such that they are suitable for CLSM. Additionally, the liquid crystal phase formation of these modified platelets is studied with CLSM.

References

[1] P. G. de Gennes and J. Prost, *The Physics of Liquid Crystals*, Oxford University Press, New York, 1995.
[2] S. Chandrasekhar, *Liquid Crystals*, Cambridge University Press, Cambridge, 1992.
[3] Q. Li, *Liquid Crystals Beyond Displays: Chemistry, Physics and Applications*, Wiley, Hoboken, New Jersey, 2012.
[4] M. R. Fisch, *Liquid Crystals, Laptops and Life,* World Scientific Publishing Co. Pte. Ltd., Singapore, 2004.
[5] D. H. Everett, *Basic principles of colloid science*, Royal Society of Chemistry, London, 1988.
[6] J. C. P. Gabriel and P. Davidson, *Adv. Mater.*, 2000, **12**, 9.
[7] P. Davidson and J. C. P. Gabriel, *Curr. Opin. Colloid In.*, 2005, **9**, 377-383.
[8] H. N. W. Lekkerkerker and G. J. Vroege, *Philos. T. R. Soc. A*, 2013, **371**, 20120263.
[9] L. Onsager, *Ann. N. Y. Acad. Sci.*, 1949, **51**, 627-659.
[10] R. Eppenga and D. Frenkel, *Mol. Phys.*, 1984, **52**, 1303-1334.
[11] A. Stroobants, H. N. W. Lekkerkerker and D. Frenkel, *Phys. Rev. Lett.*, 1986, **57**, 1452-1455.
[12] D. Frenkel, H. N. W. Lekkerkerker and A. Stroobants, *Nature*, 1988, **332**, 822-823.
[13] J. A. C. Veerman and D. Frenkel, *Phys. Rev. A*, 1992, **45**, 5632-5648.
[14] H. Zocher, Z. *Anorg. Allg. Chem.*, 1925, **147**, 91-U15.
[15] F. Bawden, N. Pirie, J. Bernal and I. Fankuchen, *Nature*, 1936, **138**, 1051-1052.
[16] J. Bernal and I. Fankuchen, *J. Gen. Physiol.*, 1941, **25**, 111-U8.
[17] I. Langmuir, *J. Chem. Phys.*, 1938, **6**, 873-896.
[18] M. J. Freiser, *Phys. Rev. Lett.*, 1970, **24**, 1041.
[19] R. Alben, *Phys. Rev. Lett.*, 1973, **30**, 778-781.
[20] J. P. Straley, Phys. Rev. A, 1974, **10**, 1881-1887.
[21] L. J. Yu and A. Saupe, *Phys. Rev. Lett.*, 1980, **45**, 1000-1003.
[22] J. Perrin, *Ann. Chim. Phys.*, 1909, **18**, 5-114.
[23] J. Perrin, *Les Atomes*, Alcan, Paris, 1913.

[24] H. N. W. Lekkerkerker, P. Coulon, R. Vanderhaegen and R. Deblieck, *J. Chem. Phys.*, 1984, **80**, 3427-3433.
[25] A. Speranza and P. Sollich, *J. Chem. Phys.*, 2002, **117**, 5421-5436.
[26] Z. Dogic and S. Fraden, *Phys. Rev. Lett.*, 1997, **78**, 2417-2420.
[27] Z. Dogic and S. Fraden, *Curr. Opin. Colloid In.*, 2006, **11**, 47-55.
[28] F. Livolant, A. M. Levelut, J. Doucet and J. P. Benoit, *Nature*, 1989, **339**, 724-726.
[29] M. Bates and D. Frenkel, *J. Chem. Phys.*, 1998, **109**, 6193-6199.
[30] Y. Martinez-Raton and J. A. Cuesta, *Mol. Phys.*, 2009, **107**, 415-422.
[31] M. P. Lettinga and E. Grelet, *Phys. Rev. Lett.*, 2007, **99**, 197802.
[32] A. R. Khokhlov and A. N. Semenov, *Macromolecules*, 1982, **15**, 1272-1277.
[33] S. Fraden, G. Maret, D. L. D. Caspar and R. B. Meyer, *Phys. Rev. Lett.*, 1989, **63**, 2068-2071.
[34] S. Fraden, G. Maret and D. L. D. Caspar, *Phys. Rev. E*, 1993, **48**, 2816-2837.
[35] J. X. Tang and S. Fraden, *Phys. Rev. Lett.*, 1993, **71**, 3509-3512.
[36] E. P. Furlani, in *Permanent Magnet and Electromechanical Devices: Materials, Analysis, and Applications.*, Academic Press: San Diego, CA, 2001, p. 518.
[37] E. Paineau, I. Dozov, K. Antonova, P. Davidson, M. Imperor, F. Meneau, I. Bihannic, C. Baravian, A. M. Philippe, P. Levitz and L. J. Michot, *Int. Congr. Cer.*, 2011, **18**, 062005.
[38] S. Zhang, C. I. Pelligra, G. Keskar, P. W. Majewski, F. Ren, L. D. Pfefferle and C. O. Osuji, *ACS Nano*, 2011, **5**, 8357-8364.
[39] X. Commeinhes, P. Davidson, C. Bourgaux and J. Livage, *Adv. Mater.*, 1997, **9**, 900.
[40] B. Abecassis, F. Lerouge, F. Bouquet, S. Kachbi, M. Monteil and P. Davidson, *J. Phys. Chem. B*, 2012, **116**, 7590-7595.
[41] L. J. Michot, I. Bihannic, S. Maddi, S. S. Funari, C. Baravian, P. Levitz and P. Davidson, *P. Natl. Acad. Sci. USA*, 2006, **103**, 16101-16104.
[42] E. Paineau, I. Dozov, A. Philippe, I. Bihannic, F. Meneau, C. Baravian, L. J. Michot and P. Davidson, *J. Phys. Chem. B*, 2012, **116**, 13516-13524.
[43] M. Dijkstra, R. van Roij and R. Evans, *Phys. Rev. E,* 2001, **63**, 051703.
[44] H. Reich and M. Schmidt, *J. Phys.: Condens. Matter*, 2007, **19**, 326103.
[45] D. de las Heras, E. Velasco and L. Mederos, *Phys. Rev. Lett.*, 2005, **94**, 017801.
[46] D. de las Heras, Y. Martinez-Raton and E. Velasco, *Phys. Chem. Chem. Phys.*, 2010, **12**, 10831-10841.
[47] D. de las Heras, Y. Martinez-Raton and E. Velasco, *Phys. Rev. E*, 2010, **81**, 021706.
[48] O. J. Dammone, I. Zacharoudiou, R. P. A. Dullens, J. M. Yeomans, M. P. Lettinga and D. G. A. L. Aarts, *Phys. Rev. Lett.*, 2012, **109**, 108303.
[49] A. Kuijk, A. van Blaaderen and A. Imhof, *J. Am. Chem. Soc.*, 2011, **133**, 2346-2349.
[50] B. Lemaire, P. Davidson, J. Ferre, J. Jamet, D. Petermann, P. Panine, I. Dozov and

J. Jolivet, *Eur. Phys. J. E*, 2004, **13**, 291-308.
[51] D. M. E. Thies-Weesie, J. P. de Hoog, M. H. H. Mendiola, A. V. Petukhov and G. J. Vroege, *Chem. Mat.*, 2007, **19**, 5538-5546.
[52] G. J. Vroege, D. M. E. Thies-Weesie, A. V. Petukhov, B. J. Lemaire and P. Davidson, *Adv. Mater.*, 2006, **18**, 2565.
[53] E. van den Pol, D. M. E. Thies-Weesie, A. V. Petukhov, G. J. Vroege and K. Kvashnina, *J. Chem. Phys.*, 2008, **129**, 164715.
[54] Q. Majorana, *C. R. Hebd. Seances Acad. Sci.*, 1902, **135**, 159-161.
[55] Q. Majorana, *Rend. Accad. Lincei*, 1902, **11**, 374.
[56] A. Cotton and Q. Majorana, *C. R. Acad. Sci.*, 1905, **141**, 317.
[57] B. Lemaire, P. Davidson, J. Ferre, J. Jamet, P. Panine, I. Dozov and J. Jolivet, *Phys. Rev. Lett.*, 2002, **88**, 125507.
[58] B. Lemaire, P. Davidson, D. Petermann, P. Panine, I. Dozov, D. Stoenescu and J. Jolivet, *Eur. Phys. J. E*, 2004, **13**, 309-319.
[59] B. Lemaire, P. Davidson, J. Ferre, J. Jamet, D. Petermann, P. Panine, I. Dozov, D. Stoenescu and J. Jolivet, *Faraday Discuss.*, 2005, **128**, 271-283.
[60] E. van den Pol, A. V. Petukhov, D. M. E. Thies-Weesie, D. V. Byelov and G. J. Vroege, *Phys. Rev. Lett.*, 2009, **103**, 258301.
[61] S. Belli, A. Patti, M. Dijkstra and R. van Roij, *Phys. Rev. Lett.*, 2011, **107**, 148303.
[62] H. H. Wensink and G. J. Vroege, *Phys. Rev. E*, 2005, **72**, 031708.
[63] E. van den Pol, A. A. Verhoeff, A. Lupascu, M. A. Diaconeasa, P. Davidson, I. Dozov, B. W. M. Kuipers, D. M. E. Thies-Weesie and G. J. Vroege, *J. Phys.: Condens. Matter*, 2011, **23**, 194108.
[64] E. van den Pol, A. Lupascu, M. A. Diaconeasa, A. V. Petukhov, D. V. Byelov and G. J. Vroege, *J. Phys. Chem. Lett.*, 2010, **1**, 2174-2178.
[65] B. Lemaire, P. Davidson, P. Panine and J. Jolivet, *Phys. Rev. Lett.*, 2004, **93**, 267801.
[66] E. van den Pol, A. V. Petukhov, D. V. Byelov, D. M. E. Thies-Weesie, A. Snigirev, I. Snigireva and G. J. Vroege, *Soft Matter,* 2010, **6**, 4895-4899.
[67] E. van den Pol, A. V. Petukhov, D. M. E. Thies-Weesie and G. J. Vroege, *Langmuir,* 2010, **26**, 1579-1582.
[68] A. M. Wierenga, T. A. J. Lenstra and A. P. Philipse, *Colloid. Surface. A*, 1998, **134**, 359-371.
[69] F. van der Kooij, K. Kassapidou and H. Lekkerkerker, *Nature*, 2000, **406**, 868-871.
[70] F. M. van der Kooij, D. van der Beek and H. N. W. Lekkerkerker, *J. Phys. Chem. B*, 2001, **105**, 1696-1700.
[71] H. H. Wensink, G. J. Vroege and H. N. W. Lekkerkerker, *J. Phys. Chem. B*, 2001, **105**, 10610-10618.
[72] D. van der Beek, T. Schilling and H. Lekkerkerker, *J. Chem. Phys.*, 2004, **121**, 5423-5426.

[73] D. van der Beek, P. B. Radstake, A. V. Petukhov and H. N. W. Lekkerkerker, *Langmuir*, 2007, **23**, 11343-11346.
[74] A. Petukhov, D. van der Beek, R. Dullens, I. Dolbnya, G. Vroege and H. Lekkerkerker, *Phys. Rev. Lett.*, 2005, **95**, 077801.
[75] A. A. Verhoeff, I. A. Bakelaar, R. H. J. Otten, P. van der Schoot and H. N. W. Lekkerkerker, *Langmuir,* 2011, **27**, 116-125.
[76] D. van der Beek, A. V. Petukhov, P. Davidson, J. Ferre, J. P. Jamet, H. H. Wensink, G. J. Vroege, W. Bras and H. N. W. Lekkerkerker, *Phys. Rev. E*, 2006, **73**, 041402.
[77] D. van der Beek, P. Davidson, H. H. Wensink, G. J. Vroege and H. N. W. Lekkerkerker, *Phys. Rev. E*, 2008, **77**, 031708.
[78] A. A. Verhoeff, R. H. J. Otten, P. van der Schoot and H. N. W. Lekkerkerker, *J. Chem. Phys.*, 2011, **134**, 044904.
[79] A. A. Verhoeff, R. H. J. Otten, P. van der Schoot and H. N. W. Lekkerkerker, *J. Phys. Chem. B*, 2009, **113**, 3704-3708.
[80] J. Wijnhoven, *J. Colloid Interf. Sci.*, 2005, **292**, 403-409.
[81] C. Vonk, S. Oversteegen and J. Wijnhoven, *J. Colloid Interf. Sci.*, 2005, **287**, 521-525.
[82] J. Wijnhoven, D. van't Zand, D. van der Beek and H. Lekkerkerker, *Langmuir*, 2005, **21**, 10422-10427.
[83] M. C. D. Mourad, A. V. Petukhov, G. J. Vroege and H. N. W. Lekkerkerker, *Langmuir,* 2010, **26**, 14182-14187.
[84] A. Petukhov, J. Thijssen, D. t Hart, A. Imhof, A. van Blaaderen, I. Dolbnya, A. Snigirev, A. Moussaid and I. Snigireva, *J. Appl. Crystallogr.*, 2006, **39**, 137-144.
[85] H. Schnablegger and Y. Singh, *The SAXS guide*, Anton Paar GmbH, Graz, Austria, 2011.

PART 1

GOETHITE

2

Ageing in a system of polydisperse board-like goethite particles

The rich liquid crystalline phase behaviour of a polydisperse system of chromium-modified goethite particles sedimenting in the earth gravitational field has been studied for five years. We observe that the particles stay highly mobile over years and the rich phase behaviour keeps developing in novel and even surprising ways. While in many other colloidal systems particle size polydispersity suppresses the formation of ordered phases, goethite particles form multiple co-existing ordered phases. The particle polydispersity problem is then solved by particle exchange between co-existing phases. One usually expects that a less ordered phase (e.g., nematic) is formed first while crystallization of the smectic and columnar crystals might take longer time. For goethite particles we find the opposite, i.e. the nematic phase grows over years at the expense of a better ordered smectic phase. Moreover, SAXS patterns revealed peak splitting for both the smectic and the columnar phase meaning that the system displays fractionated crystallization. We further discovered that the centred rectangular columnar phase (R_C) spontaneously forms out of the simple rectangular columnar phase (R_S). The reverse transition is observed as well. We explain the ease of these martensitic transitions by showing how slight rotation and translation of the particles triggers the transition.

2.1 Introduction

Suspensions of anisotropic particles are able to self-organize into various liquid crystal phases with nematic (*N*), smectic (*S*) and columnar (*C*) structures. In the *N* phase there is only orientational order. In the smectic phase the oriented particles are stacked into layers and thus have positional ordering in one direction as well. In the columnar phase the oriented particles form columns which are stacked in two dimensions.

Although much attention has been paid to organic liquid crystals which are well known for their application in liquid crystal displays, mineral liquid crystals have enhanced electrical, optical and magnetic properties and a better thermal stability [1] and therefore deserve study in their own right.

However, synthetic colloids have an inherent polydispersity which is known to suppress ordering. For example, a crystal of colloidal spheres cannot accommodate a polydispersity higher than the so-called terminal polydispersity of about 6 – 8 % [2, 3]. For dispersions of rod-like particles it is predicted on the basis of computer simulations that the smectic phase cannot contain particles with a length polydispersity above 18% because the particles will not fit into the smectic layers [4].

Some theories address the influence of fractionation, showing for example for both bidisperse and continuous systems that fractionation occurs for isotropic-nematic phase separation in dispersions of colloidal rods [5-7]. The longer rods orient first and form the nematic phase, while the shorter rods remain in the isotropic phase [8-11]. For spheres it is shown that they can display fractionated crystallization, when the polydisperse suspension splits into fractions with narrower size distributions. If local values of the polydispersity then end up below the terminal polydispersity, each of these fractions can consequently form crystals with different periods [12-17]. This fractionated crystallization has actually been observed for liquid crystals in a system of polydisperse colloidal disks [18].

Dispersions of colloidal board-like goethite (α-FeOOH) particles show rich liquid crystalline phase behaviour, including the nematic, smectic and two different types of columnar phases, the rectangular simple (R_S) and the rectangular centred (R_C) [19-24]. For a specific particle aspect ratio even biaxial nematic and smectic phases are found [25, 26]. Because of the special magnetic properties of individual goethite particles [27, 28] the system is highly susceptible to external fields as well.

Surprisingly, for goethite systems with a high polydispersity (35 - 50%) it was shown that their polydispersity does not suppress, but actually enriches the phase behaviour [29, 30]. In contrast to systems with lower polydispersity besides the nematic and smectic also columnar phases were observed. Goethite particles have a high density which makes sedimentation an important factor as well. The interplay between the high polydispersity, sedimentation and phase separation induces fractionation which locally can reduce the polydispersity by a factor of at least two [29]. It was shown that at high polydispersity the columnar phase and smectic phase coexist and that the columnar phase acts as a waste disposal for particles which

do not fit within the smectic phase. Fractionated crystallization, as was observed for plate-like particles, was expected but has never been observed before for this system.

In this chapter we have studied the phase behaviour of a highly polydisperse (30%) dispersion of chromium-modified goethite boards by small angle x-ray scattering (SAXS) and polarized light microscopy (PLM), over a span of five years. Interestingly, the initially already rich phase behaviour keeps developing over time, leading to an increasing volume of nematic phase, fractionated crystallization in smectic and columnar phases and providing a proof for the delicate balance between the two forms of the columnar phase.

2.2 Experimental

2.2.1 Synthesis and sample preparation

The chromium-modified goethite particles were obtained by the hydrolysis of iron/chromium nitrate at high pH. This was performed according to the procedure described by Lemaire *et al*. [23] but slightly adjusted to incorporate chromium ions [24, 31]. 1 M NaOH (Acros, reagent ACS, pellets 97+%) was added to a 0.1 M chromium/iron nitrate solution ($Cr(NO_3)_3.9H_2O$, Merck, p.a. and $Fe(NO_3)_3.9H_2O$, Fischer, p.a.) until the pH of the solution was 9. The precipitate was redispersed in Millipore (mp) water and NaOH was added until a pH of 11-12 was reached. The precipitate was aged at 70 °C for 10 days. The particles were washed with mp water and charged with 3M HNO_3 (Merck, 65%, p.a.). After washing with mp water the particles were dispersed in slightly acidified (with HNO_3) mp water to obtain a stable dispersion at pH = 3. The H^+ and charge-compensating NO_3^- concentrations determine the salt concentration. Therefore, the Debye length is 10 nm at most. The particle volume fraction ϕ was 0.08.

A flat glass capillary with internal dimensions of 0.2 x 4.0 x 100 mm^3 (Vitrocom W3520-100) was filled with the Cr-goethite dispersion. The capillary was flame-sealed and stored vertically to assure the formation of a density gradient.

2.2.2 Characterization

Inductively coupled plasma optical emission spectroscopy (ICPOES) showed that approximately 5% of the iron atoms were substituted by chromium. The chromium substitution increases the critical magnetic field strength B^*, which was found to be ~550 mT for the particles described in this chapter.

A Technai 10 (FEI company) transmission electron microscope (TEM) was used to determine particle size distributions. Of about 300 particles the length and width were measured with iTEM imaging software to determine the average length ($\langle L \rangle$) and width ($\langle W \rangle$) and their standard deviations (δL and δW). The length polydispersity is then defined as $\sigma L = \delta L / \langle L \rangle$. Because few particles lay on their side the

thickness *T* was hard to measure and was determined for about 10 particles. The particle dimensions were found to be <*L*> x <*W*> x <*T*> = 227 x 68 x 22 nm with a polydispersity of about 30% in all dimensions.

Small angle x-ray scattering
We have collected SAXS patterns during six measurement sessions which were done over a time span of five years using the microradian diffraction setup [32] at the BM26 DUBBLE [33] beamline and the ID02 high brilliance beamline [34] of the European Synchrotron Radiation Facility (ESRF, Grenoble, France). Patterns were collected by different 2-dimensional x-ray CCD-based detectors. Exact details of the used setup slightly varied for the different measurements but typically a photon energy of 12 - 13 keV was used, with a sample-detector distance of 7 - 10 m. During most sessions magnetic fields were applied with a variable permanent magnet (of beamline ID02) with which a field strength of up to 1.5T could be reached. By changing the distance between the NdFeB poles (which are made of stacks of NdFeB) the strength of the field could be varied and by changing the NdFeB stacks the direction of the field could be altered. Sometimes also a homemade permanent magnet was used.

Here we collect the results of the SAXS measurements to determine the character of the liquid crystal phases, which were always done before the magnetic field was applied. This means that in between the experiments the sample was able to relax its structure after magnetic field application. During every measurement the sample was measured in the middle of the capillary and patterns were obtained every mm along the vertical direction (y) of the capillary.

Polarized Light Microscopy
A polarized light microscope (Nikon LV100Pol) equipped with a 2x Nikon CFI Plan UW and a 10x Nikon CFI Plan Fluor ELDW objective was used to study the birefringence and the liquid crystal phases within the sample. The microscope was in a tilted position with the focal plane along gravity in order to allow investigation of the sample in an upright position to prevent the gravity induced density gradient in the sample from being distorted. Images were captured by a MicroPublisher 5 megapixel CCD camera (MP5, Qimaging).

2.3 Results and Discussion

2.3.1 Phase behaviour through the years

Here we present observations on a dispersion of chromium-modified goethite particles (5:95 Cr:Fe). The particles have a critical magnetic field strength (B^*) of ~550 mT above which the induced magnetic moment is larger than the permanent magnetic moment and the particles will change orientation. A flat capillary was filled

with the dispersion (ϕ = 0.08) in November 2006 and stored vertically to assure the formation of a density gradient in the gravitational field. The phase behaviour of the system has been studied by small angle x-ray scattering (SAXS) and polarized light microscopy (PLM), over a span of five years.

Fig. 2.1(a) shows a schematic overview of the development of the different liquid crystal (LC) phases formed in the capillary. PLM clearly reveals phase separation and the appearance of the LC between crossed polarizers suggests the character (*N*, *S*, *C*) of the LC phase (Fig. 2.1(b)). With a white light source Bragg reflections could be observed in both the *S* and *S* + *C* phase, which helped distinguishing between the *N* and the *S* (+*C*) phases. Furthermore, detailed structure characterization and final LC structure assignment were done with SAXS. Patterns were taken every mm along the height of the capillary. There were six measurement points with different time intervals. The first three (Jun, Aug, Nov 07) with an interval of about two to three months, the next two (Sep 08, Jun 09) with an interval of approximately a year and the last measurement (Oct 11) was done over two years later. For other research purposes magnetic fields were applied. The black arrows in Fig. 2.1(a) indicate when a magnetic field was applied, the strength of that field and in which direction. At low field strengths particles align along their *L* axis and above *B** they reorient and will align along their *T* axis. The effect of the field is always temporary; after the field is switched off the particles are eventually able to relax to their preferred configurations without field.

Fig. 2.1(a) shows that the sample displays rich and complex phase behaviour already half a year after sample preparation (Jun 07); the isotropic, nematic, a large smectic and the simple rectangular columnar phase (R_S) are observed. After sedimentation for a year also the centred rectangular columnar phase (R_C) is observed (Nov 07). After a couple of years in which both columnar phases are coexisting (Nov 07 – Jun 09) the columnar R_S phase completely disappears and the R_C columnar phase is the only columnar phase present.

For the first four measurements the large smectic phase has approximately the same size, but over time the amount of smectic phase decreases. For the nematic phase the contrary is observed; it steadily grows over time.

The last two SAXS measurements done in 2009 and 2011 showed fractionated crystallization in the smectic phase and in 2011 in the columnar phase as well. This has recently been observed in suspensions of gibbsite platelets [18] but was never seen before in goethite. In the following parts we will focus on some selected features.

2.3.2 Polydispersity induced nematic phase

The observations reported above again point to the influence of polydispersity on the phase behaviour. Normally, in sedimenting colloidal liquid crystals a density gradient is formed which induces phase separation; phases with different volume fractions are formed on top of each other, the phase with the highest density form-

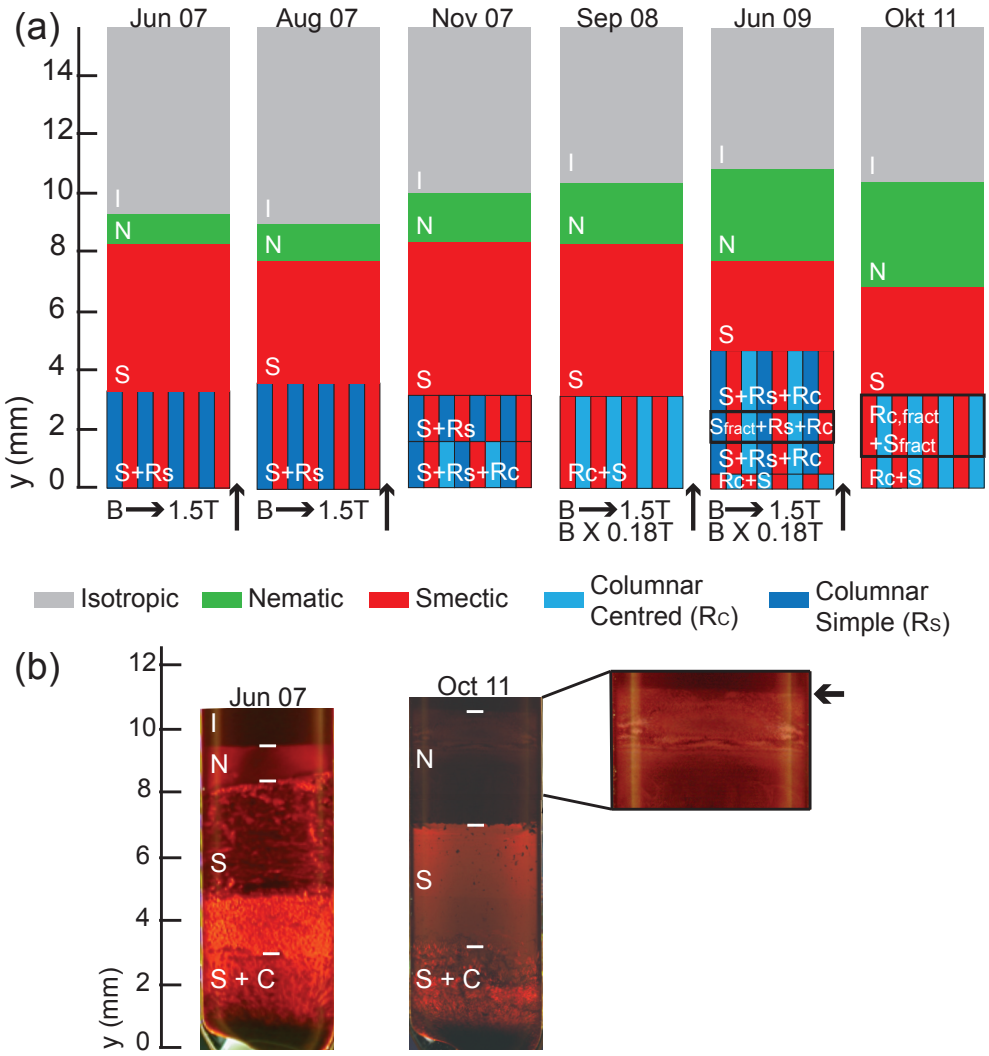

Fig. 2.1 (a) Schematic representations of the liquid crystal phases observed in the capillary constructed from SAXS (supported by PLM) measurements done at six moments over five years. SAXS patterns were obtained every mm along the vertical direction (y) of the capillary. Grey represents the *I* phase, green the *N*, red the *S* and the blue colours the two different *C* phases, R_C and R_S. The vertical arrows indicate when magnetic fields were applied. The field was always applied after the LC phases were determined. The strength of the field and direction (→ means along capillary width and x along capillary thickness) are mentioned as well. B^* = 550 mT. 0 mm is at the bottom of the capillary. (b) PLM images of the phase separated sample in Jun 07 and Oct 11. White bars mark the interfaces between the different LC phases. The enlarged area shows the *I* - *N* interface with increased picture brightness to increase visibility of the interface.

ing at the bottom of the capillary. So for this system, one would expect the most highly ordered columnar phase at the bottom, with the smectic, nematic and isotropic phase respectively on top. The higher the degree of ordering in the liquid crystal phase, the longer it normally takes for the corresponding structure to form. This means that one expects the smectic phase to grow over time, while the nematic phase decreases.

Previous research already showed that polydispersity explains the coexistence of the columnar and smectic phase at the same height: the particles too large to match the smectic periodicity in this system are expelled to the columnar phase, which acts as a waste bin.

In the present experiments we see the nematic phase steadily grow over time. This is in contrast to the size of the smectic phase which decreases over time (Fig. 2.1) after staying - within the accuracy of the measurements - approximately equal for about a year (Fig. 2.1(a)). This peculiar behaviour strongly suggests that the nematic phase is not only formed by sedimenting particles from the isotropic phase but also by smaller particles that are expelled from the smectic phase. We observed that even after phase separation the smectic phase slowly keeps developing. Fig. 2.3 shows that over time smectic domains with different periodicities, hence lower polydispersities, are formed at the same height in the capillary. This so called 'fractionated crystallization' will be discussed in the next section (section 2.3.3). Moreover, Fig. 2.1(b) shows that finally a large single, well ordered smectic domain is formed. From this it is clear that Brownian rearrangement of particles happens for a long time. To obtain this high ordering and low polydispersity in the smectic phase the particles that do not 'fit' the smectic periodicity are excluded. The columnar phase accommodates the larger particles that, due to fractionation and sedimentation, are lower in the sample. The smaller particles that are higher in the sample are easily 'absorbed' in the nematic phase which can accept a much higher polydispersity. In this respect, the nematic phase can - like the columnar phase for the longer particles - be considered a waste bin for shorter particles that do not fit within the smectic layers.

Board- or rod-like systems with high polydispersity normally favour the nematic phase over the smectic phase. By expelling the particles that do not fit the smectic periodicity the goethite system locally reduces its polydispersity and still favours the smectic phase, large rather stable smectic domains are present.

2.3.3 Fractionated crystallization

We saw before that the system deals with polydispersity by expelling the too large and too small particles into columnar and nematic phases respectively. Previous measurements [29] demonstrated that goethite systems fractionate, meaning that there is a gradient with the larger particles lower in the sample, and the smaller particles in the top of the sample. It was found that due to this effect, the local polydispersity can be twice as low as in the parent dispersion.

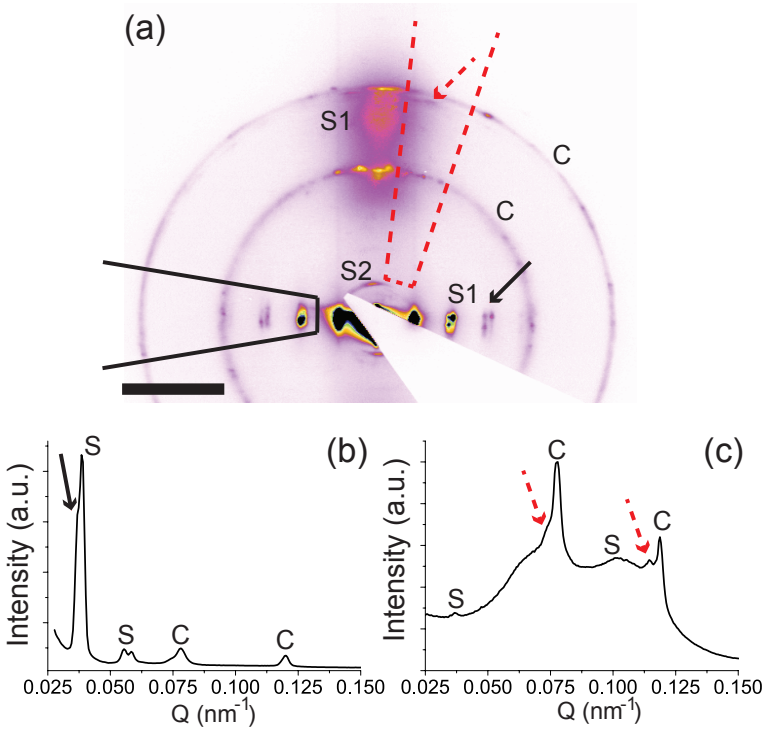

Fig. 2.2 (a) High resolution SAXS pattern of a R_c and S phase measured in the Cr-goethite sample in Oct 11 at y = 2.5 mm. Reflections labelled S1 and S2 originate from the smectic interlayer periodicity and the liquid-like interactions within the layers, respectively. Reflections labelled C originate from the Q_{11} and Q_{20} columnar reflections. The solid and dashed arrows emphasize the split Bragg peaks indicating fractionated crystallization in the smectic and the columnar phase, respectively. The black bar denotes 0.05 nm^{-1}. (b) I(Q) profile taken of the area between the black solid lines in (a). S and C again indicate reflections from the smectic and columnar phase respectively. For the 3rd order smectic reflection we clearly see split peaks. For the 2nd order it is less clear but a shoulder can be observed. (c) I(Q) profile taken of the area between the grey dashed lines in (a). Again S and C indicate reflections from the smectic and columnar phase, respectively. Here we clearly see split peaks for the columnar Q_{20} reflection and a shoulder at the Q_{11} reflection.

In this paper we show for the first time that these systems may also display fractionated crystallization (i.e. the presence of crystal domains with different periods at the same height in the sample). This was observed with SAXS for the first time in the smectic phase after three years of sedimentation (Jun 2009).

This fractionated crystallization is demonstrated in the SAXS pattern shown in Fig. 2.2(a). This pattern was measured in 2011, after five years of sedimentation. The sharp reflections in the horizontal direction and the liquid-like reflection in the vertical direction, both labelled S1, originate from one set of smectic inter- and

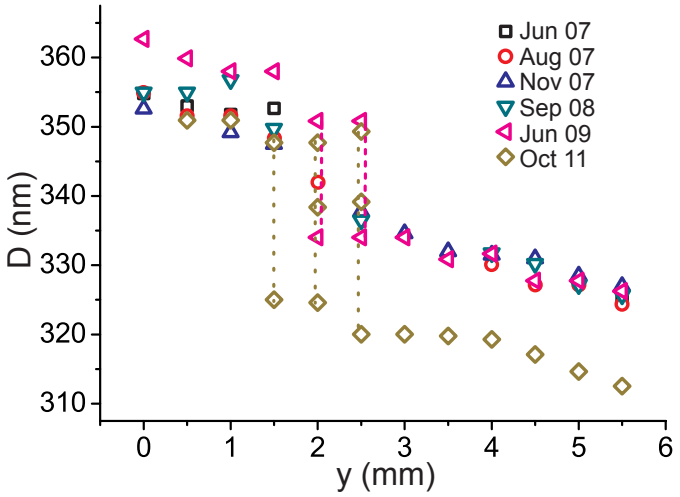

Fig. 2.3 The interlayer distances *D* measured in the *S* phase plotted against the distance from the bottom of the capillary y (0 mm is at the capillary bottom), measured at the same moments in time as the schematic drawings in Fig. 2.1(a). From 2007 till Sept 2008, there is a continuous gradient in *D* with the largest distances found at y = 0 since the largest particles are at the bottom of the capillary. However in 2009 we see a discontinuous transition (dashed lines); two characteristic interlayer distances are measured at the same position, indicating fractionated crystallization. The same can be observed for an ever larger area in the Oct 2011 measurements (dotted lines). Here, up to three different characteristic distances were detected at the same position.

intralayer distances. The weak reflection labelled S2 is from a smectic domain with another orientation. The rings labelled *C* originate from the Q_{11} and Q_{20} columnar R_C reflection. If one looks closer, one clearly sees that the sharp S1 reflections are split (black arrow), indicating that there are two characteristic interlayer distances (with almost similar orientation) at that height in the capillary. The same can be seen for the reflections of the columnar phase (dashed arrow).

This is even clearer from the intensity profiles in Fig. 2.2(b, c). One profile was taken of the area between the black lines, the first two reflections at Q = 0.038 nm^{-1} and 0.057 nm^{-1} are the 2nd and 3rd order of the smectic periodicity and especially at the 3rd order reflection double peaks can be observed. For the 2nd order reflection it is less clear, but the peak is asymmetric, a shoulder can be observed (indicated by the black arrow). The two reflections at higher Q-values originate from the columnar R_C phase. Fig. 2.2(c) shows the intensity profile of the area between the dashed lines, at low Q a weak peak is visible from the smectic periodicity, as is the liquid-like peak seen around 0.1 nm^{-1}. The two columnar reflections at 0.078 nm^{-1} and 0.120 nm^{-1} are again split proving the presence of fractionated liquid crystals.

To summarize these observations the smectic interlayer periodicity (*D*) was plotted against the height in the capillary (y) in Fig. 2.3. From 2007 through 2008 regu-

lar fractionation can be seen, there is a continuous gradient in the periodicities. The periodicity is largest at the bottom of the capillary, because larger particles sediment faster. However, in 2009 we see a discontinuous transition; two characteristic interlayer distances are observed at the same height. The same holds for the 2011 measurements, where even three characteristic distances were measured at the same position. The decrease in the interlayer distances in 2011 which can be observed for y > 3 mm is most likely due to compression of the system by aging after fractionated crystallization.

Due to the several ways the system accommodates its high polydispersity - the formation of nematic and columnar 'waste bins', both fractionation and fractionated crystallization - the system manages to form a remarkable large and stable single smectic domain over time. In 2011 the size of this single domain was more than 10 mm^2 (Fig. 2.1(b)).

For the first measurements smaller single domains were observed as well, but these might be induced by the magnetic field. However, the particles stay highly mobile, as Fig. 2.1(a) shows, and between 2009 and 2011 there was no magnetic field, indicating that the formation of this large single smectic domain is spontaneous.

2.3.4 Columnar phases

Fig. 2.1 shows that two different columnar phases were observed, the rectangular simple (R_S) and the rectangular centred (R_C) phase, depicted in Fig. 2.4(a, b) respectively. These structures were already described in ref. [24] where a simple cell model was given which shows that entropically the R_S phase is slightly favoured. The entropy difference $\Delta S = k_B(\ln \Omega_S - \ln \Omega_C)$ with Ω the configurational space per particle between the two phases varied from 0.32 k_B per particle (bare particles) up to 3.4 k_B per particle (Debye length taken into account). In the presence of a strong magnetic field the orientation of the shortest particle axis is fixed due to the induced magnetic moment in combination with excluded volume interactions (which favor alignment of T over W, see Chapter 4). In this case the model shows that the R_C phase is favoured by 0.14 to 0.22 k_B per particle. This rationalized the observation reported in that article that the R_S phase was favoured and the R_C phase was only observed after being induced by a strong magnetic field.

Here, we see for the first time that the R_C phase is also formed spontaneously. In Fig. 2.1(a) we clearly see that in November 2007 the R_S phase is present, which has spontaneously transformed into the R_C phase by September 2008. Fig. 2.4(c) shows the SAXS pattern measured in the sample. The two rings at Q = 0.064 and 0.100 nm^{-1} (Fig. 2.4(e)) originate from the R_C Q_{11} and Q_{20} reflections.

Fig. 2.1(a) shows that both phases change into each other quite easily and they even coexist, for example in November 2007 and 2009. Indeed the SAXS pattern in Fig. 2.4(d) with the accompanying intensity profile (Fig. 2.4(f)) shows reflections from both phases.

From this we can conclude that there is a fine interplay between the phases and

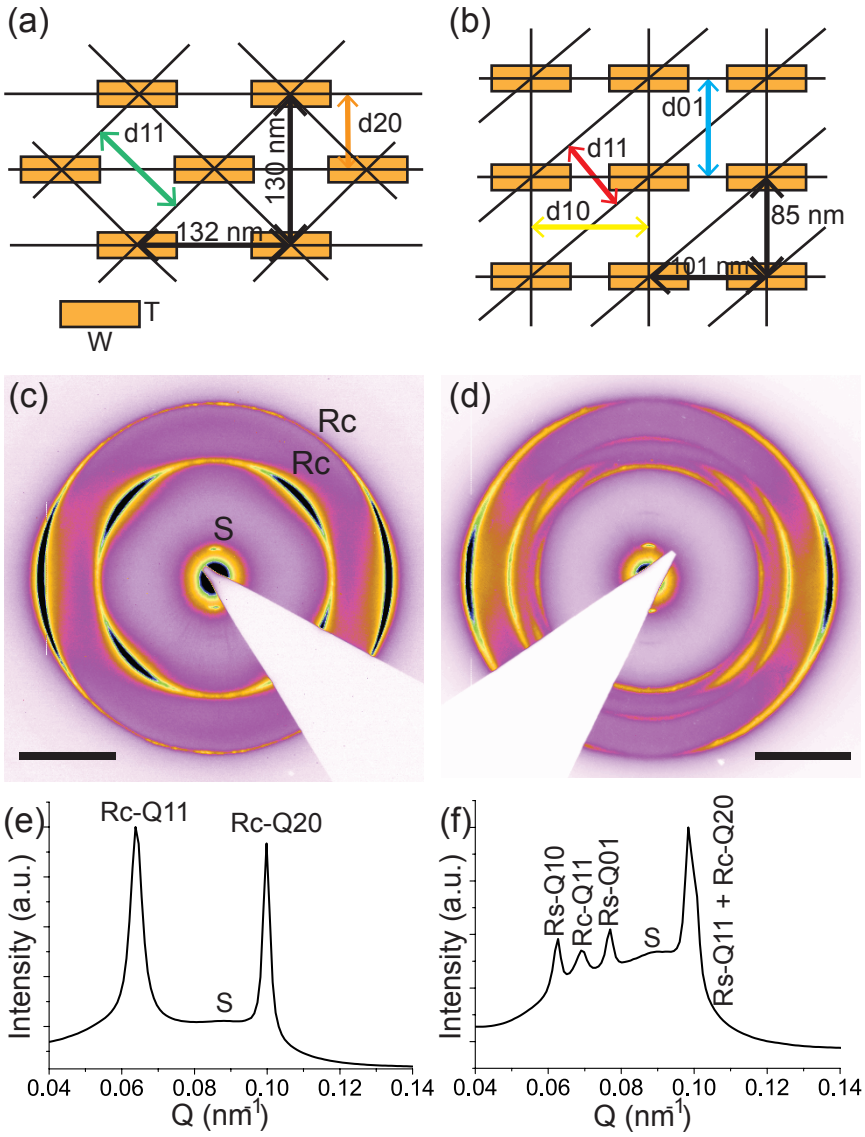

Fig. 2.4 Schematic drawings of the (a) R_C and (b) R_S phase with their characteristic cell distances shown in black. Bragg reflections are expected at $Q_{hk} = 2\pi/d_{hk}$. High resolution SAXS images of (c) the coexisting R_C and S phase measured in Sept 08 and (d) coexisting R_C, R_S and S phases measured in Nov 07. S and R_C denote reflections from the smectic and centred rectangular columnar phase respectively. The black bars denote 0.05 nm^{-1}. (e) I(Q) profile of the pattern in (c). Peaks are assigned to the R_C Q_{11} and Q_{20} reflections. (f) I(Q) profile of the pattern in (d). Peaks are assigned to the R_S Q_{10}, Q_{01} and Q_{11} reflections and the R_C Q_{11} and Q_{20} reflections, where $R_{S,Q11}$ is at the same Q as R_C.

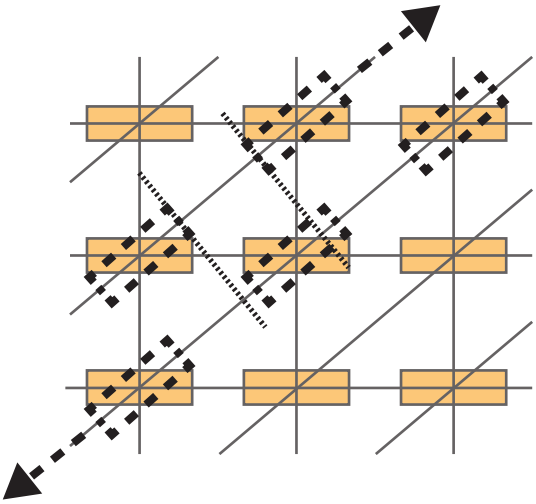

Fig. 2.5 Schematic representation of the R_S – R_C martensitic transition pathway. By rotating the particles in the R_S phase by 45° only a little sliding of the layers over each other is needed (emphasized by the dotted lines) to obtain the R_C phase.

there is no phase that is clearly favoured by the system. The model, which already predicts very small entropy differences, is probably not accurate enough to be conclusive. The spontaneous formation of the R_C phase for example cannot be explained with the model. The model does not account for polydispersity, which is playing an important role in this system. Also fractionation can influence the delicate balance between the phases.

2.3.5 Ease of the R_C – R_S martensitic transition

The fact that the phases transform into each other and coexist is easily understood if one studies the two different structures carefully. First of all, the structures both have the same particle density. Fig. 2.4(a, b) show that the R_C structure has two particles per 132 x 130 nm cell, whereas the R_S structure has one particle per 101 x 85 nm cell, which is indeed ½ x 132 x 130 nm. It is assumed that the distance between the particles in the third direction remains the same.

Besides, from Fig. 2.4(e) it is clear that the reflection $Q_{Rs,11}$ is equal to $Q_{Rc,20}$, meaning that the two structures have a common characteristic distance: $R_{S,d11} = R_{C,d20}$. It can then be seen that it is easy to transform the structures into each other (Fig. 2.5). If the particles in the R_S phase slightly rotate around their long axis (by approximately 45°) and the layers slide a little over each other, the R_C phase will be obtained. Also the other way around, a shear force created by for example moving the sample or applying a magnetic field can make the layers slide over each other which triggers the formation of the R_S phase. After or during sliding of the layers only a simple rotation is necessary to switch phases.

These transformations from one phase into the other are small and underline the

delicate balance between the two phases.

2.4 Conclusions

We have studied the phase behaviour of a polydisperse chromium-modified goethite dispersion over a span of five years using PLM and SAXS measurements. We have observed that the particles stay highly mobile over years and that the system keeps developing interesting phase behaviour. This phase behaviour is induced by the high polydispersity and a strong tendency of the system to form a smectic phase, which expels the longer particles to the columnar phase(s) [29]. We now observed that the system continues creating an increased amount of nematic phase to which too small particles from the smectic phase are expelled. We saw for the first time split Bragg reflections in SAXS patterns for both the smectic and the columnar phase meaning that the system also displays fractionated crystallization to locally decrease the polydispersity. These ways of lowering the polydispersity locally contribute to the preservation of the smectic phase. Over a period of five years, a very large and stable single smectic domain is obtained.

Moreover, we show for the first time that the centred rectangular columnar phase is spontaneously formed out of the simple rectangular columnar phase. The phases can transform into each other easily which we explained by the R_S and R_C phases having the same particle density and one equal characteristic distance so that a small transformation - sliding of the layers and simple rotations - is enough to trigger the martensitic transition between the phases.

We conclude that polydisperse aqueous goethite dispersions remain very versatile liquid crystal formers due to their particles' capacity to keep rearranging even after many years.

Acknowledgements

We would like to acknowledge first and foremost Esther van den Pol, who prepared the sample described in this chapter many years ago. Then we additionally would like to thank the staff of the BM26 and ID02 beamlines at the ESRF, in particular Giuseppe Portale, Dirk Detollenaere, Anatoly and Irina Snigirev, Kristina Kvashnina, Pierre Panine and Theyencheri Narayanan for their excellent support during the synchrotron experiments.

References

[1] P. Davidson and J. C. P. Gabriel, *Curr. Opin. Colloid In.,* 2005, **9**, 377-383.
[2] P. Bolhuis and D. Kofke, *Phys. Rev. E,* 1996, **54**, 634-643.
[3] P. Bartlett and P. Warren, *Phys. Rev. Lett.,* 1999, **82**, 1979-1982.
[4] M. Bates and D. Frenkel, *J. Chem. Phys.,* 1998, **109**, 6193-6199.

[5] H. N. W. Lekkerkerker, P. Coulon, R. Vanderhaegen and R. Deblieck, *J. Chem. Phys.,* 1984*,* **80**, 3427-3433.
[6] L. Onsager, *Ann. N. Y. Acad. Sci.,* 1949*,* **51**, 627-659.
[7] T. Odijk and H. Lekkerkerker, *J. Phys. Chem.,* 1985*,* **89**, 2090-2096.
[8] A. Speranza and P. Sollich, *J. Chem. Phys.,* 2002*,* **117**, 5421-5436.
[9] A. Speranza and P. Sollich, *J. Chem. Phys.,* 2003*,* **118**, 5213-5223.
[10] A. Speranza and P. Sollich, *Phys. Rev. E,* 2003*,* **67**, 061702.
[11] H. Wensink and G. Vroege, *J. Chem. Phys.,* 2003*,* **119**, 6868-6882.
[12] M. Fasolo and P. Sollich, *Phys. Rev. Lett.,* 2003*,* **91**, 068301.
[13] P. Bartlett, *J. Chem. Phys.,* 1998*,* **109**, 10970-10975.
[14] P. Bartlett, *J. Phys.: Condens. Matter,* 2000*,* **12**, A275-A280.
[15] R. Sear, *Europhys. Lett.,* 1998*,* **44**, 531-535.
[16] W. Kranendonk and D. Frenkel, *Mol. Phys.,* 1991*,* **72**, 679-697.
[17] P. Sollich and N. B. Wilding, *Phys. Rev. Lett.,* 2010*,* **104**, 118302.
[18] D. V. Byelov, M. C. D. Mourad, I. Snigireva, A. Snigirev, A. V. Petukhov and H. N. W. Lekkerkerker, *Langmuir,* 2010*,* **26**, 6898-6901.
[19] B. Lemaire, P. Davidson, J. Ferre, J. Jamet, P. Panine, I. Dozov and J. Jolivet, *Phys. Rev. Lett.,* 2002*,* **88**, 125507.
[20] B. Lemaire, P. Davidson, D. Petermann, P. Panine, I. Dozov, D. Stoenescu and J. Jolivet, *Eur. Phys. J. E,* 2004*,* **13**, 309-319.
[21] B. Lemaire, P. Davidson, J. Ferre, J. Jamet, D. Petermann, P. Panine, I. Dozov, D. Stoenescu and J. Jolivet, *Faraday Discuss.,* 2005*,* **128**, 271-283.
[22] B. Lemaire, P. Davidson, P. Panine and J. Jolivet, *Phys. Rev. Lett.,* 2004*,* **93**, 267801.
[23] B. Lemaire, P. Davidson, J. Ferre, J. Jamet, D. Petermann, P. Panine, I. Dozov and J. Jolivet, *Eur. Phys. J. E,* 2004, **13**, 291-308.
[24] E. van den Pol, A. V. Petukhov, D. M. E. Thies-Weesie and G. J. Vroege, *Langmuir,* 2010, **26**, 1579-1582.
[25] E. van den Pol, A. V. Petukhov, D. M. E. Thies-Weesie, D. V. Byelov and G. J. Vroege, *Phys. Rev. Lett.,* 2009, **103**, 258301.
[26] E. van den Pol, D. M. E. Thies-Weesie, A. V. Petukhov, D. V. Byelov and G. J. Vroege, *Liq. Cryst.,* 2010*,* **37**, 641-651.
[27] Q. Majorana, *Rend. Accad. Lincei,* 1902*,* **11**, 374.
[28] A. Cotton and Q. Majorana, *C. R. Acad. Sci.,* 1905*,* **141**, 317.
[29] E. van den Pol, D. M. E. Thies-Weesie, A. V. Petukhov, G. J. Vroege and K. Kvashnina, *J. Chem. Phys.,* 2008, **129**, 164715.
[30] G. J. Vroege, D. M. E. Thies-Weesie, A. V. Petukhov, B. J. Lemaire and P. Davidson, *Adv. Mater.,* 2006, **18**, 2565.
[31] E. van den Pol, D. M. E. Thies-Weesie, A. V. Petukhov, P. Panine and G. J. Vroege, *J. Phys.: Condens. Matter,* 2008, **20**, 404219.
[32] A. Petukhov, J. Thijssen, D. t Hart, A. Imhof, A. van Blaaderen, I. Dolbnya, A. Snigirev, A. Moussaid and I. Snigireva, *J. Appl. Crystallogr.,* 2006*,* **39**, 137-144.

[33] W. Bras, I. Dolbnya, D. Detollenaere, R. van Tol, M. Malfois, G. Greaves, A. Ryan and E. Heeley, *J. Appl. Crystallogr.,* 2003, **36**, 791-794.
[34] T. Narayanan, O. Diat and P. Bosecke, *Nucl. Instrum. Meth. A,* 2001, **467**, 1005-1009.

3

Phase behaviour in suspensions of goethite colloids and small spheres

We study the influence of a spherical depletant on the phase behaviour of goethite board-like particles with the length/width aspect ratio slightly larger than the width/thickness ratio. Here we present the results of an exploratory study. Using small angle x-ray scattering we find that the depletion-induced attraction between the particles leads to the formation of the smectic phase. We find isotropic - smectic phase separation for all depletant concentrations used; the nematic phase is not observed. The scattering patterns of the depletant induced smectic phase reveal smaller distances between the particles within the layers, while the smectic interlayer periodicity increases. This suggests that the depletant particles are located in between layers of goethite particles. Scattering patterns of the particle ordering within the layers reveal multiple peaks which suggests biaxial ordering. We find that the depletant-induced smectic phases are highly viscous and unresponsive to weak magnetic fields. We compare our results with theoretical work which predicts biaxial nematic phases for a similar system and similar depletant concentrations. Our results indicate that these depletant concentrations induce a sufficiently strong attraction between the particles, leading to a more highly ordered liquid crystal phase (smectic phase) superseding the nematic phase. Our results imply that for future research including nematic phases in goethite-depletant mixtures significantly lower depletant concentrations should be used.

3.1 Introduction

Suspensions of hard anisotropic (mineral) particles have the ability to self-organize into various liquid crystalline structures involving nematic (*N*), smectic (*S*) and columnar (*C*) phases [1]. In the *N* phase the particles are orientationally ordered. In the *S* and *C* phase the particles additionally have positional order in one and two dimensions, respectively. This process is predominantly entropy driven and the liquid crystal phase formed therefore depends on the particle shape and volume fraction.

The liquid crystal (LC) phase behaviour of colloidal particles can be influenced in various ways . External electric and magnetic fields are frequently used to reorient and fuse liquid crystalline domains or to induce phase transitions. Also spatial confinement is known to influence the phase behaviour: e.g. slit-pore confinement can lower the *I* – *N* [2, 3] as well as the *I* - S binodal [4].

LC phase behaviour can not only be changed by externally applied forces, but can also be influenced by changing the interactions between the particles. By changing the salt concentration of the dispersion the thickness of the double layer surrounding the particles will change. This can e.g. be used to suppress the chirality of the particles [5] or to tune the effective particle anisotropy [6].

Another way to change the particle interactions is by adding a depletant -non-adsorbing polymers or small colloidal particles- to the dispersion. The depletion interaction causes an effective attraction between colloidal particles [7, 8] which gives rise to rich phase behaviour [9]. While most studies are performed on spherical colloids a significant body of work has also been done on the addition of polymeric depletants to suspensions of rod-like and plate-like colloids. An example is the work of Dogic *et al*., who studied the addition of the polymer dextran to suspensions of fd-virus. They found that adding polymer widens the *I* – *N* coexistence region [10], while at higher dextran concentrations the *I* – *N* transition is superseded by the *I* – *S* transition [11]. This depletant-induced broadening of the *I* – *N* phase was also observed in several other studies (see ref. [9], chapter 6).

Also small colloidal spheres have been used as depletants [9]. Studies of mixtures of anisotropic particles and small colloidal spheres revealed rich phase behaviour. E.g. the addition of small silica spheres to dispersions of platelets was found to significantly broaden the *I* - *C* coexistence region [12] and to lead to a floating nematic phase sandwiched between two isotropic phases [13]. For suspensions of hard sphero-cylinders it was predicted that the addition of large spheres stabilizes the nematic phase, while the addition of small spheres stabilizes layered phases [14, 15]. Experimentally, a depletant-stabilized layered phase was observed by Adams *et al*. in mixtures of fd-virus and polystyrene spheres [16].

The depletant concentration has a large influence on the phase behaviour. Like for polymeric depletants the *I* – *S* transition was found to supersede the *I* – *N* transition for high depletant concentrations [11, 14, 16]. At even higher depletant concentrations microphase separation [16] as well as kinetically arrested phases do occur [17].

Recent theoretical work describes the effects of the depletion interaction on the phase behaviour of board-like particles [18]. Board-like particles, characterized by three distinct axes with dimensions $L > W > T$, are especially interesting; their shape is in between plates and rods and so is their phase behaviour. N, S as well as C phases have been observed. Additionally, they represent the simplest model for which the rare biaxial nematic phase (N_B) was predicted [19]. Particles in regular uniaxial nematic phases are orientationally ordered in one dimension, rods forming a prolate (N_+) and plates forming an oblate (N_-) nematic phase. In contrast, particles in the N_B phase are aligned along all three directions. The N_B phase can be interpreted as a balanced competition between rod-like (N_+) and plate-like (N_-) behaviour and is therefore predicted for board-like particles with $L/W = W/T$ [20-22]. The theoretical work of Belli *et al*. shows that the addition of a (hard) depletant, which favours N_- ordering, to a system of board-like particles with L/W slightly larger W/T, favouring N_+ competition, induces N_+ - N_- competition. As a consequence the N_B phase is predicted to be stable for a range of depletant concentrations [18].

Goethite board-like particles, known to display N, S and at higher polydispersity C phase separation [23], constitute one the few experimental realizations of the rare N_B and biaxial smectic phase [24, 25]. Unfortunately, the shape of particles is hard to control experimentally and the particles rarely satisfy the $L/W = W/T$ condition [26]. Colloidal goethite particles also have peculiar magnetic properties: a permanent magnetic moment along the L-axis combined with a magnetic easy axis perpendicular to the permanent moment. This makes them highly susceptible to an external magnetic field as they align their long axis parallel to a weak magnetic field, but realign to align their long axis perpendicular to magnetic fields with field strengths above a critical magnetic field strength B^* [27].

In this chapter we present the results of an exploratory study of the influence of a depletant on the phase behaviour of goethite board-like particles. Inspired by the theoretical work of Belli *et al*. [18] -predicting a depletant induced biaxial nematic phase- we chose goethite systems with particle aspect ratio's similar to those of the theoretical system [18]. This theoretical work does not take into account polydispersity -inherent for colloidal systems- which is known to have a significant influence on the stability of the N_B phase [28]. Therefore we use two goethite systems: one with a low (13%) and one with a high (27%) polydispersity. The volume fractions and the size of the added depletant were chosen such as to resemble the theoretical system. The experimental goethite-depletant systems, as well as the sample preparation and the experimental techniques that were used are described in section 3.2. In section 3.3 we present our results, which are then discussed in section 3.4 in the context of theoretical predictions. Finally, in section 3.5 we will conclude and give recommendations for further research.

3.2 Experimental

3.2.1 Goethite synthesis

Two different goethite systems were used: regular goethite (**gr**) and aluminium modified goethite (**ga**), in which part of the iron atoms are substituted with aluminium atoms.

Low polydisperse **gr** was synthesized according to a slightly adjusted version of the forced hydrolysis method described by Krehula *et al*. [29] 25 mL of 25% TMAH (tetramethyl ammonium hydroxide, Aldrich 25% w/w in water) was added, under vigorous stirring, to 70 mL of 0.16 M iron nitrate. The solution was aged at 100 °C for 12 days.

The aluminium modified **ga** particles were obtained by the hydrolysis of iron/aluminium nitrate ($Al(NO_3)_3.9H_2O$, Aldric, 98+%) at high pH similar to the procedure of chromium-modified goethite described in section 2.2.1. 1 M NaOH was added to a 0.1 M aluminium/iron nitrate solution until the pH of the solution was 9. After this, the precipitate was redispersed in dd water and NaOH was added until a pH of 11-12 was reached. Aging took place at 50 °C for 14 days.

The obtained dispersions were washed and stabilized in the same way as described in section 2.2.1.

3.2.2 Goethite characterization

Inductively coupled plasma optical emission spectroscopy (ICPOES) showed that approximately 4.8% of the iron atoms were substituted by aluminium. The aluminium substitution increases the critical magnetic field strength B^*, which was found to be ~450 mT for system **gr** and ~700 mT for system **ga**, but does not have an influence on the phase behaviour.

Particle size distributions were determined with TEM and iTEM imaging software as described in section 2.2.2. For both systems, the length L and width W and their corresponding polydispersities were measured of about 300 particles. T was measured of approximately 20 particles. The particle dimensions found are shown in Table 3.1. Similar to the board-like system described in the paper of Belli *et al*. [18] the goethite particles of both systems have a L/W ratio, which is slightly larger than W/T. The difference in the aspect ratio's between particles from the **gr** and the **ga** system is negligible within the experimental uncertainties.

Table 3.1 Particle dimensions and their polydispersity σ for both goethite systems.

System	$<L>$ (nm)	σ_L (%)	$<W>$ (nm)	σ_W (%)	$<T>$ (nm)
gr	184	13	57	19	~18
ga	183	27	55	28	~17

3.2.3 Sample preparation

Silica spheres were used as a depletant (ludox-cl, 30 wt% in water, Sigma). These spheres have a diameter d = 17 nm and are coated with a layer of aluminium oxide to change the surface charge from negative to positive. The density of the particles is estimated to be 2 g/cm^3 [31]. Goethite dispersions were mixed with the depletant dispersion in different ratios to obtain samples with different goethite and depletant volume fractions (ϕ_g and ϕ_d, respectively). ϕ_g ranges from 4 to 13%, ϕ_d ranges from 0 to 4.8%. The silica dispersion as obtained from the supplier has an unknown salt concentration. For the **ga**-depletant samples the silica dispersion was washed three times with slightly acidified (with HNO_3) mp water. It is assumed that the salt concentration is determined solely by the H^+ and NO_3^- ions. The Debye length is then 10 nm at most. For the **gr**-depletant samples the silica dispersion was washed once. Therefore, some additional salt might be present in these samples. All dispersions had a pH of 3.

Flat glass capillaries (Vitrocom, W3520-100 and W3510-100) were filled with the different goethite-depletant dispersions. The capillaries were flame-sealed and stored in upright position to assure the formation of a density gradient.

3.2.4 Small angle x-ray scattering

SAXS patterns were collected using the microradian diffraction set up [32] at the BM26 DUBBLE beamline [33] of the European Synchrotron Radiation Facility (ESRF, Grenoble, France). A photon energy of 12 keV was used, with a sample-detector distance of ~7 m. Patterns were collected using three different two-dimensional x-ray CCD-based detectors with a pixel size of 9, 22 (both Photonic Science) and 172 μm (Pilatus). Two homemade variable permanent magnets were used to apply magnetic fields parallel and perpendicular to the x-ray beam. By changing the distance between the poles, the field strength could be varied from 3 to ~700 mT for both magnets. The x-ray beam was estimated to have a cross-section of about 500 μm at the sample. Patterns were collected in the middle of the capillary and at different heights along the vertical (y) direction using a motorized translational stage.

3.3 Results

Using SAXS we studied the influence of a depletant on the phase behaviour of the two different goethite systems: system **gr** with a polydispersity of 13%, and system **ga** with a polydispersity of 27%. In order to properly investigate the influence of the added depletant, we first characterized the phase behaviour of the bare dispersions. This is discussed in section 3.3.1. The results of the dispersions with added depletant are described in section 3.3.2. In section 3.4 we will then discuss our results and compare them to other theoretical and experimental work.

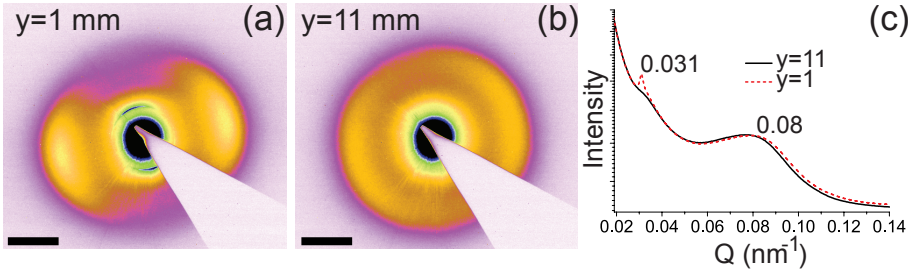

Fig. 3.1 SAXS patterns (a, b) and corresponding peak profiles (c) taken in a one month old **gr** sample with ϕ_g = 12% 1 mm above the bottom of the capillary (y = 1) and 11 mm above the bottom of the capillary (y = 11). The black bars denote 0.05 nm^{-1}. The peak profiles are taken of the entire scattering patterns.

3.3.1 Phase behaviour without depletant

*System **gr***

SAXS patterns taken in a sample with a goethite volume fraction (ϕ_g) of 12% are shown in Fig. 3.1. The sample was allowed to sediment for a month before the SAXS measurements were performed. The pattern taken at the bottom of the capillary (Fig. 3.1(a)) shows an intense and sharp reflection at Q = 0.031 nm^{-1} combined with a weak and diffuse reflection at Q = 0.08 nm^{-1}, characteristic of the smectic phase. The reflections, corresponding to real space values of 203 and 79 nm, originate from the smectic interlayer periodicity and the liquid interactions within the layers, respectively. Fig. 3.1(b) shows the pattern that was taken 11 mm higher in the sample. Also here the diffuse reflection at 0.08 nm^{-1} originating from the shortest particle dimensions can be observed. Additionally, another diffuse reflection can be observed at Q = 0.032 nm^{-1}. This characterizes the liquid crystal phase present as the nematic phase. The weak reflection at short Q originates from positional correlations of the longest particle dimension. However, the reflection is too weak and too diffuse to originate from a smectic phase. The presence of these positional correlations indicates that this nematic phase is close to the *N* - *S* interface and thus on the verge of becoming a smectic phase.

The nematic phase present appears to be a prolate uniaxial nematic phase (N_+) as only one reflection of the liquid-like interaction between particles within the layers was observed. Additionally, this diffuse reflection corresponds to a real space value of 79 nm. This is too small to originate from correlations of solely the *W*-dimension of the particles (57 nm) taking into account the Debye length (~10 nm) and the fact that within the layer -where the particles only possess orientational order- the spacing between the particles is large. It therefore appears that this reflection originates from correlations from both the particles' *W* and *T* dimensions. This indicates that the particles can freely rotate around their long axis which is characteristic of the N_+ phase.

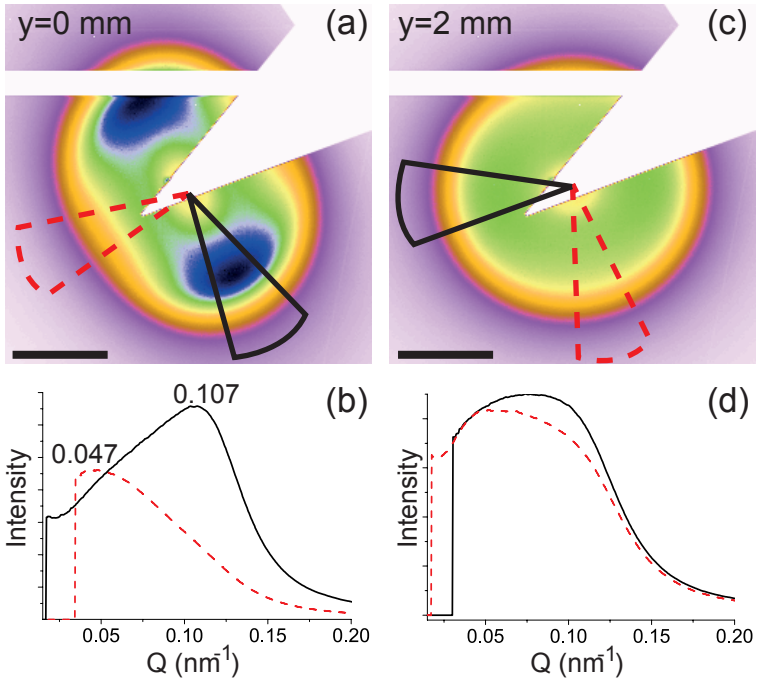

Fig. 3.2 SAXS patterns and their corresponding peak profiles taken in a six months old **ga** sample with ϕ_g = 7% at the bottom of the capillary (a, b) and 2 mm above the bottom of the capillary (c, d). Solid and dashed lines in (a) and (c) indicate the regions of which I(Q) profiles were taken. The white horizontal bars in the SAXS patterns are an artefact of the detector. The black bars denote 0.1 nm^{-1}.

*System **ga***

SAXS patterns taken in a **ga** sample with a goethite volume fraction of 7% are shown in Fig. 3.2. The sample was six months old at the time of measuring. The SAXS patterns show only diffuse reflections characteristic of the nematic phase. This can be attributed to the high polydispersity of the **ga** particles, which can inhibit positional ordering, especially on short (~months) timescales [34, 35]. The SAXS pattern taken at the bottom of the capillary (y = 0 mm, Fig. 3.2(a, b)) is highly anisotropic and displays two broad reflections in orthogonal directions at $Q_W \approx 0.047$ nm^{-1} and $Q_T \approx 0.107$ nm^{-1}. These reflections originate from correlations of the W and T particle dimensions; the ratio between Q_W and Q_T is 2.3 which closely matches the W/T ratio taken into account the Debye length (~10 nm). This indicates that the liquid crystal phase present is the biaxial nematic phase (N_B) [24].

The pattern shown in Fig. 3.2(c) is taken 2 mm above the bottom of the capillary (y = 2 mm). Also this pattern is anisotropic, but the effect is significantly less than at y = 0 mm. The I(Q) profiles taken in orthogonal directions (Fig. 3.2(d)) only vary slightly. In both directions a very broad peak consisting of reflections from correla-

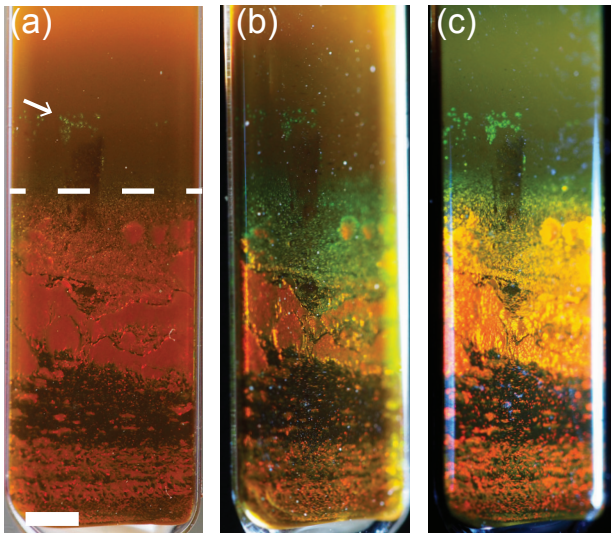

Fig. 3.3 (a) Typical photograph of a capillary containing a goethite-depletant dispersion (**gr** with ϕ_d = 3.7 and ϕ_g = 8.5%). (b) and (c) show the Bragg reflections in the capillary which are visible under illumination -under different angles- with white light. The white bar denotes 1 mm, the dashed white line indicates the transition from the *I* - *S*. The arrow points to small *S* domains nucleated on the capillary wall.

tions of both the *W* and *T* particle dimensions can be observed. In one direction the contribution from the *T* particle dimension is higher (solid line), whereas in the other direction the contribution from the *W* particle dimension is higher (dashed line). This means that the biaxial ordering is very weak. The phase resembles the prolate uniaxial nematic phase, which would display only one reflection around 0.08 nm^{-1}, as was observed for the **gr** system.

It is quite remarkable that the **ga** system, which has practically the same particle dimensions as the **gr** system, forms a N_B phase, while the **gr** system does not. This can be attributed to the higher polydispersity of the **ga** system. Belli *et al*. [28] theoretically predicted that polydispersity stabilizes the N_B phase because it induces N_- - N_+ competition. Our experimental findings confirm this theoretical prediction.

3.3.2 Phase behaviour with added depletant

*System **gr***

Using SAXS we studied the influence of a depletant by characterizing the phase behaviour in several samples with different depletant concentrations (ϕ_d = 1.2, 2.2, 2.8, 3.7 and 4.8%). The SAXS-patterns revealed *I* - *S* phase separation in all samples. Remarkably, the *N* phase, which was observed for the system without depletant and is predicted by Belli *et al*. [18], was not observed. Also optical observations indicated *I* – *S* phase separation. Fig. 3.3(a) shows a typical picture of a sample containing

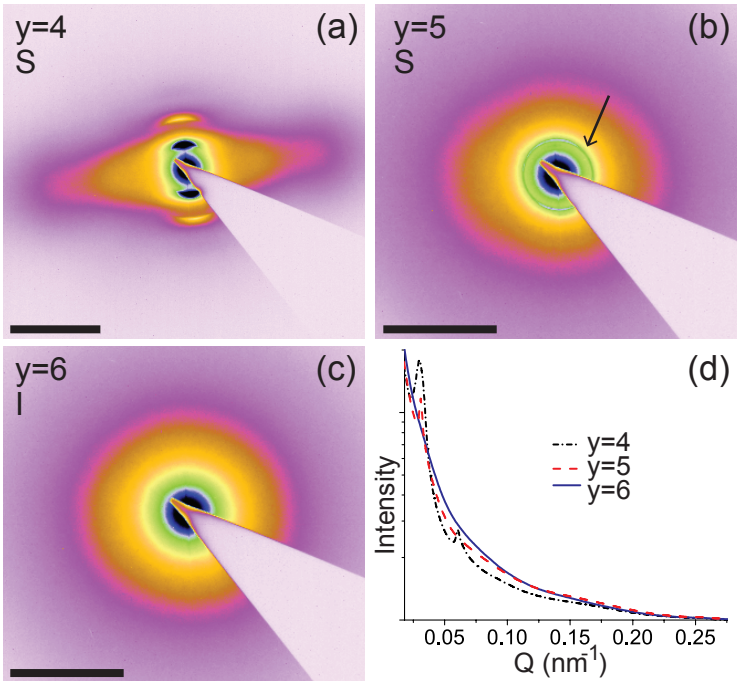

Fig. 3.4 SAXS patterns taken in a **gr** sample with ϕ_d = 3.7% and ϕ_g = 7.1% at different heights in the capillary: y = 4 (a), 5 (b) and 6 mm (c) from the bottom of the capillary. The arrow in (b) points to the reflection of the smectic interlayer periodicity. The black bars denote 0.1nm^{-1}. The peak profiles shown in (d) are averaged over all angles of the scattering patterns.

a goethite-depletant mixture (ϕ_d = 3.7 and ϕ_g = 8.5%). An isotropic phase on top of a 6.5 mm high sediment can be observed. Upon illuminating the sample with white light beautiful Bragg reflections can be observed (Fig. 3.3(b)), of which the color changes with the angle of the incident light (Fig. 3.3(c)). These reflections are characteristic of a positionally ordered -smectic or columnar- phase. The goethite particles in the **gr** system have a low polydispersity which excludes the *C* phase [23]. The Bragg reflections can be observed throughout the sediment which indicates that the entire sediment is *S*. The arrow in Fig. 3.3(a) points to small areas in the *I* phase in which Bragg reflections can be observed. These are most likely small *S* domains which nucleated on the capillary wall. Using SAXS we characterized the LC phases in detail. Below we present and discuss typical SAXS patterns of several **gr** samples.

Fig. 3.4 shows three SAXS patterns taken at different heights in a sample with a goethite volume fraction of 7.1, and a depletant volume fraction of 3.7%. The sample was allowed to sediment for eight months before SAXS patterns were taken. Both SAXS patterns taken in the 5 mm high sediment, at y = 4 and 5 mm, respectively (Fig. 3.4(a, b)), show that the system has indeed formed a smectic phase: (in-

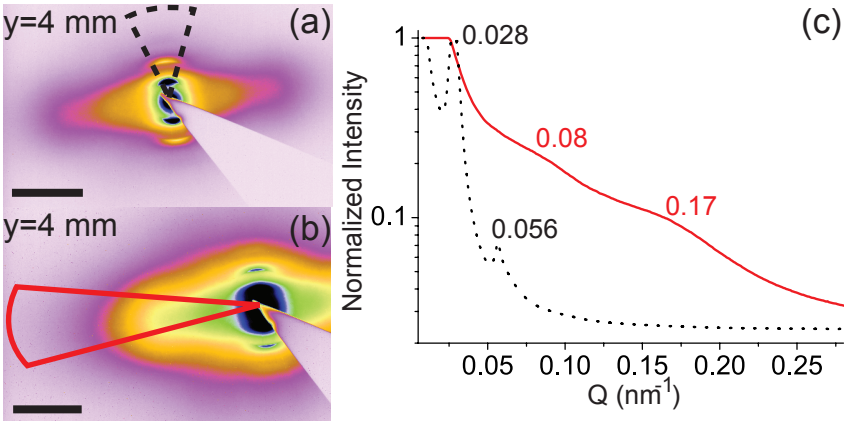

Fig. 3.5 SAXS patterns taken in a **gr** sample with ϕ_d = 3.7% and ϕ_g = 7.1% at y = 4 mm with a normal exposure time (a) and with a higher exposure time (b) and their corresponding I(Q) profiles (c). The black dashed and grey solid lines in (a) and (b) indicate the sections of the patterns of which the I(Q) profiles were taken. The black bars denote 0.1 nm^{-1}.

tense) sharp reflections originating from the interlayer periodicity can be seen at low Q. For the pattern taken at y = 4 mm (Fig. 3.4(a)) these reflections can even be observed up to the 2nd order. Diffuse and very weak reflections of the liquid-like order within the layers can be observed at higher Q-values. The SAXS pattern taken at the top layer of the smectic sediment (Fig. 3.4(b)) shows smectic reflections in all directions, indicating that multiple *S* domains are present. The main part of the smectic phase is a single smectic domain, like the pattern shown in Fig. 3.1(a).

The pattern taken directly above the sediment (Fig. 3.4(c, d)) does not show any reflections; only a steep decrease in intensity can be observed. This pattern corresponds to an isotropic phase. This confirms that the entire sediment is smectic; the *N* phase was not observed. The *I* – *S* phase separation is remarkable as the bare system also displayed, even five years after sample preparation, a *N* phase. Additionally, this goethite-depletant sample has a relatively low ϕ_g of 7.1%. In dispersions with lower volume fractions it generally takes more time for positionally ordered phases to develop [36].

The sample was studied in detail to obtain more information about the character of the *S* phase. Therefore SAXS-patterns were taken with higher exposure times to reveal the liquid-like intra-layer reflections. The patterns and corresponding peak profiles are shown in Fig. 3.5. The peak of the smectic inter-layer reflection is at Q = 0.028 nm^{-1}, with a second order peak at 0.056 nm^{-1}. This corresponds to a smectic periodicity of ~224 nm. Highly interesting is the peak profile of the liquid reflections (Fig. 3.5(c), solid line). In a regular smectic phase the particles within the layer are orientationally ordered in one dimension only; the particles can still freely rotate around their long axis. Therefore one correlation peak is expected, originating from correlations of the average of the *W* and *T* particle dimensions [23, 37].

However, in this sample the SAXS pattern displays two weak diffuse reflections at Q ≈ 0.08 (~79 nm) and 0.17 nm^{-1} (37 nm). The aspect ratio between these two reflections is ~2.1 which agrees with the ratio between the *W* and *T* particle dimensions (57 and 18 nm, respectively) taken the Debye length into account. The reflections therefore seem to originate from the particle width and thickness. Similar peaks are observed in biaxial (smectic) phases [24] and this suggests that the particles in the depletant induced smectic phase may be biaxially ordered. However, the peaks are very weak. Additionally, the fact that both reflections are observed in the same pattern points to the presence of multiple domains.

A general way to be conclusive about the biaxiality of a smectic phase is by realigning the smectic phase using a small magnetic field applied parallel to the direction of the x-ray beam. The particles align their long axis parallel to field, hence the smectic layers will then orient perpendicular to the x-ray beam. The liquid reflections originating from the two shortest particle dimensions are then revealed and can carefully be studied [24]. This was also tried for this sample. Normally, a magnetic field strength of ~60 mT is sufficient to realign the smectic phase. However, the smectic phase in this sample did not respond to magnetic fields with field strengths up to 380 mT, which is the maximum field strength that could be tried without going above the critical field strength. It appears that the addition of a depletant makes the system dense and highly viscous and therefore rather unresponsive to an external magnetic field.

The measurements were therefore repeated on a younger sample with a lower depletant density. The sample had a depletant volume fraction ϕ_d of 1.2%, a goethite volume fraction ϕ_g of 8.5% and was allowed to sediment for 1.5 months. The top row in Fig. 3.6 shows SAXS patterns taken at four different heights in the capillary, at y = 0.2, 1, 1.5 and 1.8 mm, measured before a magnetic field was applied. The patterns reveal a 1.5 mm high, single-domain, smectic sediment. The pattern at y = 1.8 mm originates from the isotropic phase, hence again the *N* phase was not observed. The second row in Fig. 3.6 shows SAXS patterns taken while a magnetic field of 15 mT was applied in the direction perpendicular to the x-ray beam. Normally goethite particles will align their long axis in a weak field, hence the smectic reflections are expected to be along the direction of the magnetic field. From the patterns it appears that only the very top layer of the sediment responded to the field as is illustrated by the arrow in Fig. 3.6, which points to the weak reflection found along the field. The main part of the smectic domain retains its original position. The SAXS patterns taken lower in the sediment did not change after applying the field, indicating that the particles in the smectic phase did not realign.

The third and the fourth row in Fig. 3.6 show the patterns taken in the sample after having been in a 100 mT magnetic field, which was first oriented perpendicular to the x-ray beam (3rd row) and finally parallel to the x-ray beam (4th row). For both cases the sample had been in the field for ~24 hours at the moment the SAXS patterns were taken. In the perpendicular field, the main part of the sediment has

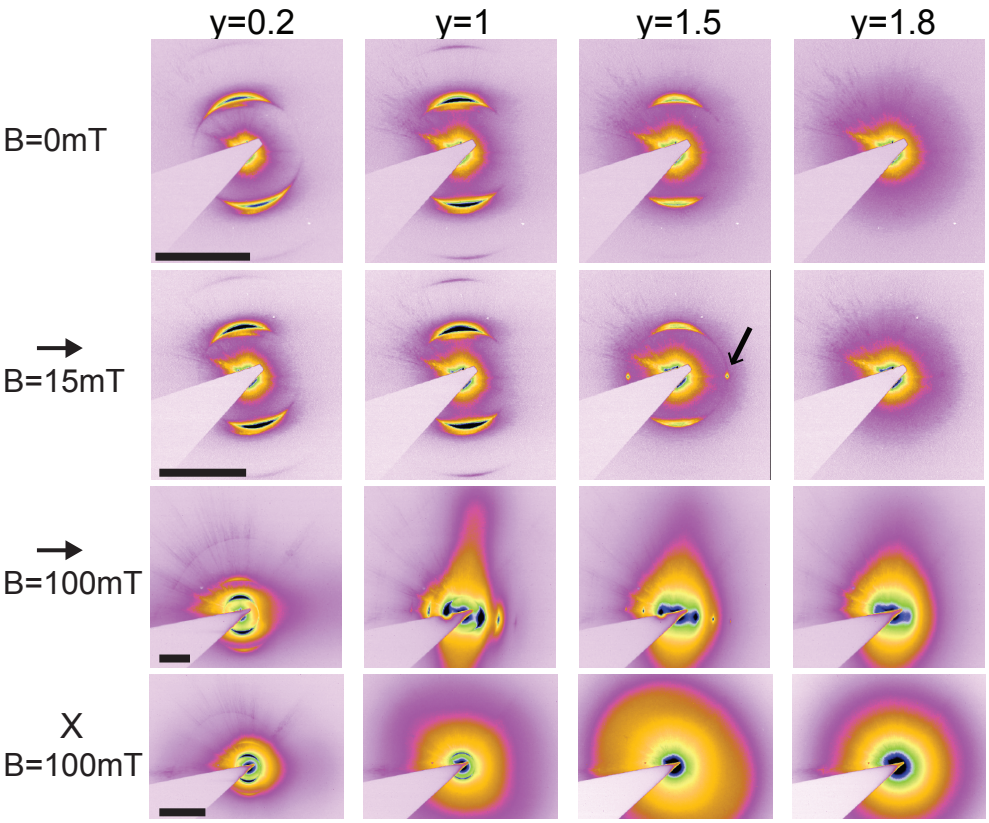

Fig. 3.6 SAXS patterns taken at four different heights in a 1.5 months old **gr** sample with ϕ_g = 8.5% and ϕ_d = 1.2% without a magnetic field (top row), in magnetic fields directed perpendicular to the x-ray beam of 15 and 100 mT (2nd and 3rd row, respectively) and in a 100 mT magnetic field which was oriented parallel to the x-ray beam (bottom row). The black bars denote 0.05 nm^{-1}.

reoriented in the field. Only the very bottom part of the sediment retains its original position. In the parallel magnetic field, again only the top ~0.5 mm of the sediment has completely realigned.

For the small part of the sediment that did align in the magnetic field the possible biaxiality of the smectic phase was studied for both directions of the magnetic field. Fig. 3.7(a, b) show the SAXS patterns taken at y = 1 and 1.5 mm in a 100 mT field directed perpendicular to the x-ray beam, respectively. The accompanying peak profiles (Fig. 3.7(c, d)) reveal that the smectic reflections are found at similar Q-values as found for the samples with ϕ_d = 3.7% (Fig. 3.4, Fig. 3.5). Additionally, two liquid reflections can be observed in the pattern taken at y = 1 mm at similar Q-values. This again reminds of biaxial ordering. However, the peaks are very weak. The pattern shown in Fig. 3.7(d) taken at y = 1.5 mm only shows one liquid

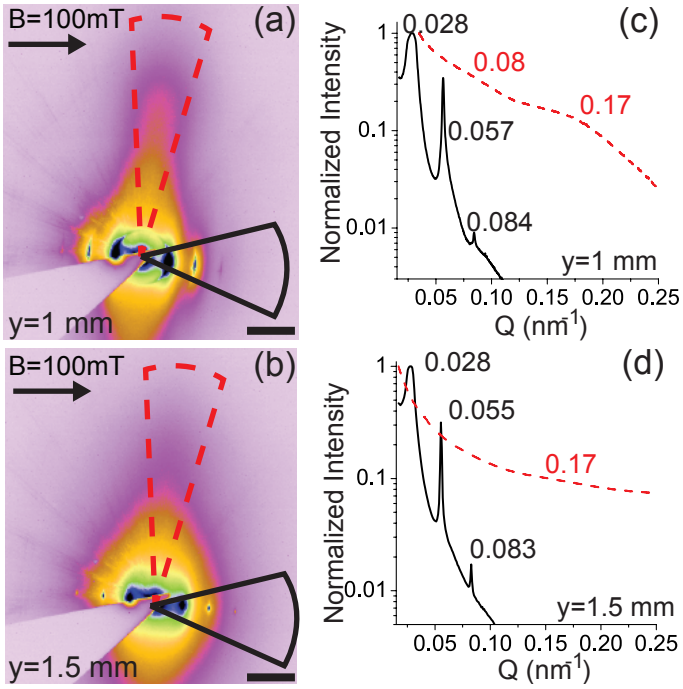

Fig. 3.7 SAXS patterns taken at y = 1 and 1.5 mm ((a), (b) respectively) in a 1.5 months old **gr** sample with ϕ_g = 8.5% and ϕ_d = 1.2% in a 100 mT magnetic field directed perpendicular to the x-ray beam. The black bars denote 0.05 nm^{-1}. The accompanying I(Q) profiles are shown in (c) (y = 1 mm) and (d) (y = 1.5 mm). The dashed and solid lines in (a) and (b) indicate the sections of the patterns of which the I(Q) profiles were taken.

reflection at Q = 0.17 nm^{-1}. This originates from correlations of the shortest particle dimension (*T*). Reflections originating from the *W*-dimension are not observed. This means that reflections of *L* and *T* are observed in orthogonal directions, which is characteristic of a single biaxial smectic domain. However, again the reflection originating from the liquid-like interactions is extremely weak and it is therefore not conclusive that this reflection originates from a biaxial phase. Fig. 3.8(a) shows the SAXS pattern taken at y = 1.5 mm in a magnetic field of 100 mT directed parallel to the x-ray beam. The pattern is asymmetric. The corresponding I(Q) profiles (Fig. 3.8(b)), taken in orthogonal directions, reveal one reflection at Q = 0.17 nm^{-1}, originating from *T*, in the horizontal direction. However in the vertical direction, reflections of correlations of both *W* and *T* can be observed. For a true biaxial smectic phase only the reflection of *W* would have been expected in this direction [24]. The azimuthal profiles of the scattering intensity are plotted along two circles at fixed Q -at Q_T = 0.17 and at Q_W = 0.08 nm^{-1}- are shown in (Fig. 3.8(c)). It is clear that the correlation peak of *T* has two maxima spaced ~180°. For a true biaxial phase one would expect the correlation peaks of *W* spaced ~180 degrees, with its maxima

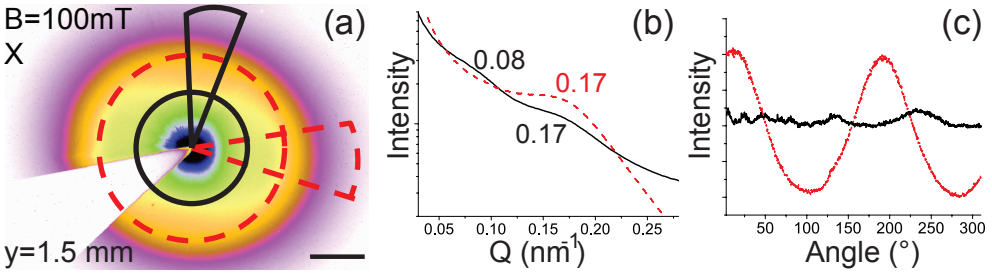

Fig. 3.8 (a) SAXS pattern taken at y = 1.5 mm in a 1.5 months old gr sample with ϕ_g = 8.5% and ϕ_d = 1.2% in a 100 mT magnetic field directed parallel to the x-ray beam. The wedge shaped lines indicate the areas of which the I(Q) profiles shown in (b) were taken. De circular lines indicate the Q-distances at which the azimuthal profiles shown in (c) were taken. The black bar denotes 0.1 nm^{-1}.

exactly in between the *T* correlation peaks. However, here the correlation peaks of *W* are weak and are very noisy. Recently, we observed that biaxiality decreases in an increasing magnetic field (see Chapter 4 and ref. [38]). This effect was found to be strongest for lower volume fractions. This effect might be observed here. We can however not be conclusive since the smectic phase in these systems cannot be aligned with a weaker magnetic field.

Comparing the found Q-values for the smectic inter- and intralayer reflections to the values found for the bare **gr** system gives valuable information about the influence of the depletant. The liquid intra-layer reflections for the depletant induced (biaxial) smectic phase are found at significantly higher Q-values; 0.17 nm^{-1} for *T* and 0.08 nm^{-1} for *W*, while for the sample without depletant, the uniaxial reflection originating from correlations of both *W* and *T* was found to be Q_{WT} = 0.08 nm^{-1} (Fig. 3.1). This indicates that the attraction induced by the depletant reduces the distance between the particles within the layer.

The smectic periodicity however, was found to be significantly larger for the samples with depletant. In combination with the decrease in particle distance within the layers, this suggests that the depletant particles are expelled from the layers and might now be located in between the smectic layers.

In summary, the addition of a depletant induces the smectic phase, thereby suppressing the nematic phase. The diffuse reflections originating from the liquid-like interaction within the layers are clearly not originating from an ordinary smectic phase. The reflections remind of biaxial ordering, however we cannot be conclusive. The smectic phase formed in the goethite-depletant dispersions is highly viscous and therefore rather unresponsive to external fields, even for the lowest depletant volume fraction of 1.2%. It appears that the depletion-induced attraction between the goethite particles is strong.

The original **gr** system without depletant already has a strong tendency to form

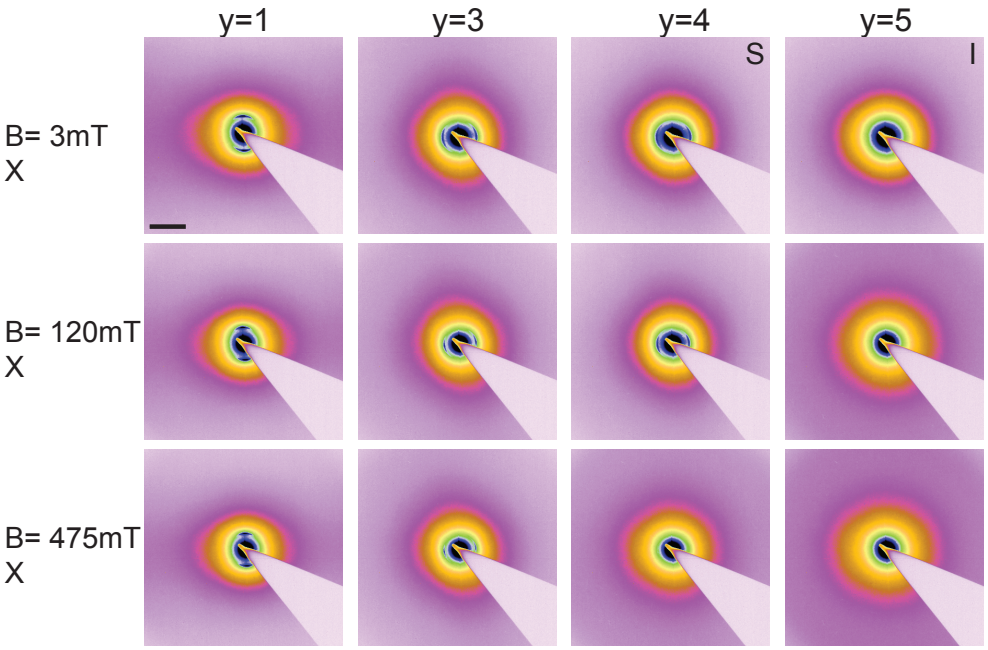

Fig. 3.9 SAXS patterns taken in a four months old **ga** sample with ϕ_d = 4.5% and ϕ_g = 6.0% at four different heights in the capillary (y = 1, 3, 4 and 5 mm) in a very weak magnetic field of 3 mT (top row) and in magnetic fields of 120 and 475 mT (middle and bottom rows, respectively). The magnetic field was applied in the direction parallel to the x-ray beam. The black bar denotes 0.05 nm^{-1}.

a smectic phase. Therefore the effects of adding a depletant were additionally studied for system **ga**, which has comparable dimensions but due to its high polydispersity only forms a (biaxial) nematic phase on a timescale of years.

*System **ga***

The phase behaviour of system **ga** with respectively 1, 2, 3, and 4.5 v/v% depletant was characterized in a similar way as system **gr** and the (SAXS) results are presented in this section. Similar to the **gr** system again only an *I* - *S* phase separation was observed, independent of the depletant volume fraction.

This is demonstrated by the SAXS patterns shown in the top row of Fig. 3.9 for a four months old sample with ϕ_d = 4.5 % and ϕ_g = 6.0 %. All patterns taken in the 4 mm high sediment reveal sharp and intense reflections at short Q originating from the smectic interlayer periodicity. Higher order peaks, characteristic of the *S* phase, are not observed but the accompanying I(Q) profiles (Fig. 3.10(c)) clearly show strong sharp reflections at low Q combined with very weak and broad reflections originating from the liquid-like intralayer interactions at high Q. This confirms that the liquid crystal phase present is smectic; for a *N* phase both reflections would be

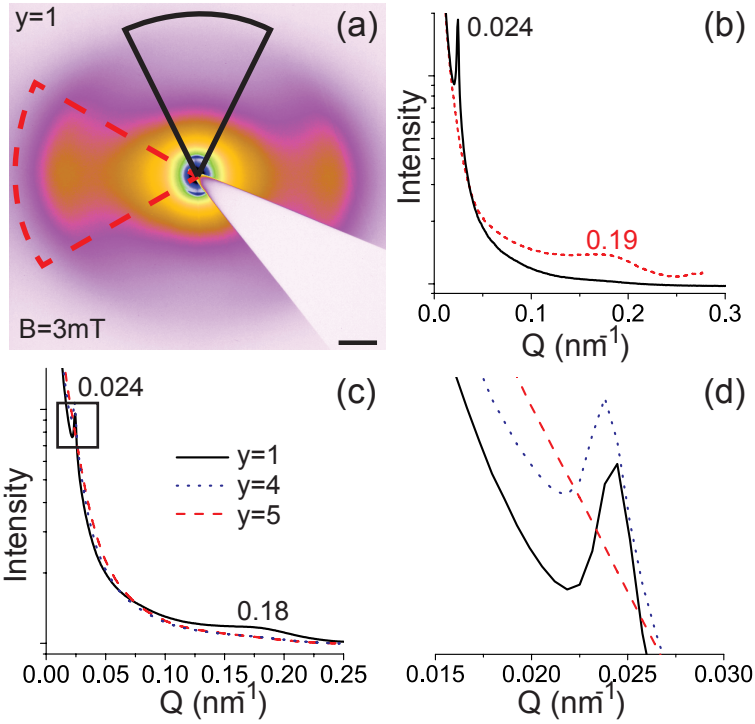

Fig. 3.10 (a) SAXS pattern taken at y = 1 mm in a four months old ga sample with ϕ_d = 4.5% and ϕ_g = 6.0% in a weak magnetic field of 3 mT. The magnetic field was applied in the direction parallel to the x-ray beam. The wedge shaped lines indicate the areas of the patterns of which the I(Q) profiles shown in (b) were taken. The black bar denotes 0.05 nm^{-1}. (c) I(Q) profiles averaged over all angles of the SAXS patterns taken at three different heights, y = 1, 4 and 5 mm in the capillary. A zoom of the area in the square is shown in (d).

broad and of the same order of intensity, with the reflection at high Q stronger than the reflection at low Q. It is quite remarkable that *I* - *S* phase separation is observed, since the bare **ga** system did not form a smectic phase on the timescale of years. Here, we observed *I* - *S* phase separation on a timescale of months. The plots in Fig. 3.10(c) reflect that the smectic phase is formed on a short timescale. Normally, in polydisperse systems like the **ga** system the smectic interlayer periodicity depends on the height in the capillary due to fractionation [23, 35]. However, in this system the change in peak position of the interlayer periodicity at short Q is negligible (Fig. 3.10(d)). The fast formation of the smectic phase might also explain the absence of higher order peaks for the smectic periodicity: individual layers will contain polydisperse particles which frustrates the positional order between smectic layers.

Again, it was tried to realign the smectic phase using an external magnetic field to study the character of the smectic phase more carefully. The SAXS patterns in the second and third row in Fig. 3.9 are taken in a parallel magnetic field of 120 and

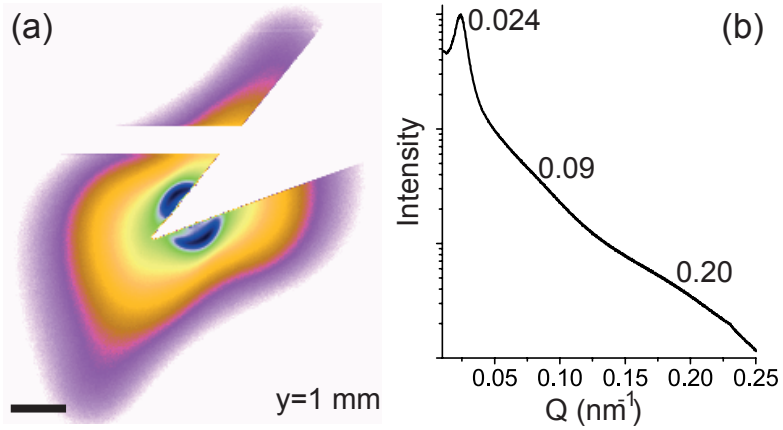

Fig. 3.11 (a) SAXS pattern taken at y = 1 mm in a **ga** sample with ϕ_d = 1.2% and ϕ_g = 11.0% and (b) its accompanying I(Q) profile (averaged over all angles of the scattering pattern). The black bar denotes 0.05 nm^{-1}.

475 mT, respectively. Like for the **gr**-depletant system, the smectic phase is rather unresponsive; only the very top layer of the smectic sediment reorients in a (rather) strong field of 475 mT. Also for a sample with a lower depletant volume fraction of 1.2 %, the sediment was unresponsive up to a field strength of 160 mT.

Despite the poor response to an external magnetic field, also here it was tried to determine the character of the smectic phase. Fig. 3.10(a, b) shows the SAXS pattern taken at y = 1 mm and the accompanying I(Q) profiles. The plot shows a sharp and strong peak at Q = 0.024 nm^{-1} and a very weak and broad reflection at Q = 0.18 nm^{-1}. In another (6 months old) sample, with ϕ_g = 11%, ϕ_d = 1.2%, the SAXS pattern (Fig. 3.11) reveals a sharp and strong reflection at Q = 0.024 nm^{-1} as well. However, here two very weak and diffuse reflections originating from the liquid-like interactions within the layers can be observed at Q = 0.09 and 0.20 nm^{-1}. The ratio between these two values ($Q_W/Q_T \approx 2.22$) suggests that the reflection observed around Q ≈ 0.09 nm^{-1} originates from correlations from the *W* particle dimension, while the reflection around Q ≈ 0.19 nm^{-1} originates from correlations of *T*. Like for the **gr** system, these reflections remind of a biaxial smectic phase. But again, these patterns alone are not fully conclusive and the systems are too viscous to align in a weak magnetic field.

The reflections of the particles within the smectic layers are often found at approximately similar Q-values as the reflections of the *N* phase [24]. Like for the **gr** system, also here the intra-layer reflections appear to be at considerably higher Q-values than in the systems without depletant (Fig. 3.2), again indicating that the depletion induced attraction reduces the distance between the particles within the layer. The reflection of the smectic periodicity found at Q = 0.024 nm^{-1} in both samples corresponds to a real space value of 262 nm and originates from the smectic interlayer periodicity. This value is significantly larger than the particle length

(183 nm) + the Debye length. It again appears that the spherical depletant particles might be located in between the smectic layers.

It is noteworthy to mention that while the particles from the **gr** and **ga** systems have practically the same dimensions, the smectic period is significantly larger for the **ga**-depletant system than for the **gr**-depletant systems. This can be attributed to the high polydispersity of this system in combination with the fast formation of the *S* phase, which inhibits fractionation.

3.4 Discussion

Our experimental results show that the addition of a depletant, in the concentration regime of ~1 – 5 v/v%, to a system of goethite board-like particles induces the formation of a smectic phase while the formation of the nematic phase is suppressed. This is quite remarkable: for the comparable theoretical system with similar particle and depletant dimensions and concentrations, stable N_B phases were predicted for depletant volume fractions up to at least 6% [18]. The theoretical work mentions that the nematic phase becomes unstable in favour of the smectic phase at higher depletant densities [18], something that is also generally observed for rod-depletant systems [11, 16, 39]. Our experimental observation of the immediate formation of smectic phase in favour of the nematic phase indicates that our system already is in the high depletant density limit. It therefore seems as if the theory underestimates the strength of the depletion-induced attraction between the board-like particles. Theoretical restrictions regarding e.g. polydispersity, which is inherent for colloidal particles, charge and possible particle orientations are inevitable. The discrepancy between our experimental results and this theoretical work again demonstrates the challenge of a quantitative comparison between theory and experiment [10].

A general trend is observed upon comparing the inter-particle distances found in our goethite-depletant system with the bare goethite systems: the distance between the particles within the smectic layers decreases while the distances between particles in adjacent layers, and thus the distance between the smectic layers, increases. Adams *et al*. [16] reported microphase separation in a system of fd-virus and small polystyrene spheres into a 'lamellar' phase, which consist of layers of aligned rods alternating with layers of spheres. Similarly, Kleshchanok *et al*. reported that in a *C* phase, formed in a platelet-sphere mixture, the depletant particles are located in between the columnar stacks [12]. We observed that, while the addition of a depletant induces attraction between the particles, the smectic layer distance increases. The observed increase was found to be larger than the sphere diameter. This suggests that also in the depletant-induced smectic phase formed in our systems the depletant might be located in between the smectic layers, similar to the 'lamellar' phase described by Adams *et al*. [14, 16]. This layered phase is predicted [13] for depletant concentrations higher than concentrations at which a miscible, nematic

phase is formed. This again suggests that the depletant volume fractions used in our work are too high for stable nematic phases to be formed.

While the theoretically predicted N_B was not observed, we did observe remarkable SAXS reflections from the particles within the layers that remind of biaxial peaks. In a regular smectic phase the particles in the layers are only ordered along their long axes and hence one perpendicular reflection, originating from both the *W* and *T* dimensions of the particles, is expected [23, 37, 40]. Here we either observed two peaks at different Q-values, or we observed one peak at a high Q-value. In the former the reflections are presumed to originate from correlations of *W* and *T*, respectively, like was previously observed for a biaxial smectic phase [24]. In the latter the peak was observed at such a high Q-value that it can only originate from correlations of solely *T*. Also this suggests biaxiality. Although the smectic phase observed in our systems clearly is not a regular uniaxial smectic, we cannot be fully conclusive about the possible biaxial ordering of the particles within the layers. The smectic phases are unresponsive to (weak) external magnetic fields and the ordering within the layers can therefore not fully be characterized.

Noteworthy to mention is the type of smectic phase that is formed in the ga-depletant system. Belli *et al*. [18] predict that the addition of a depletant to a system of elongated board-like particles can induce the formation of a N_B phase. Elongated board-like particles favour N_+ ordering, while the depletion interaction favours N_- ordering. It is clear that in our experimental system the depletant effects are strong and thus the depletant concentration is too high. The bare **ga** system already spontaneously formed a N_B phase. Upon addition of a depletant, theory then predicts the formation of a N_- phase, and at higher depletant/goethite volume fraction a smectic phase in which the particles in the smectic layers are aligned along their *T*-axis. However, we clearly observe a smectic layer periodicity corresponding to the particles longest axis. Additionally we have indications that particles within the layers are biaxially ordered. The discrepancy between the theoretical predictions and the experimental results can be understood by the fact that the positionally-ordered smectic phase is not properly included in the density-functional model described in ref. [18]. Moreover, it seems that the depletion attraction in the experiment is too high to observe the predictions of the theory. We therefore provide an order-of-magnitude estimate of the depletion attraction below.

Around each goethite particle there is a volume the depletant cannot penetrate: the excluded volume. It is entropically favourable to minimize the total excluded volume. This happens when the particles are in close proximity such that their excluded volumes overlap [9]. The volume available for the depletant will increase by the amount of the overlap volume ΔV. This leads to an increase in entropy and accordingly the depletion interaction reduces the free energy of the system by u_{depl} satisfying

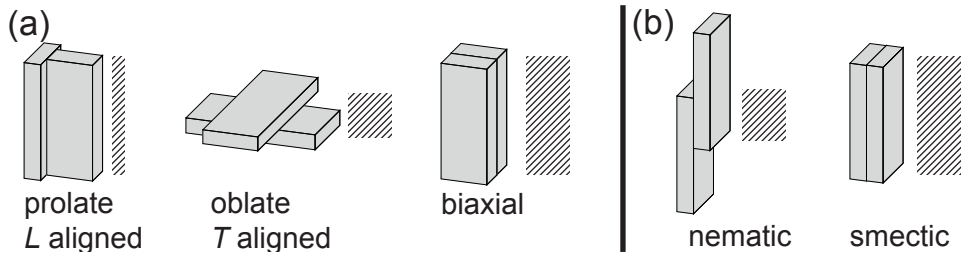

Fig. 3.12 Simplified schematic drawings illustrating two neighbouring particles and their corresponding overlap volumes (striped areas) that are (a) prolate, oblate or biaxially ordered. The same is shown in (b) but now for two neighbouring particles in the nematic and smectic phase.

$$\frac{u_{depl}}{k_B T} = -\phi_d \frac{\Delta V}{v_d}, \tag{3.1}$$

where k_B is the Boltzmann constant, T is temperature, $v_d = (\pi/6)(d)^3$ the volume of a depletant particle and ΔV the overlap volume. For the scenario's sketched in Fig. 3.12(a) we define ΔV as L x T x d, W x W x d, L x W x d, for prolate, oblate and biaxial ordering respectively. It follows from Eq. (3.1) that the most favourable particle orientation is the orientation which has the largest ΔV. It is schematically demonstrated in Fig. 3.12(a) that for this reason biaxial ordering is favoured over oblate and prolate ordering. Likewise, Fig. 3.12(b) illustrates that smectic layering is preferred over nematic alignment.

Using Eq. (3.1) we find for $\phi_d = 2\%$ that u_{depl} is -0.4 $k_B T$ for both prolate and oblate ordering and -1.4 $k_B T$ for biaxial ordering. This means that already for one of the lowest ϕ_d used in this research biaxial ordering is favoured by $\sim$1 $k_B T$, which is substantial enough for the particles to have a significant preference for biaxial ordering. Similar motivations hold for the preference of S over N ordering (Fig. 3.12(b)). The most favourable orientation is when the particles are stacked face-to-face. It is noteworthy to mention that Eq. (3.1) assumes ideal depletants. Asakura & Oosawa [41], as well as Walz and co-workers [42], calculated that the depletion interaction is greatly intensified when the depletants are charged, which is the case in our systems. It is therefore likely that the values calculated above for u_{depl} are underestimated.

The values above are calculated on a two-particle level and are meant to give an indication instead of representing the full 3-dimensional multi-particle system. However, pair-wise interactions play a large role compared to multi-body interactions in the formation dynamics of liquid crystals and the values found here are therefore relevant.

This depletion interaction is not high enough to induce bulk phase separation into a depletant rich and a goethite rich phase. For similar reasons as described above it can be understood that the depletant particles are located mostly in be-

tween the smectic layers as the loss in u_{depl} is smallest for the *W*/*T* faces of the particles. Additionally, the length polydispersity leaves room for the depletant particles to fit in between the layers [16].

3.5 Conclusions & Outlook

In this paper we present the results of an exploratory study on the influence of the depletion interaction on goethite phase behaviour. We added a depletant to a goethite system that spontaneously displays *I* - *N* - *S* phase separation, as well as to a goethite system that without depletant displays *I* - N_B phase separation. Using SAXS we found *I* – *S* phase separation for both systems. The addition of a depletant induces the formation of the smectic phase, while the formation of the nematic phase is suppressed. The depletion induced attraction decreases the particle spacing within the layers, while the interlayer periodicity increases. This suggests that the depletant induced microphase separation: the depletant particles are expelled from the layers and are subsequently located in between the layers of goethite particles.

Our results indicate extraordinary orientational ordering of the particles within the layers. From SAXS the particle ordering reminds of biaxial ordering. We can however not be conclusive and further, more systematic, research is needed.

It appears that the chosen depletant volume fractions (1 – 5%) are already sufficiently high to destabilize phases which only possess orientational order. The theoretically predicted N_B phase, which was predicted for the particle dimensions and concentrations of our systems, was not observed. It appears that the theory underestimates the strength of the depletion attraction. For future research we therefore recommend to use significantly lower depletant concentrations. The fact that in this study rather low depletant volume fractions already lead to pronounced changes in the phase diagram, like the disappearance of the *N* phase, can also be ascribed to the depletant particles carrying a charge. This intensifies the depletion interaction. We therefore also recommend using neutral depletants. An additional option to lower the strength of the depletion interaction is using a polymeric depletant. Polymers can deform around the board-like colloids and the depletion effect is therefore expected to be weaker than for the solid particles that were used in this research.

Acknowledgements

We would like to thank Simone Belli for his input during interesting discussions. Esther van den Pol is acknowledged for providing the goethite particles. The staff of the beamline 'DUBBLE' at the ESRF (European Synchrotron Radiation Facility) is thanked for their help during the SAXS measurements.

References

[1] J. C. P. Gabriel and P. Davidson, *Adv. Mater.*, 2000, **12**, 9.
[2] M. Dijkstra, R. van Roij and R. Evans, *Phys. Rev. E*, 2001, **63**, 051703.
[3] H. Reich and M. Schmidt, *J. Phys.: Condens. Matter,* 2007, **19**, 326103.
[4] D. de las Heras, E. Velasco and L. Mederos, *Phys. Rev. Lett.*, 2005, **94**, 017801.
[5] K. Kang and J. K. G. Dhont, *Europhys. Lett.*, 2008, **84**, 14005.
[6] B. Peng, *Control over colloidal particle morphology by dispersion polymerization*, 2013.
[7] S. Asakura and F. Oosawa, *J. Chem. Phys.*, 1954, **22**, 1255-1256.
[8] A. Vrij, *Pure Appl. Chem.*, 1976, **48**, 471-483.
[9] R. Tuinier and H. N. W. Lekkerkerker, *Colloids and the depletion interaction*, Springer, 2011.
[10] Z. Dogic, K. Purdy, E. Grelet, M. Adams and S. Fraden, *Phys. Rev. E*, 2004, **69**, 051702.
[11] Z. Dogic, *Phys. Rev. Lett.*, 2003, **91**, 165701.
[12] D. Kleshchanok, A. V. Petukhov, P. Holmqvist, D. V. Byelov and H. N. W. Lekkerkerker, *Langmuir*, 2010, **26**, 13614-13621.
[13] D. de las Heras, N. Doshi, T. Cosgrove, J. Phipps, D. I. Gittins, J. S. van Duijneveldt and M. Schmidt, *Scientific Reports*, 2012, **2**, 789.
[14] Z. Dogic, D. Frenkel and S. Fraden, *Phys. Rev. E*, 2000, **62**, 3925-3933.
[15] T. Koda, M. Numajiri and S. Ikeda, *J. Phys. Soc. Jpn*., 1996, **65**, 3551-3556.
[16] M. Adams, Z. Dogic, S. Keller and S. Fraden, *Nature*, 1998, **393**, 349-352.
[17] D. Kleshchanok, J. Meijer, A. V. Petukhov, G. Portale and H. N. W. Lekkerkerker, *Soft Matter*, 2011, **7**, 2832-2840.
[18] S. Belli, M. Dijkstra and R. van Roij, *J. Phys.: Condens. Matter*, 2012, **24**, 284128.
[19] C. Tschierske and D. J. Photinos, *J. Mater. Chem.*, 2010, **20**, 4263-4294.
[20] R. Alben, *Phys. Rev. Lett.*, 1973, **30**, 778-781.
[21] B. Mulder, *Phys. Rev. A*, 1989, **39**, 360-370.
[22] J. P. Straley, *Phys. Rev. A*, 1974, **10**, 1881-1887.
[23] E. van den Pol, D. M. E. Thies-Weesie, A. V. Petukhov, G. J. Vroege and K. Kvashnina, *J. Chem. Phys.*, 2008, **129**, 164715.
[24] E. van den Pol, A. V. Petukhov, D. M. E. Thies-Weesie, D. V. Byelov and G. J. Vroege, *Phys. Rev. Lett.*, 2009, **103**, 258301.
[25] E. van den Pol, D. M. E. Thies-Weesie, A. V. Petukhov, D. V. Byelov and G. J. Vroege, *Liq. Cryst.*, 2010, **37**, 641-651.
[26] D. M. E. Thies-Weesie, J. P. de Hoog, M. H. H. Mendiola, A. V. Petukhov and G. J. Vroege, *Chem. Mat.*, 2007, **19**, 5538-5546.
[27] B. Lemaire, P. Davidson, J. Ferre, J. Jamet, P. Panine, I. Dozov and J. Jolivet, *Phys. Rev. Lett.*, 2002, **88**, 125507.
[28] S. Belli, A. Patti, M. Dijkstra and R. van Roij, *Phys. Rev. Lett.*, 2011, **107**, 148303.
[29] S. Krehula, S. Popovic and S. Music, *Mater. Lett.*, 2002, **54**, 108-113.

[30] B. Lemaire, P. Davidson, J. Ferre, J. Jamet, D. Petermann, P. Panine, I. Dozov and J. Jolivet, *Eur. Phys. J. E*, 2004, **13**, 291-308.
[31] A. Lecloux, J. Bronckart, F. Noville, C. Dodet, P. Marchot and J. Pirard, *Colloid. Surface.*, 1986, **19**, 359-374.
[32] A. Petukhov, J. Thijssen, D. t Hart, A. Imhof, A. van Blaaderen, I. Dolbnya, A. Snigirev, A. Moussaid and I. Snigireva, *J. Appl. Crystallogr.*, 2006, **39**, 137-144.
[33] W. Bras, I. Dolbnya, D. Detollenaere, R. van Tol, M. Malfois, G. Greaves, A. Ryan and E. Heeley, *J. Appl. Crystallogr.*, 2003, **36**, 791-794.
[34] M. Bates and D. Frenkel, *J. Chem. Phys.*, 1998, **109**, 6193-6199.
[35] A. B. G. M. Leferink op Reinink, E. van den Pol, D. V. Byelov, A. V. Petukhov and G. J. Vroege, *J. Phys.: Condens. Matter*, 2012, **24**, 464127.
[36] M. C. D. Mourad, D. V. Byelov, A. V. Petukhov, D. A. M. de Winter, A. J. Verkleij and H. N. W. Lekkerkerker, *J. Phys. Chem. B*, 2009, **113**, 11604-11613.
[37] E. van den Pol, A. V. Petukhov, D. V. Byelov, D. M. E. Thies-Weesie, A. Snigirev, I. Snigireva and G. J. Vroege, *Soft Matter*, 2010, **6**, 4895-4899.
[38] A. B. G. M. Leferink op Reinink, S. Belli, R. van Roij, M. Dijkstra, A. V. Petukhov and G. J. Vroege, *Soft Matter*, 2014, **10**, 446-456
[39] Z. Dogic and S. Fraden, *Philos. T. R. Soc. A*, 2001, **359**, 997-1014.
[40] G. J. Vroege, D. M. E. Thies-Weesie, A. V. Petukhov, B. J. Lemaire and P. Davidson, *Adv. Mater.*, 2006, **18**, 2565.
[41] S. Asakura and F. Oosawa, *J. Pol. Sci.*, 1958, **33**, 183-192.
[42] J. Walz and A. Sharma, *J. Colloid Interf. Sci.*, 1994, **168**, 485-496.

4

Tuning biaxiality of nematic phases of board-like colloids by an external magnetic field

We study the influence of a magnetic field on the biaxial nematic phase of board-like goethite colloids both experimentally and theoretically. Using synchrotron small angle x-ray scattering techniques we find that applying a magnetic field along the main director of the biaxial nematic phase leads to a clear decrease in biaxiality with increasing magnetic field strength. Above a certain magnetic field strength the biaxiality is completely suppressed and the biaxial nematic phase transforms into an ordinary prolate uniaxial nematic phase. In order to interpret the physical mechanism behind this phenomenon, we develop a mean-field theory for the liquid crystal phase behaviour of the suspension. Within this theory the magnetic properties of the particles are modelled by taking into account the effect of both the permanent and the induced magnetic dipoles. The resulting phase diagrams support our experimental findings of the field-induced biaxial nematic to prolate uniaxial nematic transition. They additionally predict that for more plate-like particles, which initially would only display oblate nematic ordering of the shortest axis, the rare biaxial phase can be induced by applying a magnetic field with a carefully chosen field strength, a parameter which can be easily tuned.

4.1 Introduction

Anisotropic particles, like rod-, board- and plate-like particles, have the ability to form liquid crystals. There are various liquid-crystalline phases of which the nematic phase (N), in which the particles are orientationally ordered, is most common. Liquid crystals are of great fundamental interest but are also widely used in for example liquid-crystal displays (LCDs) [1]. In LCDs an external electric field controls the polarization of light by switching the orientation of particles or molecules in the nematic phase. The liquid crystals that are predominantly used in LCDs are thermotropic (molecular) liquid crystals [1]. However, lyotropic liquid crystals of mineral particles might be promising candidates for application in LCDs as well: they are cheap, have an enhanced susceptibility to external fields and a high thermal stability [2, 3].

The spontaneous formation of lyotropic liquid crystals is an entropy-driven process. Already in the 1940s Onsager explained in his seminal work the isotropic - nematic (I - N) phase transition for rod-like particles on basis of particle shape alone [4]. He showed that at sufficiently high volume fraction the loss in orientational entropy is compensated by the gain in excluded volume entropy.

There exist different nematic phases. In the usual (uniaxial) nematic phase the particles' main axes orient along a common direction. This is either the long particle axis in rod-like systems, the resulting nematic being the *prolate* uniaxial nematic (N_+) phase, or the short particle axis in plate-like systems, alignment of which results in the *oblate* uniaxial nematic phase (N_-). Additionally, there is the *biaxial* nematic (N_B) phase, in which particles orient along both axes. The appearance of this N_B phase in the phase diagram was theoretically predicted by Freiser [5] in 1970 and immediately attracted significant attention [6-10] since the improved alignment makes biaxial nematic phases promising candidates for LCDs. Unfortunately, the biaxial nematic phase is rare. There are few experimental examples, most of which are still under debate [11-13].

Board-like colloidal particles of the mineral goethite (α-FeOOH) constitute one of the few known experimental realizations [14] of the N_B phase. Above a volume fraction of typically 0.1, the goethite particles - characterized by their length L > width W > thickness T - not only spontaneously orient their L-axis but their W- and T-axes as well. Depending on the degree of polydispersity and volume fraction of the particles, this can either be a biaxial nematic phase, a biaxial smectic phase (in which the particles are stacked in layers), or both [14-16].

Understanding the factors determining the formation of biaxial liquid crystal phases is important for possible applications [17]. Biaxial nematic stability can be interpreted as a balanced competition between rod-like and plate-like behaviour. Theoretically, biaxial phases are found for specific particle dimensions close to the condition (L/W) = (W/T), hence for particles with a shape in between rod- and plate-like [18]. However for the goethite system unexpectedly a direct I - N_B phase transition was also found for slightly elongated board-like particles with a shape

parameter ($\upsilon \equiv (L/W)$ - (W/T)) of 0.1 [14]. Theory explained [19] that the stability of the goethite N_B phase could be attributed to the system's high polydispersity (~25%) which leads, similar to the effect of a depletant [20], to N_+ - N_- competition.

Colloidal goethite particles have very peculiar magnetic properties which makes them highly susceptible to an external magnetic field [21]. They possess a permanent magnetic moment along their long axis, but their magnetic easy axis is perpendicular to this axis [21]. Therefore, particles align parallel to a weak magnetic field but reorient to align their long axis perpendicular to a magnetic field with a field strength higher than the critical magnetic field strength (B^*) [21-26]. Since the particles easily align in a (weak) magnetic field, magnetic fields are often used to reorient goethite (biaxial nematic) liquid crystal phases [26, 27].

In this chapter we investigate the effect of a magnetic field on the stability of the goethite biaxial nematic phase both experimentally, using small angle x-ray scattering (SAXS), and theoretically, by means of a mean-field theory. In section 4.2 we describe the experimental goethite system, sample preparation and the SAXS set-up. In section 4.3 we describe the theoretical framework: a mean-field theory where the magnetic properties of the particles are modelled taking into account the effect of the permanent and induced magnetic moments. Section 4.4 and section 4.5 then describe the experimental and theoretical results, respectively. Finally, in section 4.6 we draw our conclusions.

4.2 Experimental

4.2.1 Goethite synthesis, characterization and sample preparation

Goethite particles were obtained by hydrolysis of iron nitrate at high pH similar to the procedure described in section 2.2.1. However, particle ageing now took place at room temperature for 9 days. The obtained dispersions were washed and stabilized in the same way as described in section 2.2.1.

Particle size distributions were determined with TEM and iTEM imaging software as described in section 2.2.2. The length L and width W and their corresponding polydispersities were determined of 600 particles. Thickness T and the polydispersity in T were determined from 150 particles. The average particle dimensions were found to be L x W x T = 254 x 83 x 28 nm with a polydispersity of 25% in all dimensions. The shape parameter $\upsilon \equiv (L/W - W/T) \approx 0.1$. Since T was measured independently from W an estimate of the variation in υ cannot be given [28].

A flat glass capillary with internal dimensions of 0.2 x 4.0 x 100 mm^3 (Vitrocom W3520-100) was filled with the goethite dispersion. The initial goethite volume fraction (ϕ_g) was 12.5%. The capillary was flame sealed and stored in upright position to assure the formation of a density gradient by the gravitational field of the earth.

4.2.2 Small angle x-ray scattering measurements

SAXS measurements were performed at the BM26 DUBBLE beamline [29] of the European Synchrotron Radiation Facility (ESRF, Grenoble, France) in a similar way as described in section 3.2.4. The patterns were collected using a CCD detector with a pixel size of 22 μm (Photonic Science). The two homemade variable permanent magnets described in section 2.2.2 were used to apply magnetic fields parallel or perpendicular to the x-ray beam. Relative goethite volume fractions were determined from the x-ray adsorption measured at different heights in the sample.

4.3 Theoretical framework

We developed a mean-field density functional theory to predict the phase behaviour of hard board-like particles under the effect of a magnetic field. By calculating the excluded volume between two uniaxial rods as a function of their orientation, Onsager was able to predict the stability of a nematic liquid crystal phase [4]. Unfortunately, the corresponding expression for the excluded volume of a pair of board-like particles is not available. Hence, in the present analysis we circumvent the problem by adopting a discrete-orientation model [30].

In Ref. [30] it is shown that the isotropic-nematic transition of uniaxial rods remains first-order if the number of allowed orientations is gradually decreased from infinity (Onsager's continuum) [4] to three (the Zwanzig model of rods) [31]. Although a similar study for board-like particles has not been performed yet, the results of Ref. [30] suggest that the nature of the isotropic-nematic transition is robust with discretising the orientation degrees of freedom. Note, however, that the location of the binodal, the magnitude of the phase gap, and the nematic ordering of the coexisting nematic state in Ref. [30] all do depend on the degree of discretization. Therefore, one should expect the predictions of the discrete-orientation model for the present system to be mainly qualitative.

Within this model the total number of orientations is reduced to the i = 1,..., 6 independent ways a board-like particle can align its main axes along those of a fixed Cartesian reference frame. Moreover, we assume each particle to carry a permanent magnetic dipole directed along the longest axis. We indicate with α = +,- when the magnetic dipole is oriented parallel and antiparallel to the Cartesian axis, respectively. As a result, the orientation of a single board-like particle can be identified with the pair ($i\alpha$), giving rise to a total of the 12 independent orientations depicted in Fig. 4.1.

4.3.1 Density functional theory

We consider a system of N identical board-like particles with dimensions L x W x T in a volume V at room temperature T under the effect of the homogenous external energy field $u_{i\alpha}$. Let us indicate with $\rho_{i\alpha}$ the number density of particles with orientation ($i\alpha$) in a homogeneous phase, satisfying the normalization condition

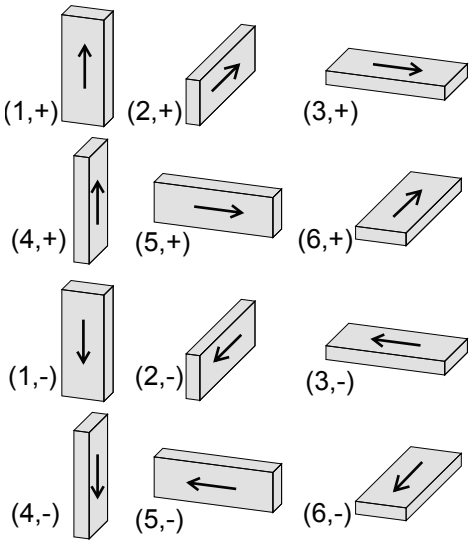

Fig. 4.1 Orientational degrees of freedom of a magnetic board-like particle in the restricted-orientation model.

$$\sum_{i,\alpha} \rho_{i\alpha} = \frac{\phi}{v}, \tag{4.1}$$

where $\phi = Nv/V$ is the particle volume fraction and $v = L$ x W x T is the single-particle volume. The free-energy functional per unit volume is defined as [32]

$$\beta f[\rho_{i\alpha}] = \sum_{i,\alpha} \rho_{i\alpha} [\log(\rho_{i\alpha} \Lambda^3) - 1] + \beta f_{exc}[\rho_{i\alpha}] + \sum_{i,\alpha} \rho_{i\alpha} \beta u_{i\alpha}, \tag{4.2}$$

where $\beta = (k_B T)^{-1}$, k_B is the Boltzmann constant and Λ is the thermal wavelength. The first term on the right-hand side of Eq. (4.2) represents the ideal-gas contribution, whereas f_{exc} is the excess free energy per unit volume due to particle-particle interactions. The excess free energy cannot be evaluated exactly and hence has to be approximated. In the present study we employ the second-virial approximation, according to which

$$\beta f_{exc}[\rho_{i\alpha}] = \frac{G(\phi)}{2} \sum_{i,i'} E_{ii'} (\rho_{i+} + \rho_{i-})(\rho_{i'+} + \rho_{i'-}), \tag{4.3}$$

where $E_{ii'}$ is the excluded volume of two particles with orientations i and i', respectively, due to the interparticle repulsion [19, 20]. In the present model magnetic interactions between particles are disregarded due to the relatively negligible strength of their magnetic dipoles. The term $G(\phi)=(1-3/4\phi)/(1-\phi)^2$ in Eq. (4.3) is a Parsons-Lee correction term [32-35], introduced in order to reduce the quantitative deviations expected in the second-virial approach. Finally, the last term on the

right-hand side of Eq. (4.2) represents the external energy contribution to the free energy of the system, which is discussed in the following section. Once an approximation for the excess free energy f_{exc} is established, the equilibrium single-particle density is found as the minimum of Eq. (4.2) under the constraint of Eq. (4.1). In other words, the equilibrium single-particle density at the packing fraction ϕ is calculated by solving the Euler-Lagrange equation

$$\rho_{i\alpha} = \frac{\phi}{v} \frac{\exp\left[-G(\phi)\sum_{i',\alpha'} E_{ii'}\rho_{i'\alpha'} - \beta u_{i\alpha}\right]}{\sum_{i'',\alpha''} \exp\left[-G(\phi)\sum_{i',\alpha'} E_{i''i'}\rho_{i'\alpha'} - \beta u_{i''\alpha''}\right]}. \tag{4.4}$$

Due to its non-linear character Eq. (4.4) cannot be solved analytically. However, standard algorithms such as the Picard method can be applied to its numerical solution.

From the knowledge of the equilibrium single-particle density $\rho_{i\alpha}$ one can investigate the broken symmetries of the phase point under consideration by calculating the nematic order parameters. In case the nematic director is the vertical axis in Fig. 4.1, the (prolate) uniaxial nematic order parameter can be expressed as

$$U.O.P. = \frac{v}{\phi}\sum_{\alpha}\left\{\rho_{1\alpha} + \rho_{4\alpha} - \frac{1}{2}\left[\rho_{2\alpha} + \rho_{3\alpha} + \rho_{5\alpha} + \rho_{6\alpha}\right]\right\}. \tag{4.5}$$

This order parameter takes positive values in case of prolate nematic ordering, while negative values for oblate nematic. On the other hand, a zero value describes an isotropic phase. Additionally, in order to take into account the possibility of biaxial ordering, one has to introduce a biaxial order parameter, which we define as

$$B.O.P. = \frac{v}{\phi}\left|\sum_{\alpha}\rho_{1\alpha} - \rho_{4\alpha}\right|. \tag{4.6}$$

4.3.2 Magnetic energy

Let us consider the energy of a single goethite particle in a constant external magnetic field with strength B directed along the z axis. Let m = 1.7 x 10^{-20} Am^2 be the strength of the particle's permanent magnetic dipole [36]. By referring to Fig. 4.1, one finds that in the absence of an induced magnetic dipole the magnetic energy in the present discrete-orientation model reads

$$u_{i\alpha} = -mB(\delta_{i1} + \delta_{i4})(\delta_{\alpha+} - \delta_{\alpha-}), \tag{4.7}$$

where δ is the Kronecker delta. On the other hand, most of the peculiar magnetic properties of goethite particles are due to the presence of an induced magnetic dipole [21, 22, 24]. Such an induced dipole is known to develop in the plane perpendicular to the permanent dipole, that is, along the shortest and the intermediate

particle axes. In order to account for such an induced magnetic dipole, Eq. (4.7) has to be substituted by the following expression

$$u_{i\alpha} = -mB(\delta_{i1} + \delta_{i4})(\delta_{\alpha+} - \delta_{\alpha-}) - KB^2(\delta_{i2} + \delta_{i3} + \delta_{i5} + \delta_{i6}), \tag{4.8}$$

where

$$K = \frac{v|\Delta\chi|}{2\mu_0}. \tag{4.9}$$

In the previous equations $v = L$ x W x T is the single-particle volume, $\mu_0 = 4\pi$ x 10^{-7} NA^{-2} the magnetic permeability and $\Delta\chi = \chi_{//} - \chi_{\perp}$ the susceptibility anisotropy with respect to the long axis of the particle. Experimental measurements for the susceptibility anisotropy of such particles exist and suggest a value varying between -3 x 10^{-4} (in ref. [23]) and -7 x 10^{-4} (in ref. [36]). In principle, one could plug these values into Eq. (4.9) to obtain an estimate for the coefficient K. In practice, however, the large uncertainty of the particle volume v due to the relatively high degree of polydispersity of the sample does not allow for a sufficiently accurate estimate of K. In order to overcome this limitation, we apply our model to predict the value of the constant K. We chose K such that at room temperature in the dilute limit the critical magnetic field takes the experimental value of 250 mT. The corresponding value of K was found to be K = 2.9 x 10^{-20} $A^2m^4J^{-1}$. This corresponds to a susceptibility anisotropy of -1.2 x 10^{-4} which is close to the values found in literature.

4.4 Experimental results

The sample was allowed to sediment for three months before SAXS patterns were taken. The liquid crystal phases formed in the sample were first characterized in a very weak magnetic field of 3 mT applied parallel to the x-ray beam. This is the lowest field possible with the magnet poles at maximum spacing. At low volume fractions, such a weak field might partially direct the main director along the field but does not change the liquid-crystal phase itself. SAXS patterns were taken every 0.5 mm along the y-direction (Fig. 4.2) of the capillary and revealed an isotropic phase on top of a 3 mm high nematic sediment. The left column in Fig. 4.2 shows the collected SAXS patterns taken in a magnetic field of 3 mT at three different heights in the sediment: at the capillary bottom (y = 0 mm) and at 1.5 and 2 mm above the capillary bottom. All three patterns show similar diffuse reflections characteristic of a (biaxial) nematic phase. The patterns are highly anisotropic; two orthogonal peaks can be observed at large scattering vectors. The radial profiles corresponding to the SAXS-pattern taken at y = 0 mm (black line in Fig. 4.3(b)) reveal Q-values of 0.045 (140 nm) and 0.086 nm^{-1} (73 nm) respectively. They originate from the correlations of the W and T dimensions of the particles, respectively. The ratio between the Q-values of the two peaks Q_T/Q_W = 1.9 agrees reasonably well with the particle aspect ratio W/T taken into account the Debye length (~10 nm). Additionally, the

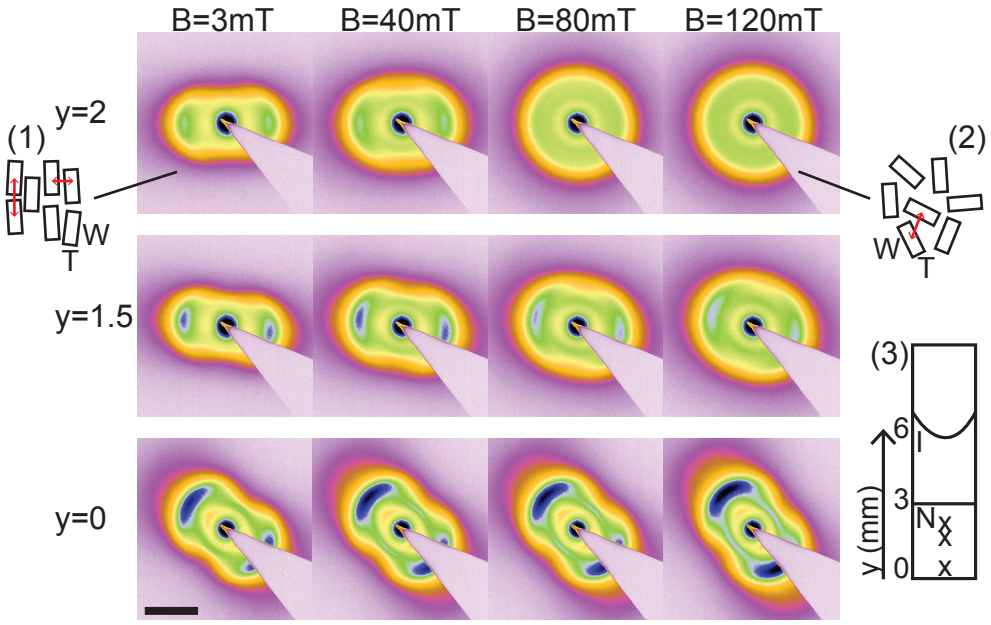

Fig. 4.2 SAXS patterns taken at three different heights in the capillary (y = 0, 1.5 and 2 mm) submitted to an external magnetic field of 3, 40, 80 and 120 mT, respectively. The magnetic field direction is parallel to the x-ray beam. (1) & (2) Schematic drawings illustrating the N_B and N_+ phase seen along the *L*-axis, respectively. (3) Schematic drawing of the capillary. Liquid crystal phases are denoted by *I* (isotropic) and *N* (nematic). The presented SAXS patterns were taken at the positions denoted by x. The black bar denotes 0.1 nm^{-1}.

sample had been sedimenting for only three months, which means that ϕ_g is relatively low and thus that the inter-particle spacing is large compared to the particle dimensions. For the pattern taken at y = 2 mm (Fig. 4.3(d)) reflections are found at slightly smaller Q-values. Due to sedimentation the goethite volume fraction decreases with the height in the sample ($\phi_{g,y=0}$ = 1.27 x $\phi_{g,y=2}$) hence the particle spacing is slightly larger at y = 2 mm. Azimuthal profiles of the scattering intensity along circles at the Q-values corresponding to the correlation peaks are shown in Fig. 4.3(a, c). The different correlation peaks clearly appear along orthogonal directions of each other. From the plots and the patterns it is clear that the particles are orientationally ordered in three dimensions hence the patterns taken at 3 mT originate from the biaxial nematic liquid crystal phase (N_B) (Fig. 4.2) [14].

To study the influence of an external magnetic field on the N_B phase SAXS-patterns were taken while stepwise increasing the magnetic field strength. The measurements were taken at the same heights in the capillary as before. The magnetic field strength ranges from 40 to 120 mT. This is far below the critical magnetic field strength, hence the particles align their long axis along the field. The resulting SAXS patterns are shown in Fig. 4.2. For the patterns taken at y = 0 mm, there is no sig-

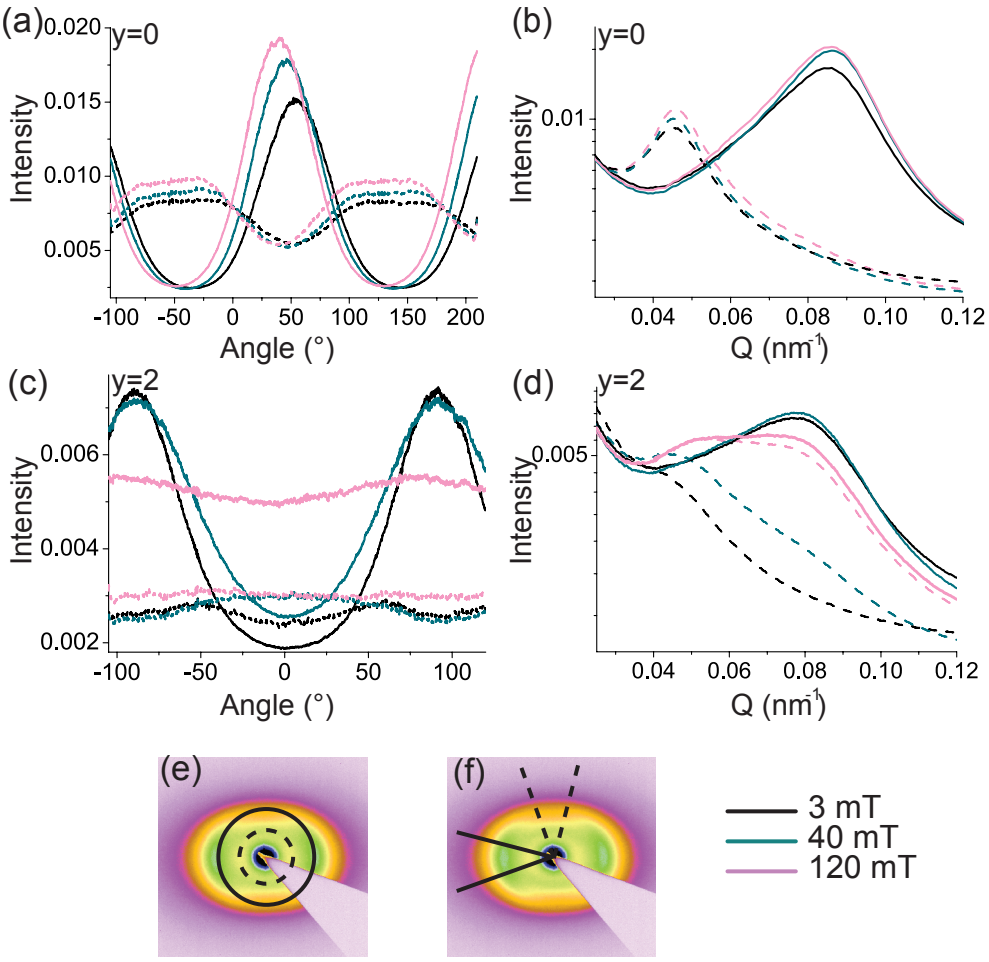

Fig. 4.3 Plots of selected SAXS patterns shown in Fig. 4.2 illustrating the decrease in biaxiality as a function of the height in the capillary y and of the magnetic field strength. (a) and (c) show the azimuthal plots at Q_W (dashed lines) and Q_T (solid lines) for y = 0 and y = 2 mm respectively (taken as illustrated in (e)). (b) and (d) show the radial profiles taken along two orthogonal directions corresponding to the *W* (dashed lines) and *T* (solid lines) reflections respectively (taken as illustrated in (f)).

nificant change due to the increase of the magnetic field strength. Compared to the pattern taken at 3 mT, a subtle increase in intensity can be observed, as well as a slight change in the directions in which the reflections can be found. This is due to the particles aligning in the field. Similar conclusions can be drawn from the radial profiles (Fig. 4.3(a, b)). Fig. 4.3(b) shows the subtle increase in intensity for the patterns taken at B > 3mT. However, the positions of the peaks are unchanged. The azimuthal profiles (Fig. 4.3(a)) confirm this, as well as the slight change in ori-

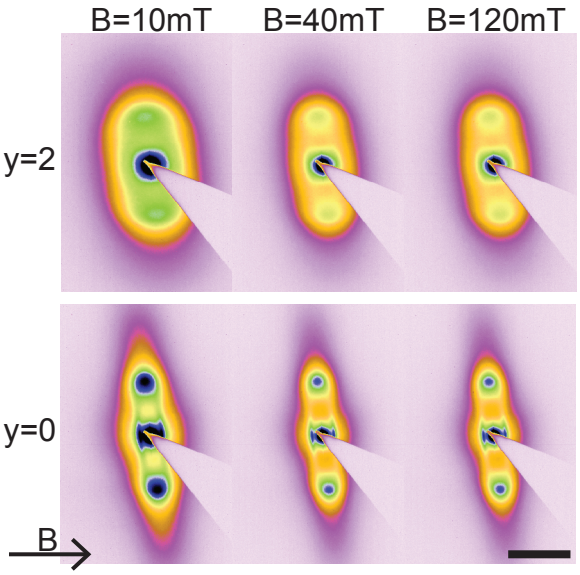

Fig. 4.4 SAXS patterns taken at two positions in the capillary (y = 0 and 2 mm), in a magnetic field varying from 10 to 120 mT. The magnetic field direction is perpendicular to the x-ray beam and is denoted by the black arrow. The black bar denotes 0.1 nm^{-1}.

entation of the nematic reflections. The observed reflections however still clearly indicate the biaxial ordering of the nematic phase for all magnetic field strengths. Whereas the magnetic field effects on the N_B phase at y = 0 mm are small, the effect on the N_B phases is significant at y = 1.5 and 2 mm, where the volume fraction ϕ_g is lower. For the patterns taken at y = 1.5 mm, the anisotropy of the pattern decreases when the magnetic field strength increases (Fig. 4.2). This indicates that the actual biaxial order decreases upon increasing the magnetic field. The sharp character of this transition is manifested upon going from 40 to 80 mT.

The decrease in biaxial ordering is even more pronounced for the patterns taken at y = 2 mm; at 80 and 120 mT the patterns appear to be isotropic. This indicates that the particles lost their biaxial ordering and formed a prolate uniaxial nematic phase (N_+) instead (schematic drawing Fig. 4.2). The magnetic field-induced N_B to N_+ transition observed at y = 2 mm is confirmed by the radial and azimuthal profiles shown in Fig. 4.3(c, d). The I(Q) plots originating from the pattern taken at 120 mT given in Fig. 4.3(d) show that the combined reflections of both the *W* and *T* correlations of the particles are present in both orthogonal directions. The radial profiles are even almost identical. Additionally, the peaks of the independent *W* and *T* reflections are barely visible; they almost entirely fused to form one reflection at a Q-value in between Q_W and Q_T. This is characteristic of the uniaxial nematic phase and confirms the N_B to N_+ transformation. The azimuthal plots (Fig. 4.3(c)) show the loss of biaxial order with increasing field strength as well. Already at 40 mT the peaks have become broader and at 120 mT the different positional correlation peaks barely appear along orthogonal directions. For the profile taken at Q_W, the integrated intensity of the reflection is equal for the entire profile. The angular

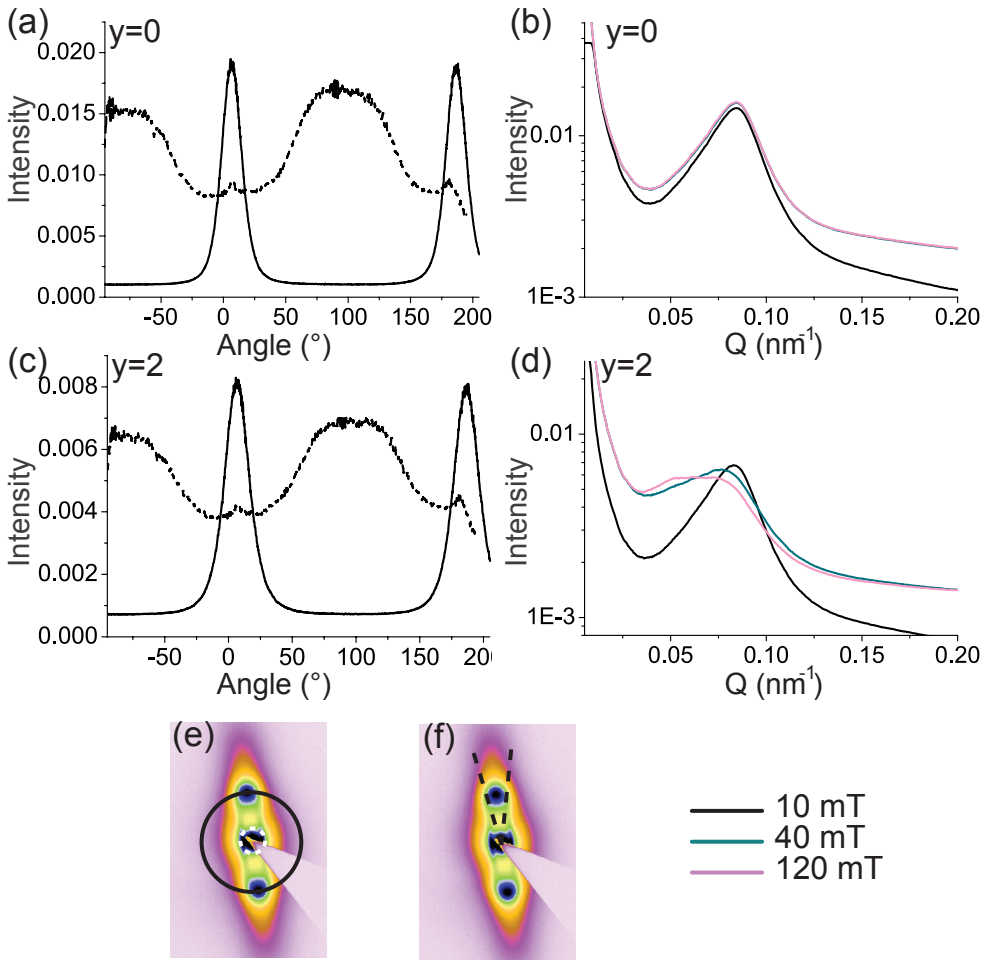

Fig. 4.5 Plots of selected SAXS patterns shown in Fig. 4.4 illustrating the decrease in biaxiality as a function of height in the capillary y and the magnetic field strength. (a) and (c) show the azimuthal plots (taken as illustrated in (e)) at Q_T (~0.08 nm^{-1} (solid lines)) and at Q_L (~0.017 nm^{-1} (dashed lines)) for y = 0 and y = 2 mm respectively in a 10 mT magnetic field. Both plots show the biaxiality of the nematic phase. (b) and (d) show the radial profiles taken along the direction of the reflection at large Q for 10, 40 and 120 mT (taken as illustrated in (f)).

extension of the diffuse reflections indicates that the particles can now freely rotate around their *L*-axis, indicating N_+ ordering once more.

To confirm these observations the biaxiality was studied by applying the magnetic field in the direction perpendicular to the x-ray beam. SAXS patterns and the corresponding radial and azimuthal profiles are shown in Fig. 4.4 and Fig. 4.5, respectively. The patterns taken at y = 0 mm show a reflection at short Q originating

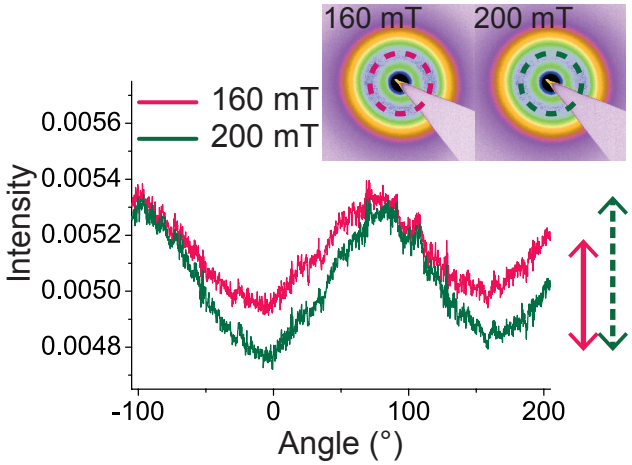

Fig. 4.6 Azimuthal plots of the SAXS patterns (inset) taken at y = 2 in magnetic fields of 160 and 200 mT. The magnetic field direction is parallel to the x-ray beam. The integrated area is illustrated by the dashed circles in the inset. The solid and dashed arrows represent the peak height for the 160 mT and the 200 mT plots respectively. It is clear that the peak height of the 200 mT plot is larger than the peak height of the 160 mT plot. This indicates that biaxiality has increased again at 200 mT.

from the longest axis of the particles combined with a reflection at Q = 0.084 nm^{-1}, originating from particles' shortest dimension. Reflections of the *W*-correlation of the particles are not observed, thus confirming the biaxiality of the nematic phase. Upon increasing the magnetic field strength, the reflection of *T* remains at fixed Q, confirming the biaxiality of the nematic phase at y = 0 mm in a magnetic field of 120 mT (Fig. 4.5(b)).

The SAXS-pattern taken at y = 2 mm and B = 10 mT shows the reflections of the N_B phase: a weak reflection at short Q originating from *L* and in the orthogonal direction the *T*-reflection at Q = 0.083nm^{-1}. It is clear from the I(Q) profiles of the patterns taken at B = 40 and 120 mT that the peak at large Q is shifting to lower Q-values (Fig. 4.5(d)). This indicates that reflections are not solely originating from the *T*-dimension of the particles but from the *W*-dimension as well. This means that the particles are able to rotate around their long axis and are no longer biaxially ordered.

It is also interesting to investigate the influence of the magnetic field when the magnetic field strength is getting closer to the critical magnetic field strength B^*. It is known that, due to goethite's specific magnetic properties, particles in the nematic phase align their *L*-axis in weak magnetic fields (B < B^*) but reorient to align their *T*-axis in strong magnetic fields (B > B^*). As a result the N_+ phase transforms into a rotated N_B phase -where the particles' long axis is now aligned perpendicular to the field- when submitted to a strong magnetic field. Here we observed the N_B to N_+

transition in magnetic fields weak compared to the critical magnetic field, where the particles do not rotate yet and the induced magnetic moment does not have a significant influence on the phase behaviour. In Fig. 4.6 we present SAXS patterns with their corresponding azimuthal plots taken at y = 2 mm in magnetic fields with field strengths (B =160 and 200 mT) closer to B^* (250 mT). The profile of the pattern taken at B = 160 mT is similar to the profile at 120 mT, the differences are negligible. However if the profile corresponding to the pattern taken at 200 mT is compared to the one of 160 mT, it appears that the amplitude of the peaks has increased. This suggests that the biaxial ordering slightly increased again. This might indicate that the perpendicular induced magnetic moment starts playing a role: the particles start aligning their T-axes as well thereby increasing the biaxial ordering of the board-like particles.

4.5 Theoretical results

The theoretical framework described in section 4.3 was applied to predict phase diagrams for board-like particles submitted to an external magnetic field. Fig. 4.7 shows the well-known [7, 37] zero-field case as a function of the shape parameter ($\upsilon \equiv L/W\text{-}W/T$) and volume fraction ($\phi$). A system of board-like particles undergoes a transition to a prolate uniaxial nematic phase (N_+) if $\upsilon > 0$, to an oblate uniaxial nematic (N_-) if $\upsilon < 0$ and to a biaxial nematic (N_B) if $\upsilon = 0$. Such isotropic-nematic phase transitions are in general discontinuous, albeit very weakly, and become continuous in a Landau critical point only if $\upsilon = 0$. Here and in what follows we focus on low enough volume fractions so that the stability of inhomogeneous phases (e.g., smectic, crystals, ...) can be neglected.

The phase diagrams for board-like particles submitted to magnetic fields of intensity 3, 40, 80 and 120 mT are shown in Fig. 4.8. For comparison the zero field case is shown by the white lines. Let us first focus on Fig. 4.8(a), which reports the phase diagram of board-like particles in the presence of a 3 mT magnetic field. In spite of the low field strength, the effect of the explicit breaking of the rotational symmetry due to the field is already evident. First, due to the coupling between the permanent magnetic dipole and the field, the particles acquire a weak tendency to align their long axis L along the field even at very low volume fraction. As a consequence, the symmetry of the low-density isotropic phase (Fig. 4.7) becomes the same as that of the prolate uniaxial nematic phase (red region in Fig. 4.7 and Fig. 4.8). Such a phenomenon closely resembles the phase behaviour of rods under the effect of an external magnetic field which couples to the orientation of their main axis [38]. In the latter context, the low-density phase which acquires the same symmetries as the higher-density nematic phase is termed "*para*-nematic". The distinction between a nematic and a *para*-nematic phase is needed as long as the two phases are separated by a discontinuous phase transition. This happens to be the case as long as the field strength is sufficiently low. However, at high enough field strength such

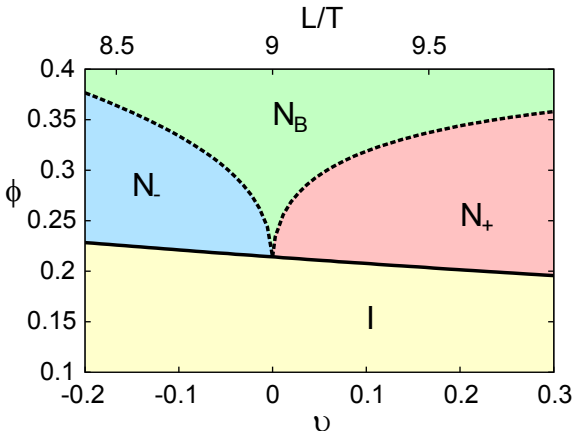

Fig. 4.7 Phase diagram of magnetic board-like particles in the absence of a magnetic field. ϕ = volume fraction. Here and in the following plots the shape parameter υ (≡ L/W – W/T) is modified by changing the aspect ratio L/T while keeping W/T fixed at 3. Solid lines indicate (very weakly) first order transitions, whereas dashed lines indicate continuous transitions. Liquid crystal phases are denoted by I (isotropic), N_-, N_+ and N_B (oblate uniaxial, prolate uniaxial and biaxial nematic, respectively).

a phase transition becomes continuous, and the two phases merge into the same nematic phase [38]. As pointed out in the analysis of the zero-field case (cf. Fig. 4.7), in the present model the isotropic-nematic phase transition of board-like particles is very weakly discontinuous. This means that at a magnetic field strength as low as 3 mT this phase transition is already continuous, and the distinction between *para*-nematic and nematic phases is pointless. The second manifest effect of the external field on the phase behaviour of board-like particles is the disappearance of the oblate uniaxial nematic phase (blue region in Fig. 4.7) in favour of the biaxial nematic (green region in Fig. 4.7 and Fig. 4.8). It is important to realize that at such a low magnetic field the deviations from the zero-field case play the role of a very weak symmetry-breaking perturbation. This statement is confirmed by the fact that the transition line (black dashed line) between the only two phases left in the phase diagram, that is the N_+ and the N_B, does not change appreciably from the zero-field case. In contrast, relevant deviations in the N_+ - N_B transition develop at higher magnetic field strengths. The phase diagram in Fig. 4.8(b) shows that already at 40 mT the original N_B phase formed close to the Landau critical point, where ϕ is relatively low, has transformed into a N_+ phase. The phase diagrams for magnetic fields of 80 and 120 mT (Fig. 4.8(c, d)) show that the N_B - N_+ transition line shifts to higher volume fractions with increasing magnetic field strengths. This indicates that more and more of the original N_B phase is transformed into a N_+ phase.

An alternative way to visualize the data is offered in Fig. 4.9, where we report the phase diagram of a system of board-like particles with fixed shape parameter $\upsilon = 0$ (L/T=9; W/T=3) as a function of the magnetic field strength. This plot shows

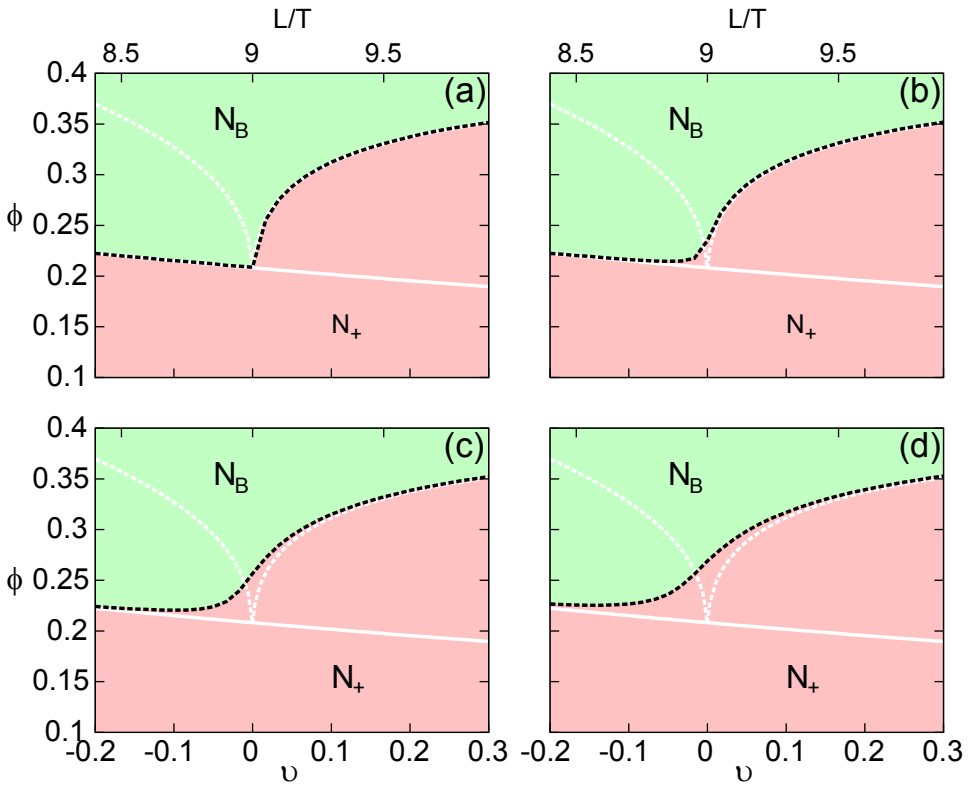

Fig. 4.8 Theoretical prediction of phase diagrams of magnetic board-like particles in a magnetic field of (a) 3 mT, (b) 40 mT, (c) 80 mT and (d) 120 mT under the effect of the external potential in Eq. (4.8). White lines represent the zero-field phase diagram. N_+ and N_B denote the prolate uniaxial and biaxial nematic liquid crystal phase, respectively.

explicitly the variation of the N_B to N_+ transition with the intensity of the field. The transition line shows that the magnetic field strength needed to induce the N_+ phase increases with increasing volume fraction. Above a certain volume fraction the particles remain in the N_B phase for all field strengths lower than B^*. These theoretical predictions agree with the experimental observations of the field-induced N_B to N_+ transition. Our experimental results also indicated that the biaxial order is restored when the magnetic field strength approaches the critical magnetic field strength (B^* = 250 mT). Also this is supported by theory. The black arrow in Fig. 4.9 clearly shows the re-entrant N_B to N_+ to N_B transition. Interestingly, Fig. 4.9 also shows that for field strengths above B^*, where alignment along the short axis T is favoured, the N_B phase again loses biaxial order but now in favour of oblate uniaxial ordering.

It is crucial to keep in mind that in the present model the N_B - N_+ transition is continuous. This means that the biaxial ordering and the prolate uniaxial ordering close to the transition line are weak, hence those phases do not differ as drasti-

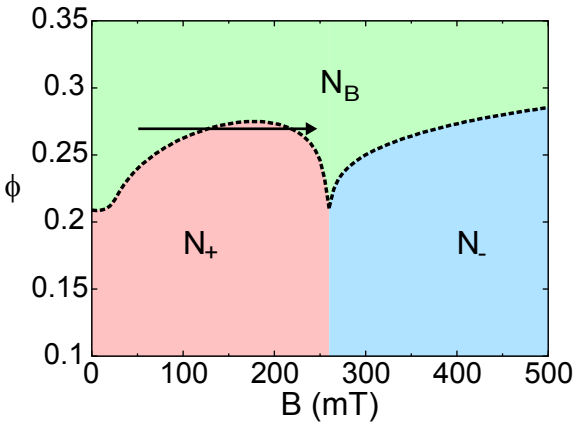

Fig. 4.9 Theoretical prediction of the phase diagram of magnetic board-like particles with shape parameter $\upsilon = 0$ (L x W x T = 9 x 3 x 1) as a function of volume fraction ϕ and magnetic field strength. The black arrow illustrates the re-entrant N_B to N_+ to N_B transition with increasing field strength.

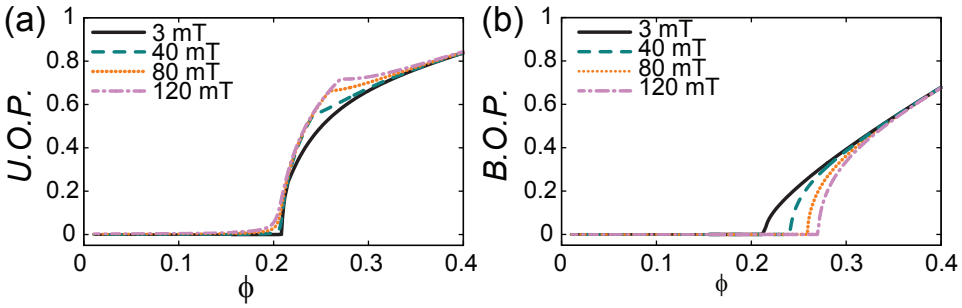

Fig. 4.10 (a) Uniaxial order parameter (*U.O.P.*) and (b) biaxial order parameter (*B.O.P.*) plotted as a function of volume fraction ϕ for four magnetic field strengths (3, 40, 80 and 120 mT respectively) for particles with $\upsilon = 0$ (L x W x T = 9 x 3 x 1).

cally from each other as appears from the phase diagram at first glance. This is also emphasized by the order parameter plots shown in Fig. 4.10. At a volume fraction of ~0.23 the N_B phase transforms into the N_+ phase in a field of 40 mT for particles with $\upsilon = 0$ (Fig. 4.8(b), Fig. 4.9). It is however apparent from the order parameter plots (Fig. 4.10(b)) that the corresponding decrease in the biaxial nematic order parameter is not drastic upon going from 3 to 40 mT. The biaxial order parameter decreases with increasing B and at high enough field strengths, e.g. 80 mT for a volume fraction of 0.23, eventually becomes zero, indicating that the particles are no longer biaxially ordered. The uniaxial order parameter along L plotted in Fig. 4.10(a), in contrast to the biaxial order parameter, increases with increasing field strength. The discontinuities in the curves' first derivatives represent the N_+ - N_B transition points.

The theoretical predictions of the influence of the magnetic field on the other liquid crystal phases are also interesting. As expected, the phase diagrams in Fig. 4.8(a) show that the magnetic field breaks the symmetry of the isotropic phase and induces the N_+ phase, which in turn transforms into the N_- phase for B > B^* (Fig. 4.9). Especially interesting is the influence of the magnetic field on the N_- phase, which is expected at zero field for particles with $\upsilon < 0$. The phase diagrams in Fig. 4.8 clearly show that the N_- phase transforms into the rare biaxial nematic phase under the influence of a magnetic field. Alignment of the particles' L-axes in the field breaks the symmetry of the N_- phase which leads to the formation of the N_B phase. Again, one has to realize that the induced N_B phase in a 3 mT magnetic field has very weak biaxial ordering; the corresponding biaxial order parameter (not shown) increases with increasing field strength.

4.6 Conclusions & Outlook

Using SAXS we observed that goethite particles in the N_B phase lose their biaxial ordering upon applying a magnetic field along the main director of the N_B phase. The extent of the loss of biaxial ordering strongly depends on the strength of the magnetic field. The field-induced N_B to N_+ transition can be understood in terms of the entropy balance that drives lyotropic liquid crystal formation. The stability of the N_B phase can be interpreted as a balanced competition between rod-like (N_+) and plate-like (N_-) behaviour. The interaction of the applied magnetic field with the permanent magnetic moment along the L-axis of the particles substantially narrows the orientation distribution function which describes the orientation of the particles. 'Fixing' the L-axis of the particles in the field releases more space for the particles to rotate freely along their L-axis. This increases the orientational entropy and pushes the particles towards N_+ ordering.

We additionally found that the extent of the loss of biaxial ordering strongly depends on the goethite volume fraction ϕ_g. At high volume fractions the field-induced observed decrease in biaxiality is significantly less; and is even negligible for sufficiently high ϕ_g. This can be explained by the excluded-volume entropy that favours N_B ordering and whose contribution to the total entropy strongly increases with increasing volume fraction.

The loss of biaxial ordering persists up to a field strength of B ≈ 160 mT. For higher magnetic fields strengths, closer to B^*, the biaxial order was found to increase again as a result of alignment of the particles' T-axes due to the increasing induced magnetic moment.

Theoretically the influence of a magnetic field was studied using a mean-field theory in which the magnetic properties of the particles were modelled by taking into account the effect of both the permanent and the induced magnetic dipoles. The theoretical results agree well with the experimental findings in spite of the approximations required. Moreover, polydispersity, which is known to have a sig-

nificant influence on goethite phase behaviour [15, 19, 28, 39], is not accounted for in the present analysis. Therefore the absolute values given in the theoretical phase diagrams and the order parameter plots presented in this paper are not expected to be quantitatively trustworthy. Nevertheless, the theory gives reliable qualitative predictions on the effect of the magnetic field on the phase behaviour of magnetic board-like particles.

Interestingly, the theory also predicts that the rare N_B phase can be formed upon applying a magnetic field to a N_- ordered phase of particles with a negative shape parameter. This magnetic-field induced N_B phase opens up new possibilities. Normally a very specific shape of (goethite) board-like particles is required ($L/W = W/T$) to create a biaxial nematic phase. There is a small N_B window around $\upsilon = 0$ that will be truncated by the smectic phase at higher volume fractions [40]. However, the shape of the particles is an experimental parameter that is hard to tune [41]. Our new findings predict that the rare N_B phase can easily be induced by applying a magnetic field with a carefully chosen field strength to a N_- phase. The magnetic field strength is a parameter that is easy to tune and the field-induced N_- to N_B transition is not limited to the goethite system presented here. Our theoretical work implies that for any system of board-like particles that carry a magnetic (or electric) dipole along their longest axis and favours N_- ordering in zero field, the N_B phase can be induced by applying a weak magnetic (or electric) field.

It is also worth mentioning that our theoretical model indicates that it is not necessarily true that the T-axis aligns in a strong magnetic field because it is the magnetic easy axis, which has generally been assumed [21, 22, 24-26]. This assumption was always made from the experimental observation that goethite particles in the *nematic* phase align along T in a strong magnetic field. However, in the nematic phase other factors like the excluded volume entropy have a strong influence on the alignment of the particles. The theoretical work presented in this paper shows that even when the magnetic susceptibilities along W and T are equal, particles align along T since alignment along W is strongly suppressed due to the excluded volume interactions. For future work it is therefore interesting, although challenging, to investigate the alignment of particles in very dilute suspensions to exclude the effects of multiple-particle interactions.

To summarize, the results presented in this paper show that a magnetic field is a useful 'tool' to control nematic phases of board-like particles. Carefully choosing the volume fraction and the magnetic field strength, parameters that are both easy to tune, enables the formation of the N_B phase (out of N_-) as well as the N_+ phase (out of N_B). Additionally, Belli *et al*. [20] already theoretically predicted that the addition of a depletant can induce both the N_B and N_- phase in systems of board-like particles with a positive shape parameter. Both options open up possibilities to engineer the desired character of the nematic phase for a range of particle shapes. This is especially useful since the rare biaxial nematic phase can now be induced.

Acknowledgements
The work in this chapter is done in collaboration with Simone Belli, who is greatly acknowledged for his theoretical contribution to this chapter. Additionally we would like to thank the staff of the BM26 beamline "DUBBLE" at the ESRF, as well as Vera Meester and Antara Pal for their support during the synchrotron experiments.

References
[1] D. K. Yang and S. T. Wu, in *Fundamentals of Liquid Crystal Devices*, Wiley, 2006, p. 378.
[2] J. C. P. Gabriel and P. Davidson, *Adv. Mater.*, 2000, **12**, 9.
[3] H. N. W. Lekkerkerker and G. J. Vroege, *Philos. T. R. Soc. A*, 2013, **371**, 20120263.
[4] L. Onsager, *Ann. N. Y. Acad. Sci.*, 1949, **51**, 627-659.
[5] M. J. Freiser, *Phys. Rev. Lett.*, 1970, **24**, 1041.
[6] R. Alben, *Phys. Rev. Lett.*, 1973, **30**, 778-781.
[7] J. P. Straley, *Phys. Rev. A*, 1974, **10**, 1881-1887.
[8] P. I. C. Teixeira, A. J. Masters and B. M. Mulder, *Mol. Cryst. Liq. Cryst. Sci. Technol. Sect. A-Mol. Cryst. Liq. Cryst.*, 1998, **323**, 167-189.
[9] B. Mulder and T. Ruijgrok, *Physica A*, 1982, **113**, 145-167.
[10] R. van Roij and B. M. Mulder, *J. Phys. II*, 1994, **4**, 1763-1769.
[11] L. J. Yu and A. Saupe, *Phys. Rev. Lett.*, 1980, **45**, 1000-1003.
[12] J. Lee, T. Lim, W. Kim and J. Jin, *J. Appl. Phys.*, 2007, **101**, 034105.
[13] Y. Galerne, A. Neto and L. Liebert, *J. Chem. Phys.*, 1987, **87**, 1851-1855.
[14] E. van den Pol, A. V. Petukhov, D. M. E. Thies-Weesie, D. V. Byelov and G. J. Vroege, *Phys. Rev. Lett.*, 2009, **103**, 258301.
[15] E. van den Pol, A. A. Verhoeff, A. Lupascu, M. A. Diaconeasa, P. Davidson, I. Dozov, B. W. M. Kuipers, D. M. E. Thies-Weesie and G. J. Vroege, *J. Phys.: Condens. Matter*, 2011, **23**, 194108.
[16] E. van den Pol, D. M. E. Thies-Weesie, A. V. Petukhov, D. V. Byelov and G. J. Vroege, *Liq. Cryst.*, 2010, **37**, 641-651.
[17] J. P. F. Lagerwall and G. Scalia, *Curr. Appl. Phys.*, 2012, **12**, 1387-1412.
[18] P. Camp and M. Allen, *J. Chem. Phys.*, 1997, **106**, 6681-6688.
[19] S. Belli, A. Patti, M. Dijkstra and R. van Roij, *Phys. Rev. Lett.*, 2011, **107**, 148303.
[20] S. Belli, M. Dijkstra and R. van Roij, *J. Phys.: Condens. Matter*, 2012, **24**, 284128.
[21] B. Lemaire, P. Davidson, J. Ferre, J. Jamet, P. Panine, I. Dozov and J. Jolivet, *Phys. Rev. Lett.*, 2002, **88**, 125507.
[22] B. Lemaire, P. Davidson, D. Petermann, P. Panine, I. Dozov, D. Stoenescu and J. Jolivet, *Eur. Phys. J. E*, 2004, **13**, 309-319.
[23] B. Lemaire, P. Davidson, J. Ferre, J. Jamet, D. Petermann, P. Panine, I. Dozov and J. Jolivet, *Eur. Phys. J. E*, 2004, **13**, 291-308.
[24] B. Lemaire, P. Davidson, J. Ferre, J. Jamet, D. Petermann, P. Panine, I. Dozov, D.

Stoenescu and J. Jolivet, *Faraday Discuss.*, 2005, **128**, 271-283.
[25] E. van den Pol, A. Lupascu, M. A. Diaconeasa, A. V. Petukhov, D. V. Byelov and G. J. Vroege, *J. Phys. Chem. Lett.*, 2010, **1**, 2174-2178.
[26] E. van den Pol, A. V. Petukhov, D. V. Byelov, D. M. E. Thies-Weesie, A. Snigirev, I. Snigireva and G. J. Vroege, *Soft Matter*, 2010, **6**, 4895-4899.
[27] E. van den Pol, A. Lupascu, P. Davidson and G. J. Vroege, *J. Chem. Phys.*, 2010, **133**, 164504.
[28] E. van den Pol, D. M. E. Thies-Weesie, A. V. Petukhov, G. J. Vroege and K. Kvashnina, *J. Chem. Phys.*, 2008, 129, 164715.
[29] W. Bras, I. Dolbnya, D. Detollenaere, R. van Tol, M. Malfois, G. Greaves, A. Ryan and E. Heeley, *J. Appl. Crystallogr.*, 2003, **36**, 791-794.
[30] K. Shundyak and R. van Roij, *Phys. Rev. E*, 2004, **69**, 041703.
[31] R. Zwanzig, *J. Chem. Phys.*, 1963, **39**, 1714.
[32] R. Evans, *Adv. Phys.*, 1979, **28**, 143-200.
[33] S. Lee, *J. Chem. Phys.*, 1987, **87**, 4972-4974.
[34] S. Lee, *J. Chem. Phys.*, 1988, **89**, 7036-7037.
[35] J. Parsons, *Phys. Rev. A*, 1979, **19**, 1225-1230.
[36] E. van den Pol, *Goethite liquid crystals and magnetic field effects*, Utrecht University, 2010.
[37] B. M. Mulder, *Phys. Rev. A*, 1989, **39**, 360-370.
[38] A. R. Khokhlov and A. N. Semenov, *Macromolecules*, 1982, **15**, 1272-1277.
[39] A. B. G. M. Leferink op Reinink, E. van den Pol, D. V. Byelov, A. V. Petukhov and G. J. Vroege, *J. Phys.: Condens. Matter*, 2012, **24**, 464127.
[40] M. Taylor and J. Herzfeld, *Phys. Rev. A*, 1991, **44**, 3742-3751.
[41] D. M. E. Thies-Weesie, J. P. de Hoog, M. H. H. Mendiola, A. V. Petukhov and G. J. Vroege, *Chem. Mat.*, 2007, **19**, 5538-5546.

5

Alignment pathway of the goethite columnar liquid cyrstal phase studied by SAXS

The alignment of board-like goethite particles in the dense rectangular centred columnar liquid crystal phase in an external magnetic field is studied using small angle x-ray scattering (SAXS). Transient SAXS-patterns show broadening of the columnar reflections in specific directions. While the reflections along the field stay at a constant Q-value, the other reflections do not. These results imply a certain pathway of reorientation. It appears that alignment proceeds via collective rotation of domains inducing 'nanoshear' between the layers of particles, which slide over each other. The results support the recently suggested martensitic transition pathway for the simple and centred rectangular columnar phases, which were found to spontaneously transform into each other in another goethite system. The results also provide a fine example of how SAXS can be used to study reorientation behaviour of liquid crystals at the nanoscale.

5.1 Introduction

When dispersed in a fluid, anisometric colloidal particles form complex fluids with remarkable properties. For example, their advanced rheological properties such as high yield stress and strong shear thinning are of interest for numerous applications and have been studied in detail for both rod-like [1] and plate-like particles [2, 3]. Anisometric colloidal particles in suspension are also able to self-organize into various liquid crystalline phases including isotropic (*I*), nematic (*N*), smectic (*S*) and columnar (*C*) phases [4].

Until now a rich variety of liquid crystalline phases was reported in suspensions of plate-like [5-8] and rod-like [9, 10] particles.

These lyotropic liquid crystals are very susceptible to external fields and have a high thermal stability. A remarkable example displaying unique properties is provided by suspensions of board-like goethite particles (α-FeOOH) which were found to form *N* as well as *S* and *C* phases. The inherent polydispersity of the particles surprisingly does not suppress, but actually enhances the phase behaviour (Chapter 2). It was found to induce the columnar phase, which is only found in polydisperse (>20%) goethite - coexisting with a smectic phase - and acts as a 'waste bin' for the particles that do not fit the smectic periodicity [11, 12].

In addition goethite particles also have peculiar magnetic properties [13]; they possess a permanent magnetic moment along their longest axis and an induced magnetic moment with its easy axis perpendicular to the permanent moment. Therefore particles in suspension align their long axis parallel to a small magnetic field but reorient to align their shortest axis parallel to a strong magnetic field (with B^* the critical field strength where particles realign from parallel to perpendicular to the field, see also Chapter 4). These alignment and reorientation phenomena open wide possibilities for easy manipulation of the liquid crystal phases by an external magnetic field (Chapter 4). It has been shown that a strong magnetic field induces formation of the columnar phase; both the $N \rightarrow C$ and $S \rightarrow C$ reversible transitions have been observed [11, 14].

The particle properties of goethite can be changed by partially substituting iron by different elements (Chapter 2, Chapter 43 and ref. [15]). For example chromium-modified goethite shows similar phase behaviour but has a higher B^*. Moreover, two types of columnar structures, centred rectangular columnar (R_C) and simple rectangular columnar (R_S), have been observed [16]. The two columnar structures can spontaneously transform into each other but this martensitic transition between them can also be induced by a magnetic field (Chapter 2, [17]).

Small angle x-ray scattering (SAXS) is a key technique in characterizing the static liquid crystal structures of colloidal particles, whether or not formed spontaneously or induced by a magnetic field. Here we show that SAXS is also a powerful technique to study alignment pathways by studying the reorientation behaviour of the goethite columnar phase in a strong magnetic field. Deformed transient SAXS-patterns suggest the presence of specific deformations induced by microscopic local shear

between layers of particles. These new insights are similar to the martensitic R_S - R_C pathway that was suggested earlier (ref. [17] and Chapter 2).

5.2 Experimental

5.2.1 Synthesis, characterization & sample preparation

Experiments were performed on two different goethite dispersions, dispersion **g1** and dispersion **g2**. Dispersion **g1** consists of the same goethite particles as described in section 4.2.1. These particles have dimensions L x W x T = 254 x 83 x 28 nm with a polydispersity of ~25% in all directions.

The goethite particles for dispersions **g2** were synthesized following the same protocol as for the **g1** particles (according to the method described in section 4.2.1). The **g2** particles have slightly different dimensions of L x W x T = 282 x 68 x ~25 nm with an overall polydispersity of ~35%.

Flat glass capillaries with internal dimensions of 0.2 x 4.0 x 100 mm^3 were filled with dispersions **g1** and **g2** with initial goethite volume fractions of 10.6 and 5.2%, respectively. The capillaries were flame-sealed and stored in upright position.

5.2.2 Small angle x-ray scattering

SAXS measurements were performed to study the liquid crystalline phase behaviour and the orientation dynamics in an external magnetic field. These measurements were performed at the BM-26 DUBBLE beamline of the European Synchrotron Radiation Facility (ESRF, Grenoble, France) [18], using the microradian resolution setup developed by Petukhov *et al*. [19]. The selected energy of the x-ray beam was 12.4 keV. Two different CCD detectors (both Photonic Science) were used, one with a pixel size of 22 μm x 22 μm and one with a pixel size of 9 μm x 9 μm. Both detectors were placed at a distance of 7 m from the sample. A variable permanent magnet (from the ID02 beamline) was used, which uses two stacks of NdFeB permanent magnets to generate magnetic fields up to 1.5 T by adjusting the distance between the NdFeB stacks.

5.3 Results and Discussion

First we present observations in a capillary filled with goethite dispersion **g1** with an initial volume fraction of 10.6%. The sample was allowed to sediment for almost six years during which an equilibrium density profile was formed. Despite careful gluing of the capillary the solvent slowly evaporated, the overall volume fraction at the moment of measuring was estimated to be 25%. Before a magnetic field was applied, SAXS measurements were done at different positions along the vertical direction of the capillary to determine the different liquid crystal structures that were formed. The measurements revealed rich phase behaviour: from the top to the

bottom of the capillary respectively an isotropic, nematic, smectic and a columnar phase coexisting with a smectic phase were found.

The columnar phase was monitored while a stepwise increasing magnetic field was applied. The magnetic field was perpendicular to the x-ray beam. Fig. 5.1(a) shows the SAXS pattern of the columnar phase coexisting with the smectic phase in a weak field of 3 mT, which is the weakest field achievable for this set up with the magnet poles at maximum spacing. The dense columnar phase does not respond to such a low field, hence this pattern can be considered as without field. The pattern shows the 11 and 20 reflections, at Q = 0.083 and 0.139 nm^{-1}, respectively, characteristic of the centred rectangular columnar phase with unit cell dimensions of 119 by 90 nm as illustrated in Fig. 5.1(c). The reflections appear as 'rings', indicating that there are numerous columnar domains with different orientations. The weak 02 reflection is not visible in this pattern but was observed with increased exposure time. This reflection is weak since it is in the vicinity of the form factor minimum. The bright reflections observed at small angles originate from the interlayer periodicity from an adjacent smectic domain.

The columnar reflections were undisturbed up to a magnetic field strength of ~300 mT, which is approximately 50 mT above the critical magnetic field strength B^*. At higher field strengths – where the particles will align their shortest axis T parallel to the field – the columnar reflections slowly started to change. The SAXS pattern of the columnar phase at 440 mT is shown in Fig. 5.1(b). The intensity of the 11 and 20 columnar reflections is increasing in specific directions, meaning that the different domains have started to reorient in the field. While some columnar domains grow, other domains, that are unfavourable in the magnetic field, melt. This effect is increasing with increasing magnetic field strength. Fig. 5.1(d) shows the SAXS pattern of the R_C phase after 30 minutes in a strong magnetic field of 1.4 T. Indeed, the R_C columnar reflections are now found in certain directions only, meaning that a large single columnar domain is formed. Highly interesting is the deformation of the 11 reflection which is broadened and is more rod- rather than arc-like, which is emphasized by the dashed circle at fixed scattering vector (Q). It therefore appears that the 11 reflection has broadened and can now be found over a small range of Q-values varying from 0.078 to 0.087 nm^{-1}, which includes values both larger and smaller than the original Q-value. In contrast, the 20 reflection along the field is found at the fixed Q-value of 0.139 nm^{-1}, hence the d_{20} spacing is undisturbed.

The observed broadening of the 11 reflection suggests certain deformations within the columnar domains, which presumably arise during the reorientation process. In general, the alignment of ordered phases in an external field can proceed via various scenarios. For example, it can involve growth of favoured domains at the expense of domains with incorrect orientation. Alternatively, reorientation can involve collective rotation of domains to attain the proper orientation. Previous studies have revealed rather complex reorientation pathways of smectic domains in thermotropic [20] and lyotropic [21] liquid crystals.

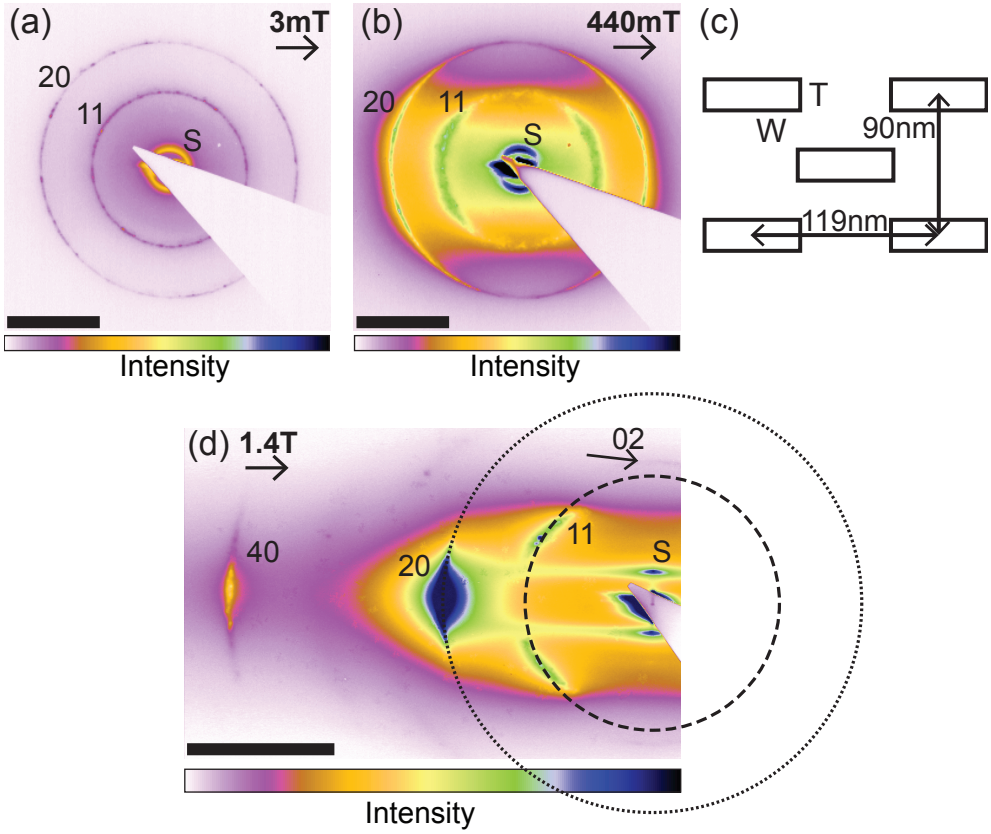

Fig. 5.1 (a) SAXS pattern of the multidomain centred rectangular (R_C) phase before the strong magnetic field was applied showing the 20 and 11 columnar reflections. (b) Transient SAXS-pattern of the R_C columnar phase in a field of 440 mT. The columnar reflections are more pronounced in the direction along the magnetic field. (c) Schematic drawing of the R_C unit cell with dimensions of 199 by 90 nm. (d) Deformed transient SAXS pattern of the R_C phase in a field of 1.4 T. The 11 reflection is rod-like and can be found at different Q-values which is emphasized by the smallest circle which is at fixed Q from the centre. The 20 reflection remains at a constant Q-value. In all three scattering patterns, reflections from the smectic phase can be observed as well, they are denoted with "S". Black arrows indicate the direction of the magnetic field. The black bars denote 0.1 nm^{-1}.

The data presented in Fig. 5.1 can shed some light on the reorientation pathway of the columnar liquid crystalline domains. The peculiar peak broadening can be understood as a result of collective rotation of domains in a viscous environment created by other domains. The interactions between the particles and the magnetic field will generate a torque applied to each particle and, via the interparticle interactions, to the whole domain. During rotation a domain will experience a shear field, applied opposite to the rotation direction. As a result of the applied shear, the

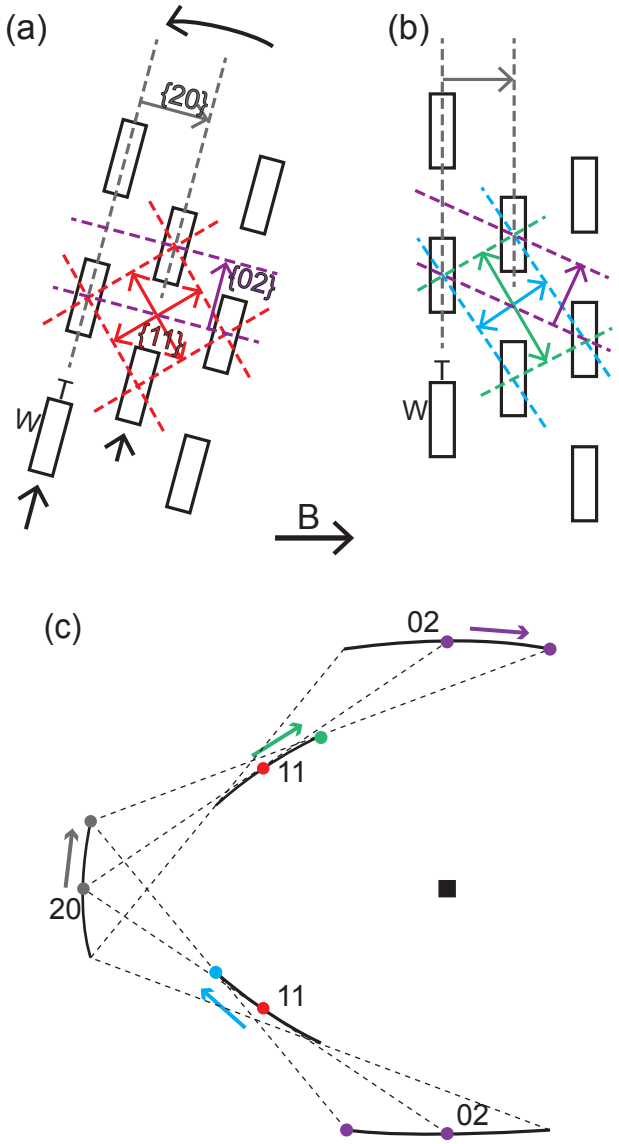

Fig. 5.2 (a) Schematic drawing of the R_C phase and its characteristic distances. The top black arrow indicates the reorientation direction of the structure induced by the B-field. The two black arrows at the bottom represent the subsequent sliding of the {20} planes over each other. (b) Schematic drawing of the transient deformed columnar phase in the B-field. The distance between the {11} crystal planes has changed and is both larger (green lines) and smaller (blue lines) than the original distance. *W* and *T* in the schematic drawings represent the width and thickness of the particles. (c) Schematic drawing of the expected SAXS pattern for the transient columnar phase shown in (b). The same colours are used for the changes in the 11, 20 and 02 reflections respectively as in (a) and (b).

{20} crystal planes can slightly slide relative to each other leading to a deformed crystal structure, as schematically illustrated in Fig. 5.2(a, b). Fig. 5.2(b) clearly shows how the spacing between the {11} crystal planes has changed and is now larger (green lines) in one specific direction and smaller (blue lines) perpendicular to that direction than the original spacing. Note that the deformation in Fig. 5.2(b) is slightly exaggerated compared to true experimental values as Fig. 5.2(b) is meant to illustrate the principle. For a domain approaching the most favourable orientation from another direction, the applied shear field will result in a similar deformation but applied in a different direction. At the moment of observation different domains possess a different degree of deformation. Their ensemble then produces the peculiar broadening seen in Fig. 5.1(d). The spacing between the {20} planes remains the same. The {02} distance also changes but the effect is less pronounced than for the {11} crystal planes.

The expected SAXS pattern for this type of deformed structure (Fig. 5.2(b)) is schematically drawn in Fig. 5.2(c). The 11 reflection (red) is split and shifts to Q-values both larger (blue) and smaller (green) than the original value, whereas the 20 reflections (grey) along the magnetic field remain at fixed Q. Similar to the 11 reflection, the 02 reflection can be found at range of different Q-values but this range is considerably smaller than for the 11 reflection. This schematic pattern indeed corresponds to the observed SAXS pattern in Fig. 5.1(d). The 02 reflections can be seen in the SAXS pattern but are still weak due to the proximity of the form factor minimum. However, these reflections were properly observed in measurements with longer exposure times. This confirms the reorientation pathway in which the magnetic field induced nanoshear induces the layers of columns to slide over each other.

The specific broadening of the 11 reflection observed in the SAXS pattern (Fig. 5.1(d)) obtained in this sample was also observed in a capillary with goethite dispersion **g2** (Fig. 5.3(b)) when similar experiments were performed. The observed behaviour illustrates a typical phenomenon that is frequently observed in the goethite columnar phase in an external magnetic field.

The **g2** sample of which the patterns are shown in Fig. 5.3 had been sedimenting for roughly 3.5 years. The patterns were taken 0.5 mm above the bottom of the capillary (where the osmotic pressure is high). Fig. 5.3(a) shows the SAXS pattern before the strong magnetic field was applied. The 11 and 20 reflections characteristic of the centred rectangular columnar (R_C) phase can be observed up to the 2nd order. This pattern was taken with a lower exposure time, hence the 02 reflections are not visible. Also here the magnetic field was applied perpendicular to the x-ray beam and the field strength was stepwise increased up to 1.5 T. Fig. 5.3(b) shows the SAXS pattern taken approximately 30 minutes after the magnetic field reached a strength of 1.5 T. Like for the **g1** sample, the 11 reflection is smeared out over a range of Q-values while the 20 reflection remains at a fixed Q. The range of Q-values

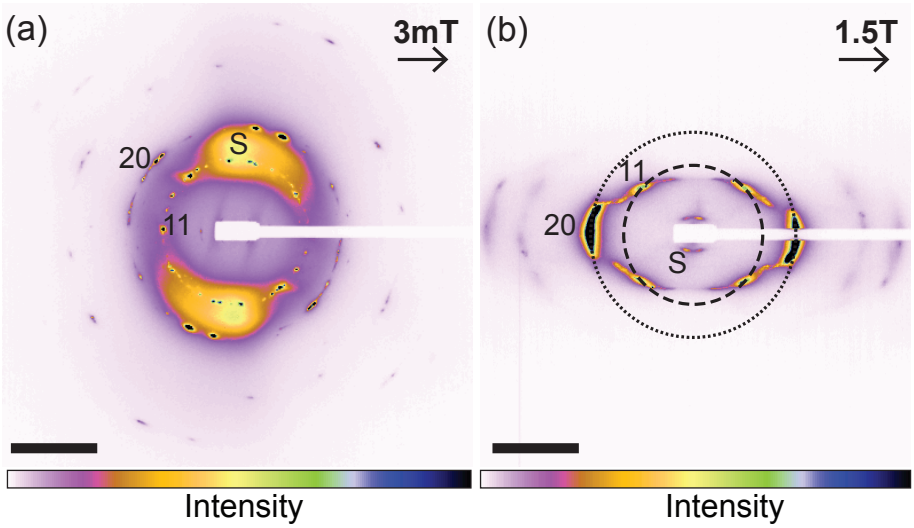

Fig. 5.3 (a) SAXS pattern of the multidomain centred rectangular (R_C) phase before the strong magnetic field was supplied showing the 11 and 20 columnar reflections. (b) Transient SAXS pattern of the R_C phase in a field of 1.5 T. The 11 reflection is rod-like and smeared out over a range of Q-values, as is emphasized by the dashed circle, whereas the 20 reflection remains at fixed Q (emphasized by dotted circle). Reflections labelled S originate from the smectic intra-(a) and interlayer (b) reflections. Black arrows indicate the direction of the applied magnetic field. The black bars denote 0.1 nm^{-1}.

at which the 11 reflection can be found appears to be larger in the **g2** sample than in the **g1** sample. This indicates that in this sample the deformation of the crystal structure, due to the field-induced shear between the layers of particles, is even more pronounced.

The SAXS patterns in Fig. 5.1 and Fig. 5.3 also show reflections from the smectic phase. This smectic phase transforms (for the greater part) into the columnar phase in the strong magnetic field. The field-induced $S \rightarrow R_C$ transition follows a complex mechanism and is partly described in the paper by Van den Pol *et al*. [21]. The smectic and columnar phases are in adjacent macroscopic domains and it is therefore assumed that the influence of the evolution of the smectic phase on the reorientation of the columnar phase is negligible.

Chapter 2 in this thesis describes a study on a sample of chromium-modified goethite to which magnetic fields were applied over time. In this study it was observed that the R_S and R_C columnar phases transform into each other via a martensitic transition. A closer look at the structures predicted a shear induced transition pathway (Chapter 2, ref. [17]). This prediction is now supported by the new information presented in this work, which suggests a very similar scenario. The fact that the R_C phase is more often observed experimentally suggests that the R_S phase is probably a metastable structure. The present data suggest that the deformations induced by

local shear can promote a transition to the metastable R_S structure.

It is also worth noticing that the connection between micro-rheological properties of complex fluids with their macroscopic viscosity can be rather non-trivial [22, 23]. Although the micro-rheology methods were not applied in the present study, the results show that transient SAXS patterns are able to reveal the local deformations at the nanoscale in response to a microscopic shear. The method is not limited to our goethite system and can be applied to various types of complex colloidal fluids and applied forces. An advantage of using SAXS is that there is no need to use tracer particles or to adapt the colloids, like fluorescently label them, which is necessary for popular micro-rheology techniques [22]. Therefore, SAXS might be an additional technique, which is able to complement the micro-rheological studies of complex colloidal fluids. E.g. for suspensions of plate-like clay particles [7, 24] as well as rod-like virus particles [25] it is reported that the local structure determined by SAXS could be connected to the systems' rheological properties. In this work we did not specifically study temporal dynamics. Normally, patterns were measured some minutes after application of the field. The rotation process was shorter than that. However relaxation of the structural deformations is much longer since the patterns shown in Fig. 5.1(d) and Fig. 5.3(b) did not change significantly on the scale of an hour. Future studies can therefore include more detailed observations of real-time reorientation dynamics.

5.4 Conclusions

We have studied the reorientation behaviour of the goethite columnar phase in a strong external magnetic field using SAXS. It was found that during reorientation the magnetic field induces shear between the layers which makes them slide over each other. The SAXS pattern of the resulting transient deformed columnar crystal structure shows broadening of the columnar reflections in specific directions. The reflections along the field stay at constant Q-value, whereas other reflections do not. With these new observations we support the shear induced transition pathway which was proposed in Chapter 2 for the R_S – R_C martensitic transition in chromium-modified goethite [17].

Furthermore, we showed that SAXS is a useful technique not only for characterization of static crystal structures but can also be used to study alignment pathways and orientation dynamics at the nanoscale.

Acknowledgements

Esther van den Pol is acknowledged for her contribution to this chapter. Again, we would like to thank the staff of the BM26 beamline at the ESRF, in particular Giuseppe Portale and Dirk Detollenaere for support and NWO for provided beamtime. We would also like to thank Dmytro Byelov for his help during the SAXS measure-

ments and Ivan Dozov and Patrick Davidson for useful discussions.

References

[1] M. Ripoll, P. Holmqvist, R. G. Winkler, G. Gompper, J. K. G. Dhont and M. P. Lettinga, *Phys. Rev. Lett.*, 2008, **101**, 168302.
[2] M. P. Lettinga, P. Holmqvist, P. Ballesta, S. Rogers, D. Kleshchanok and B. Struth, *Phys. Rev. Lett.*, 2012, **109**, 246001.
[3] D. Kleshchanok, V. Meester, C. E. Pompe, J. Hilhorst and H. N. W. Lekkerkerker, *J. Phys. Chem. B*, 2012, **116**, 9532-9539.
[4] J. C. P. Gabriel and P. Davidson, *Adv. Mater.*, 2000, **12**, 9.
[5] E. Paineau, K. Antonova, C. Baravian, I. Bihannic, P. Davidson, I. Dozov, M. Imperor-Clerc, P. Levitz, A. Madsen, F. Meneau and L. J. Michot, *J. Phys. Chem. B*, 2009, **113**, 15858-15869.
[6] F. van der Kooij, K. Kassapidou and H. Lekkerkerker, *Nature*, 2000, **406**, 868-871.
[7] J. O. Fossum, *Eur. Phys. J.- Spec. Top.*, 2012, **204**, 41-56.
[8] J. Fossum, E. Gudding, D. Fonseca, Y. Meheust, E. DiMasi, T. Gog and C. Venkataraman, *Energy*, 2005, **30**, 873-883.
[9] Z. Dogic, K. Purdy, E. Grelet, M. Adams and S. Fraden, *Phys. Rev. E*, 2004, **69**, 051702.
[10] Z. Zhang and J. van Duijneveldt, *J. Chem. Phys.*, 2006, **124**, 154910.
[11] G. J. Vroege, D. M. E. Thies-Weesie, A. V. Petukhov, B. J. Lemaire and P. Davidson, *Adv. Mater.*, 2006, **18**, 2565.
[12] E. van den Pol, D. M. E. Thies-Weesie, A. V. Petukhov, G. J. Vroege and K. Kvashnina, *J. Chem. Phys.*, 2008, **129**, 164715.
[13] B. Lemaire, P. Davidson, J. Ferre, J. Jamet, P. Panine, I. Dozov and J. Jolivet, *Phys. Rev. Lett.*, 2002, **88**, 125507.
[14] B. Lemaire, P. Davidson, P. Panine and J. Jolivet, *Phys. Rev. Lett.*, 2004, **93**, 267801.
[15] E. van den Pol, D. M. E. Thies-Weesie, A. V. Petukhov, P. Panine and G. J. Vroege, *J. Phys.: Condens. Matter*, 2008, **20**, 404219.
[16] E. van den Pol, A. V. Petukhov, D. M. E. Thies-Weesie and G. J. Vroege, *Langmuir*, 2010, **26**, 1579-1582.
[17] A. B. G. M. Leferink op Reinink, E. van den Pol, D. V. Byelov, A. V. Petukhov and G. J. Vroege, *J. Phys.: Condens. Matter*, 2012, **24**, 464127 (Chapter 2 of this thesis).
[18] W. Bras, I. Dolbnya, D. Detollenaere, R. van Tol, M. Malfois, G. Greaves, A. Ryan and E. Heeley, *J. Appl. Crystallogr.*, 2003, **36**, 791-794.
[19] A. Petukhov, J. Thijssen, D. t Hart, A. Imhof, A. van Blaaderen, I. Dolbnya, A. Snigirev, A. Moussaid and I. Snigireva, *J. Appl. Crystallogr.*, 2006, **39**, 137-144.
[20] P. D. Brimicombe, S. D. Siemianowski, S. Jaradat, Y. K. Levine, P. Thompson, W. Bras and H. F. Gleeson, *Phys. Rev. E*, 2009, **79**, 031706.

[21] E. van den Pol, A. V. Petukhov, D. V. Byelov, D. M. E. Thies-Weesie, A. Snigirev, I. Snigireva and G. J. Vroege, *Soft Matter*, 2010, **6**, 4895-4899.
[22] A. Mukhopadhyay and S. Granick, *Curr. Opin. Colloid Interface Sci.*, 2001, **6**, 423-429.
[23] A. Kozina, P. Diaz-Leyva, C. Friedrich and E. Bartsch, *Soft Matter*, 2012, **8**, 1033-1046.
[24] I. Bihannic, C. Baravian, J. F. L. Duval, E. Paineau, F. Meneau, P. Levitz, J. P. de Silva, P. Davidson and L. J. Michot, *J. Phys. Chem. B*, 2010, **114**, 16347-16355.
[25] J. Dhont, M. Lettinga, Z. Dogic, T. Lenstra, H. Wang, S. Rathgeber, P. Carletto, L. Willner, H. Frielinghaus and P. Lindner, *Faraday Discuss.*, 2003, **123**, 157-172.

PART 2

GIBBSITE

6

3D structure of nematic and columnar phases of gibbsite platelets

We present small angle x-ray scattering data of single-domain nematic and columnar liquid crystal phases in suspensions of sterically stabilized gibbsite platelets. The measurements are performed with different sample orientations to obtain information about the 3D structure of the liquid crystalline phases. With the x-ray beam incident along the director of the nematic phase a strong correlation peak is observed corresponding to the side-to-side interparticle correlations, which suggests a columnar nematic structure. Upon sample rotation this side-to-side correlation peak of the nematic shifts to higher Q-values suggesting the presence of strong fluctuations of small stacks of particles with different orientations while the overall particle orientation is constant. In the hexagonal columnar phase clear Bragg inter-columnar reflections are observed. Upon rotation, the Q-value of these reflections remains constant while their intensity monotonically decreases upon rotation. This indicates that the column orientation fluctuates together with the particle director in the columnar phase. This difference between the behaviour of the columnar and the nematic reflections upon sample rotation is used to assign the liquid crystal phase of a suspension consisting of larger platelets, where identification can be ambiguous due to resolution limitations.

6.1 Introduction

Suspensions of anisotropic colloidal particles, such as rods and platelets, show rich phase behaviour involving nematic (*N*), smectic (*S*) and columnar (*C*) lyotropic liquid crystalline states. The first observations of the *N* phase were already made in 1925 by Zocher of spontaneously self-organizing ribbon-like vanadium pentoxide (V_2O_5) particles [1]. Later *N* phases were also found to occur in suspensions of tobacco mosaic virus [2, 3], goethite rods [4] and clay plate-like particles [5]. Nowadays a rich variety of different liquid crystalline phases are reported in suspensions of rod-like [6-8], board-like [9, 10] and plate-like particles [11-21]. For the plate-like particles these include the observations of the *I* - *N* phase transition in suspensions of mixed metal hydroxides [15], F-hectorite [16], nontronite [13] and beidellite [14], as well as the observation of the *I* - *C* phase transition in nickel hydroxides [11] and the occurrence of the *I* - *S* phase transition in extended sheet materials [12].

Several techniques are available to study liquid crystalline systems, ranging from polarized light microscopy [22, 23], (cryo) transmission and scanning electron microscopy (cryoTEM/SEM) [24], NMR [12, 25] and neutron scattering [26-28] to wide and small angle x-ray scattering (WAXS/SAXS) [28] and more recently, transmission x-ray microscopy (TXM) [29]. Of these methods, polarized light microscopy is most commonly used, as it reveals phase separation and indicates particle orientation. For structure characterization in the range of approximately of 5 to 500 nm SAXS has proven to be a powerful technique. Since the detailed atomic structure is irrelevant, scattering is sensitive only to the particle shape and their ordering.

Gibbsite (γ-$Al(OH)_3$) suspensions are a unique plate-like system as it displays a well-defined *I* - *N* - *C* phase separation [19]. It was extensively studied with polarized light microscopy and SAXS for both sterically and charge stabilized particles [19, 21, 24]. The hexagonally shaped disk-like particles have a thickness significantly smaller than the diameter. These can be synthesized with varied sizes using the seeded growth method [30] and it has been shown that 560 nm sized sterically stabilized gibbsite platelets are also able to form hexagonal columnar liquid crystals [31]. Larger particles have the advantage that they can be made visible with confocal microscopy but they are more challenging for x-ray scattering as resolution becomes an issue, due to disorder and size fractionation [21, 31, 32].

So far the SAXS measurements are usually reported with a single orientation of the sample which often coincides with the particle normal, due to anchoring at the container wall. A more profound characterisation of the 3D structure can be achieved by studying large single domain samples under various sample orientations. Moreover, for large particle systems this information is crucial for unambiguous phase identification.

In this article we show that characterization of the full 3D structure is an effective method to distinguish between different liquid crystalline phases especially when the resolution becomes an issue. In a system with small (~200 nm) platelets

the *N* phase with columnar nematic (N_C) structure and the *C* phase are studied in 3D. In the N_C structure small particle stacks are formed which have a stack axis that can fluctuate while the average particle normal remains constant. This decoupling causes a characteristic increase in the scattering vector Q upon rotation. In the *C* phase there is no decoupling hence Q remains constant when the sample is rotated. With the obtained information the technique is then applied to a system of larger platelets (~400 nm) and used to determine its 3D liquid crystal structure.

6.2 Experimental

6.2.1 Materials

Two different particle suspensions were used, one consisting of small and one of larger sterically stabilized gibbsite platelets referred to as system 1 (**S1**) and system 2 (**S2**), respectively. The **S1** hexagonal colloidal gibbsite platelets (γ-$Al(OH)_3$) were prepared from an acidic aqueous aluminium alkoxide solution, according to the procedure of Wijnhoven *et al*. [33]. The particles were subsequently grafted with end-functionalised polyisobutene and were dispersed in toluene [34]. For **S2** large particles were synthesized via the seeded growth method from small gibbsite platelets; a detailed description of the procedure is described in section 7.2.1 of this thesis. The particles obtained after five growth steps were grafted with polyisobutene and suspended in tetralin.

Transmission electron microscopy (TEM) was used to determine the surface area of over 200 particles for both systems. The particle diameter *D* was determined to be 232 nm for **S1** and 411 nm for **S2** with a polydispersity of 20% and 10% respectively. In solution the thickness of the stabilizing layer is expected to be 2-3 nm, giving effective diameters D_{eff} of 237 nm for **S1** and 416 nm for **S2** (Table 6.2).

Table 6.2 Properties of the different gibbsite systems **S1** and **S2**.

System	D_{eff} (nm)	σ (%)
S1	237	20
S2	416	10

6.2.2 Sample preparation

To promote the formation of large single columnar crystals non-adsorbing polymer (poly-dimethylsiloxane, M_w = 423 kDa) was added at a concentration of 0.8 g/l to a dispersion of **S1** with a volume fraction of 0.38 [21, 35]. The suspension was placed in a flat capillary with internal dimensions of 0.3 x 3 mm. For **S2** a home made flat capillary consisting of two coverslips (24 x 50 x 0.15 mm and 24 x 24 x 0.15 mm) glued together with internal dimensions of 0.15 x 20 mm was made and filled with a highly viscous suspension of **S2**. The capillaries were stored upright for a period

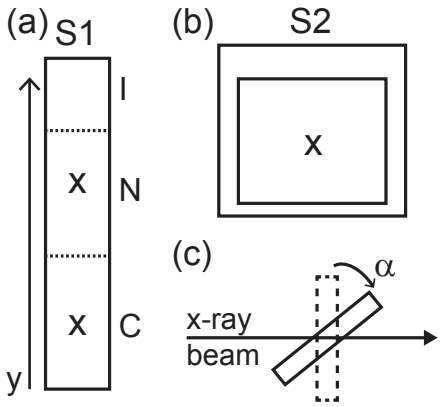

Fig. 6.1 Schematic representation of the sample cells of (a) **S1** and (b) **S2**. Crosses mark the positions in the samples where SAXS patterns were taken. (c) Illustration of sample rotation around y (seen from top).

of one year for **S1** and 40 days for **S2**, which allows the establishment of a gravity controlled profile of osmotic pressure in the samples. In Fig. 6.1 a schematic representation of the sample cells and the sedimentation profiles as observed between crossed polarisers is shown. In **S1** the *I* - *N* - *C* phase transitions were observed as indicated with the dotted lines. In **S2** birefringence was observed but the liquid crystal phase was unassigned.

6.2.3 Small angle x-ray scattering

X-ray studies were performed at the Dutch-Belgian beamline BM-26 DUBBLE [36] of the European synchrotron radiation facility (ESRF) in Grenoble, France using a microradian setup [20, 37]. The selected energy of the x-ray beam was 11 keV for **S1** and 13 keV for **S2**. The CCD detector used (Photonic Science) had a pixel size of 22 x 22 μm and was placed at a distance of 8 m from the sample. The sample cell was mounted perpendicular to the x-ray beam on remotely controlled, motorized translation and rotation stages. The samples were scanned along their y-axis and the measurements discussed in this article were done at the positions marked with a cross in Fig. 6.1(a, b). At these positions the sample was rotated around its y-axis over an angle α as shown in Fig. 6.1(c), in the range of 0° – 50°.

6.3 Results and Discussion

6.3.1 System 1 (S1)

In **S1** SAXS measurements were done at several positions along the y-axis. 3D measurements were performed at two positions, one in the domain determined to be nematic and one in the domain determined to be columnar at positions marked in

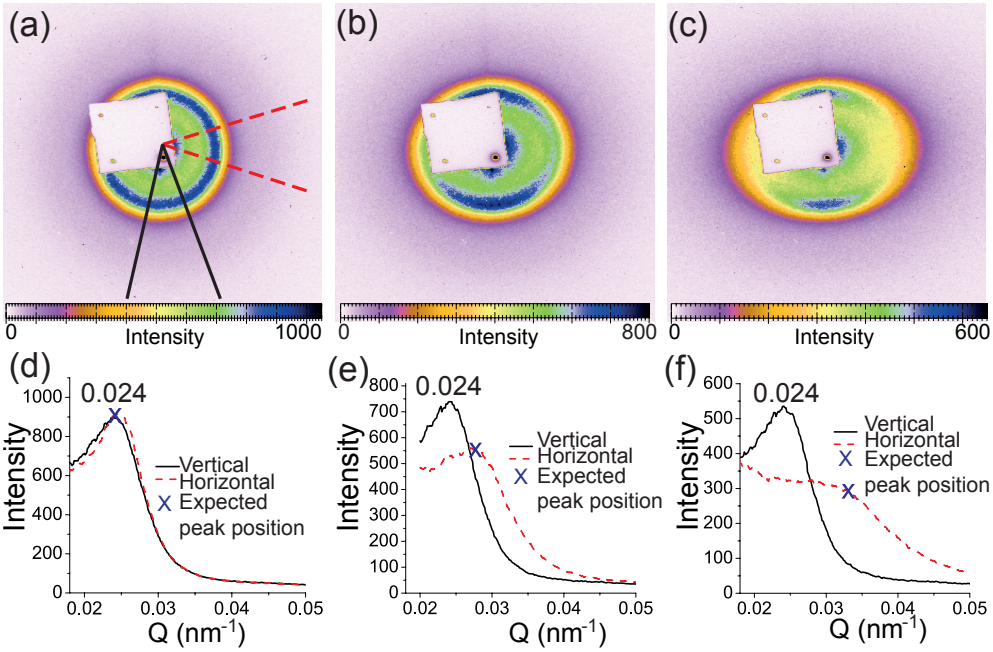

Fig. 6.2 High resolution SAXS-patterns of a single *N* domain with N_C structure in **S1** at α = (a) 0° (b) 30° and (c) 50° and (d-f) accompanying vertical and horizontal intensity profiles. Black en red lines in (a) show the areas of which intensity profiles were taken in the vertical and horizontal direction, respectively. Blue crosses mark the expected horizontal peak position for N_C, according to Q_0 / cos α. The direct beam was absorbed by a square-shaped lead beamstop.

Fig. 6.1(a). In the capillary the platelets will align flat against the glass wall; hence the x-ray beam is parallel to the platelet normal for α = 0°.

In Fig. 6.2 the SAXS diffraction patterns as well as the corresponding horizontal and vertical intensity profiles measured in the *N* domain are shown for α = 0°, 30° and 50°. Intensity profiles are obtained by integration of the pattern over the area between the black and red lines as shown in Fig. 6.2(a). The diffraction pattern measured at α = 0° (Fig. 6.2(a)) shows a broad ring-like reflection with a maximum at scattering vector Q = 0.024 nm^{-1} (Fig. 6.2(d)). This corresponds to a distance in real space of 262 nm, which is in the order of *D*. This broad and strong reflection indicates presence of pronounced side-to-side correlations, which is a signature of the columnar nematic structure (N_C) [38]. In this phase the platelets form short stacks that in turn display nematic ordering. As illustrated in Fig. 6.3(a), in these short stacks the lateral correlations between the particle positions give rise to a stack axis Ξ parallel to the particle normal ξ. This leads to strong side-to-side correlations and hence an intense scattering peak.

The patterns measured at α = 30° and 50° (Fig. 6.2(b, c), respectively) both show

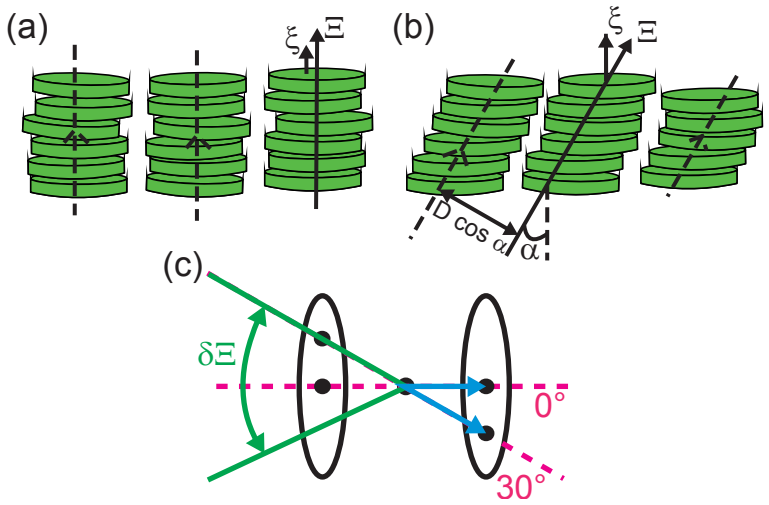

Fig. 6.3 Schematic representations of N_C structure where short particle stacks are formed where ξ and Ξ are (a) coupled and (b) decoupled due to the rotation of Ξ over an angle α causing the side-to-side correlation to be shorter according to D cos α and (c) top view representation of N_C reciprocal space and the broadening in side-to-side correlations due to δΞ variations (green lines). The intersections represent the observed patterns at α = 0° and α = 30° rotation resulting in a larger scattering vector (blue arrows).

elongation of the ring-like pattern and a decrease in intensity in the horizontal direction. As expected, the peak position in the vertical direction (along the rotation axis) remains the same, as is confirmed by the intensity profiles shown in Fig. 6.2(d, e).

The increase in Q suggests the presence of an apparent correlation length shorter than D when the structure is seen at an angle. This can be understood as follows: the stacks in the N_C phase can also be formed by platelets which are slightly shifted with respect to each other as illustrated in Fig. 6.3(b). While the average particle normal ξ is constant and approximately perpendicular to the capillary wall, the stack axes Ξ fluctuates and is as a result decoupled from ξ. When the structure is seen at angle α, the apparent side-to-side distance will then be D cos α.

Fig. 6.3(c) illustrates how the variation in the axes of the stacks δΞ broadens the side-to-side reflections in reciprocal space leading to an increase in Q via $Q_\alpha = Q_0 /$ cos α, with Q_a and Q_0 the scattering vectors measured at α and α = 0°, respectively. The expected peak positions for α = 30° and 50° are marked with a blue cross in the intensity profiles in Fig. 6.2(e, f) and correspond well to the measured peak maxima.

The SAXS pattern and corresponding intensity profile in the horizontal directions obtained in a large single columnar domain of approximately 8 mm in sample **S1** at

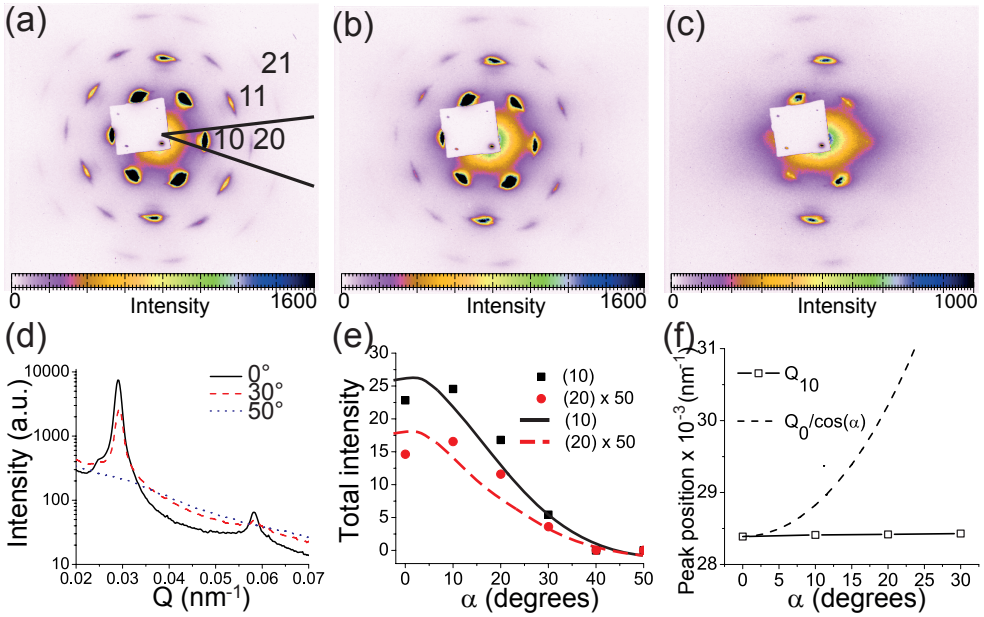

Fig. 6.4 High resolution SAXS-patterns of the **S1** *C* phase at α = (a) 0° (b) 30° and (c) 50°, with (d) accompanying intensity profiles. (e) Decrease in intensity for increasing α of the 10 and the 20 columnar reflections. Dots and squares represent experimental data, lines are a guide for the eye. (f) Positions of Q_{10} as determined for α and the expected position for a N_C structure. Black lines in (a) shows the area of which intensity profiles were taken. The direct beam was absorbed by a square-shaped lead beamstop.

α = 0° are shown in Fig. 6.4(a, d). Strong Bragg reflections can be observed at Q = 0.029 and 0.058 nm^{-1}. These values relate to each other as 1:2, confirming that they originate from the 10 and the 20 reflections of the hexagonal columnar structure. The 11 and 21 reflections can also be observed but these are not discussed here as the horizontal part of the pattern is integrated as indicated with the black lines in Fig. 6.4(a).

The patterns measured at α = 30° and 50° (Fig. 6.4(b, c)) and the corresponding intensity profiles (Fig. 6.4(d, e)) show a decrease in intensity in the horizontal direction, whereas the peak positions remain constant. In the highly ordered hexagonal *C* phase the particles are stacked into perfect columns, which in turn order in a hexagonal structure. The result is a column axis coupled to the average particle orientation (which is determined by the glass wall), hence Ξ = ξ and the Bragg reflections will be sharp point-like features in the 3D reciprocal space. It is therefore expected that the 10 and 20 reflections are only visible at α = 0°. However, our results do show some of the 10 and 20 reflections upon rotation. This indicates presence of domains with slightly different column orientations where the directions of both Ξ and ξ can fluctuate. However, the fact that the value of Q is constant upon rotation

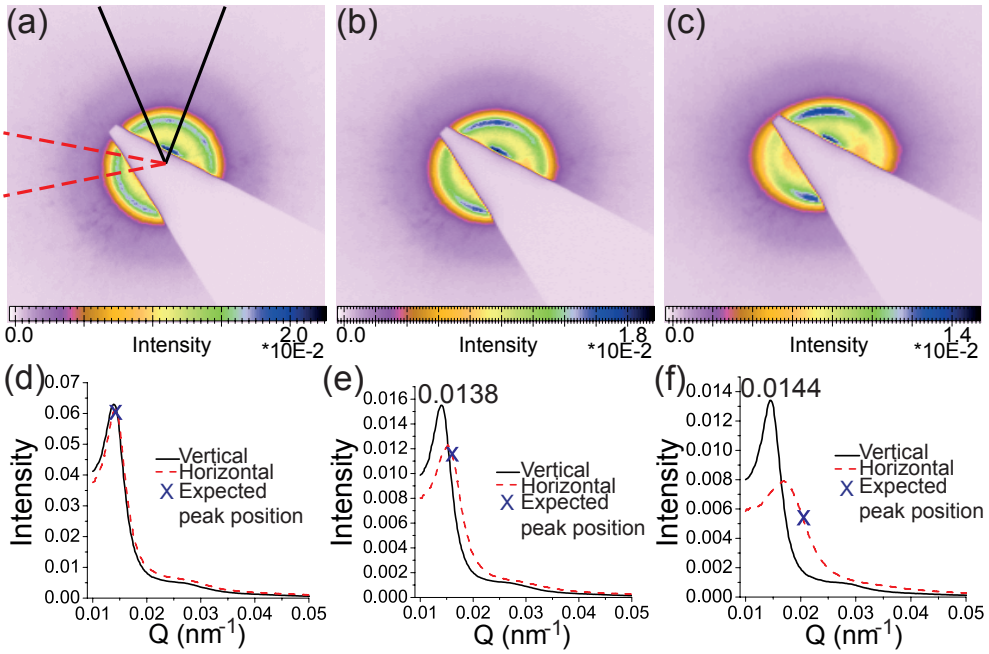

Fig. 6.5 High resolution SAXS-patterns of **S2** at α = (a) 0° (b) 30° and (c) 45° with (d-f) accompanying intensity profiles for vertical and horizontal directions. Black and red lines in (a) show the areas over which intensity profiles were taken in the vertical and horizontal direction, respectively. The blue crosses mark the Q-values of the expected peak positions for N_C. The direct beam was absorbed by a wedge-shaped tantalum beamstop.

indicates that here the coupling between these Ξ and ξ still holds: Ξ = ξ. Fig. 6.4(e) shows the angular dependence of the 10 and 20 intensity and indicates that most fluctuations of Ξ (and ξ) occur over a range of 20° with a maximum of 30°. These domains are most likely situated in the centre of the capillary where the influence of the glass walls is expected to be smallest. Fig. 6.4(f) emphasizes the drastic difference in the α-dependence of the 10 peak positions for the *C* phase when compared to the expected position for the N_C structure.

6.3.2 System 2 (S2)

In **S2** the liquid crystal phase could not be determined from polarization microscopy experiments. Due to the large dimensions of the platelets in sample **S2**, it is challenging to determine the intrinsic width of the reflections, which occur at considerably lower Q-values. Another complication is that in liquid crystals consisting of large platelets (columnar) reflections can be seriously broadened by disorder of different types [21, 31] and by the presence of size fractionated crystals [32]. To determine the liquid crystal structure the sample was therefore measured with SAXS along its y-axis and 3D SAXS was done at the marked position in Fig. 6.1(b).

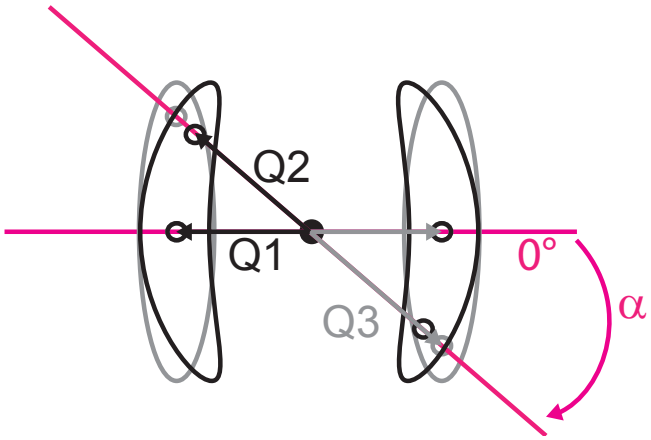

Fig. 6.6 Schematic representation of N_C reciprocal space where ξ is constant (grey lines) and ξ fluctuates (black lines) which causes the broadening of side-to-side correlations to be distorted. At α = 0° Q1 is equal for both, but at an angle α Q2 (fluctuating ξ) is found to be shorter than Q3 (constant ξ).

Fig. 6.5(a) shows the SAXS pattern measured at α = 0°. A circular pattern with strong side-to-side correlations with a maximum at Q = 0.0136 nm^{-1} and a much weaker reflection at Q = 0.028 nm^{-1} are observed. These might be assigned to 10 and 20 reflections, as observed in the *C* phase in **S1**, but they are relatively weak and broad. It is thus ambiguous to assign the liquid crystal phase based on this alone. In Fig. 6.5(b-f) the SAXS patterns and the accompanying intensity profiles measured at α = 30° and 45° are shown. Here the elongation in the horizontal direction with an increase in Q can be observed. Since this is specific for the N_C structure the phase can be unambiguously identified as such.

However, in Fig. 6.5(e, f) it can be seen that the increase in Q_{max} is not as high as expected according to the dependence $Q_a = Q_0/\cos\alpha$ observed in the *N* phase of **S1**. Thus, the results obtained in **S2** are in between those seen in the *N* phase (Ξ fluctuates, ξ is constant on average) and the *C* phase (both Ξ and ξ fluctuate keeping Ξ = ξ on average) of **S1**. This points to the presence of significant fluctuations of not only the axes Ξ of the stacks, but also average particle orientation ξ. It is the combination of the fluctuations of both Ξ (broadening the reflections along a line orthogonal to Q) and ξ (broadening the reflections along an arc), which lead to the observed shape of the side-to-side reflections, which is illustrated in Fig. 6.6. The fluctuation of ξ can have several causes. First of all, the larger particle size leads to a shorter sedimentation time. As a result, the particles have less chance to reorient themselves. Secondly, the difference in the sample age can also be an important factor [39]. Thirdly, there is no non-absorbing polymer added in **S2**, which in **S1** could have caused stronger anchoring at the capillary wall.

The information obtained on the 3D structure of **S2** clearly shows that the sam-

ple has a *N* phase with a N_C structure with several domains where both Ξ and ξ fluctuate and are decoupled. The expectations are that after some time the particles in the **S2** system will align better to the walls resulting in a single N_C domain.

6.4 Conclusions

We have studied and identified different liquid crystal phases of suspensions of small and large gibbsite platelets using SAXS measurements. By rotating the samples around the vertical axis by an angle α, information about the 3D structure of the *N* and *C* phase was obtained. For the *N* phase in a suspension of 237 nm sized platelets a N_C structure is found, where fluctuations of the stack axes Ξ are decoupled from a constant overall particle normal ξ. This led to an apparent decrease in the side-to-side correlation distance with α.

On the contrary, in the *C* phase Ξ and ξ are coupled causing the side-to-side correlation and hence Q-values to remain constant. With this information the liquid crystal phase of a gibbsite dispersion consisting of large (416 nm) platelets was studied and the structure was identified as N_C with several domains. This conclusion could not have been based on a scattering pattern at $\alpha = 0°$ alone and illustrates the importance of exploring the 3D reciprocal space for unambiguous identification of the liquid crystal structure. With the obtained knowledge we would like to take the 3D research further in the future by measuring a range of angles so that the full 3D reciprocal space can be reconstructed as was for example done in Ref. [40] and [41] for a system of hard colloidal spheres.

Acknowledgements

We would like to thank the staff of the DUBBLE beamline and Anatoly Snigirev for excellent support, David van der Beek for supplying the **S1** sample and Jan Hilhorst for discussions. This work is part of the research program SFB TR6 of the ''Stichting voor Fundamenteel Onderzoek der Materie (FOM),'' which is financially supported by the ''Nederlandse Organisatie voor Wetenschappelijk Onderzoek (NWO)'' and ''Deutsche Forschungsgemeinschaft (DFG).'' The beam time is provided by the NWO.

References

[1] H. Zocher, *Z. Anorg. Allg. Chem.*, 1925, **147**, 91-U15.
[2] F. Bawden, N. Pirie, J. Bernal and I. Fankuchen, *Nature*, 1936, **138**, 1051-1052.
[3] J. Bernal and I. Fankuchen, *J. Gen. Physiol.*, 1941, **25**, 111-U8.
[4] K. Coper and H. Freundlich, *T. Faraday Soc.*, 1937, **33**, 0348-0349.
[5] I. Langmuir, *J. Chem. Phys.*, 1938, **6**, 873-896.
[6] M. P. B. van Bruggen, F. M. van der Kooij and H. N. W. Lekkerkerker, *J. Phys.: Condens. Matter*, 1996, **8**, 9451.

[7] Z. Zhang and J. van Duijneveldt, *J. Chem. Phys.*, 2006, **124**, 154910.
[8] H. N. W. Lekkerkerker and G. J. Vroege, *Philos. T. R. Soc. A*, 2013, **371**, 20120263.
[9] E. van den Pol, A. V. Petukhov, D. M. E. Thies-Weesie, D. V. Byelov and G. J. Vroege, *Phys. Rev. Lett.*, 2009, **103**, 258301.
[10] G. J. Vroege, D. M. E. Thies-Weesie, A. V. Petukhov, B. J. Lemaire and P. Davidson, *Adv. Mater.*, 2006, **18**, 2565.
[11] A. Brown, S. Clarke and A. Rennie, *Langmuir*, 1998, **14**, 3129-3132.
[12] J. Gabriel, F. Camerel, B. Lemaire, H. Desvaux, P. Davidson and P. Batail, *Nature*, 2001, **413**, 504-508.
[13] L. J. Michot, I. Bihannic, S. Maddi, S. S. Funari, C. Baravian, P. Levitz and P. Davidson, *P. Natl. Acad. Sci. USA*, 2006, **103**, 16101-16104.
[14] E. Paineau, K. Antonova, C. Baravian, I. Bihannic, P. Davidson, I. Dozov, M. Imperor-Clerc, P. Levitz, A. Madsen, F. Meneau and L. J. Michot, *J. Phys. Chem. B*, 2009, **113**, 15858-15869.
[15] S. Liu, J. Zhang, N. Wang, W. Liu, C. Zhang and D. Sun, *Chem. Mat.*, 2003, **15**, 3240-3241.
[16] J. Fossum, E. Gudding, D. Fonseca, Y. Meheust, E. DiMasi, T. Gog and C. Venkataraman, *Energy*, 2005, **30**, 873-883.
[17] D. M. Fonseca, Y. Meheust, J. O. Fossum, K. D. Knudsen and K. P. S. Parmar, *Phys. Rev. E*, 2009, **79**, 021402.
[18] H. Hemmen, N. I. Ringdal, E. N. De Azevedo, M. Engelsberg, E. L. Hansen, Y. Meheust, J. O. Fossum and K. D. Knudsen, *Langmuir*, 2009, **25**, 12507-12515.
[19] F. van der Kooij, K. Kassapidou and H. Lekkerkerker, *Nature*, 2000, **406**, 868-871.
[20] A. Petukhov, J. Thijssen, D. 't Hart, A. Imhof, A. van Blaaderen, I. Dolbnya, A. Snigirev, A. Moussaid and I. Snigireva, *J. Appl. Crystallogr.*, 2006, **39**, 137-144.
[21] A. Petukhov, D. van der Beek, R. Dullens, I. Dolbnya, G. Vroege and H. Lekkerkerker, *Phys. Rev. Lett.*, 2005, **95**, 077801.
[22] J. C. P. Gabriel and P. Davidson, *Adv. Mater.*, 2000, **12**, 9.
[23] A. A. Verhoeff, I. A. Bakelaar, R. H. J. Otten, P. van der Schoot and H. N. W. Lekkerkerker, *Langmuir*, 2011, **27**, 116-125.
[24] M. C. D. Mourad, D. V. Byelov, A. V. Petukhov, D. A. M. de Winter, A. J. Verkleij and H. N. W. Lekkerkerker, *J. Phys. Chem. B*, 2009, **113**, 11604-11613.
[25] L. Li, M. Marjanska, G. Park, A. Pines and A. Alivisatos, *J. Chem. Phys.*, 2004, **120**, 1149-1152.
[26] S. Koizumi, H. Iwase, J. Suzuki, T. Oku, R. Motokawa, H. Sasao, H. Tanaka, D. Yamaguchi, H. M. Shimizu and T. Hashimoto, *Physica B*, 2006, **385-86**, 1000-1006.
[27] E. Maier, R. Krause, M. Deggelmann, M. Hagenbuchle, R. Weber and S. Fraden, *Macromolecules*, 1992, **25**, 1125-1133.
[28] D. Yamaguchi, N. Miyamoto, S. Koizumi, T. Nakato and T. Hashimoto, *J. Appl. Crystallogr.*, 2007, **40**, S101-S105.
[29] D. V. Byelov, J. Meijer, I. Snigireva, A. Snigirev, L. Rossi, E. van den Pol, A. Kuijk,

A. Philipse, A. Imhof, A. van Blaaderen, G. J. Vroege and A. V. Petukhov, *Rsc Advances*, 2013, **3**, 15670-15677.
[30] J. Wijnhoven, *J. Colloid Interf. Sci.*, 2005, **292**, 403-409.
[31] M. C. D. Mourad, A. V. Petukhov, G. J. Vroege and H. N. W. Lekkerkerker, *Langmuir*, 2010, **26**, 14182-14187.
[32] D. V. Byelov, M. C. D. Mourad, I. Snigireva, A. Snigirev, A. V. Petukhov and H. N. W. Lekkerkerker, *Langmuir*, 2010, **26**, 6898-6901.
[33] J. Wijnhoven, D. van't Zand, D. van der Beek and H. Lekkerkerker, *Langmuir*, 2005, **21**, 10422-10427.
[34] M. C. D. Mourad, E. J. Devid, M. M. van Schooneveld, C. Vonk and H. N. W. Lekkerkerker, *J. Phys. Chem. B*, 2008, **112**, 10142-10152.
[35] F. van der Kooij, M. Vogel and H. Lekkerkerker, *Phys. Rev. E*, 2000, **62**, 5397-5402.
[36] M. Borsboom, W. Bras, I. Cerjak, D. Detollenaere, D. van Loon, P. Goedtkindt, M. Konijnenburg, P. Lassing, Y. Levine, B. Munneke, M. Oversluizen, R. van Tol and E. Vlieg, *J. Synchrot. Radiat.*, 1998, **5**, 518-520.
[37] J. H. J. Thijssen, A. V. Petukhov, D. C. 't Hart, A. Imhof, C. H. M. van der Werf, R. E. I. Schropp and A. van Blaaderen, *Adv. Mater.*, 2006, **18**, 1662.
[38] M. C. D. Mourad, D. V. Byelov, A. V. Petukhov and H. N. W. Lekkerkerker, *J. Phys.: Condes. Matter*, 2008, **20**, 494201.
[39] M. C. D. Mourad, A. A. Verhoeff, D. V. Byelov, A. V. Petukhov and H. N. W. Lekkerkerker, *J. Phys.: Condens. Matter*, 2009, **21**, 474218.
[40] A. A. Eliseev, D. F. Gorozhankin, K. S. Napolskii, A. V. Petukhov, N. A. Sapoletova, A. V. Vasilieva, N. A. Grigoryeva, A. A. Mistonov, D. V. Byelov, A. V. Petukhov, K. O. Kvashnina, D. Y. Chernyshov, A. A. Bosak and S. V. Grigoriev, *J. Exp. Theor. Phys. Lett.*, 2009, **90**, 272-277.
[41] K. S. Napolskii, N. A. Sapoletova, D. F. Gorozhankin, A. A. Eliseev, D. Y. Chernyshov, D. V. Byelov, N. A. Grigoryeva, A. A. Mistonov, W. G. Bouwman, K. O. Kvashnina, A. V. Lukashin, A. A. Snigirev, A. V. Vassilieva, S. V. Grigoriev and A. V. Petukhov, *Langmuir*, 2010, **26**, 2346-2351.

7

Gibbsite systems for confocal microscopy studies

We adapt the plate-like gibbsite system such that the particles, and the liquid crystals they form, can be studied in real time and space with confocal laser scanning microscopy (CLSM). We synthesize gibbsite platelets with dimensions larger than the resolution of the confocal microscope using two different methods: a one-step synthesis and a seeded-growth synthesis in which regular gibbsite platelets are used as seeds. We then fluorescently label the particles in two ways: either through attaching a dye to a steric polymeric stabilizer on the particle surface, or through incorporating a dye into a silica layer which is grown around the particle. We study the liquid crystal structures formed with confocal microscopy, supported by small angle x-ray scattering. With CLSM single particles can be observed, their (local) ordering can be resolved and the liquid crystal phase can be determined. We show that CLSM is a technique complementary to the techniques generally used to study liquid crystal phase behaviour and shows promise for future experiments. We do however find that the dye influences the inter-particle interactions. As a consequence it is challenging to obtain stable dispersions. Additionally, liquid crystal phase formation becomes more difficult due to the large particle size; the particles have a high sedimentation speed which inhibits the formation of a true long-range positionally ordered columnar phase. We therefore give suggestions and recommendations for improvement of the system for further research.

7.1 Introduction

Anisotropic particles such as rod-, board- and plate-like particles have the ability to spontaneously form liquid crystals (LCs). Their phase behaviour is predominantly entropy driven and the phase formed depends on the particle shape and volume fraction [1-4]. Various liquid crystalline phases exist, including nematic (*N*), smectic (*S*) and columnar (*C*) phases. In the *N* phase the particles only possess orientational order. In the *S* and the *C* phase the particles additionally possess positional order in one and two dimensions, respectively. Also colloidal mineral particles are known to display rich phase behaviour [5, 6]. In the first part of this thesis we described in detail the phase behaviour of board-like goethite (α-FeOOH). Other examples are rod-like boehmite (γ-AlOOH), fd-virus and silica rods [7, 8]. Examples of plate-like particles include nickel hydroxide and natural clays like bentonite and beidellite [6]. An exceptional system of plate-like particles is gibbsite (γ-$Al(OH)_3$). These synthetic clay platelets display an isotropic *I* – *N* – *C* phase separation [9].

There are various ways to influence the liquid crystal formation. As colloidal (mineral) particles are highly susceptible to external fields, electric and magnetic fields are frequently used to engineer LC phases [10]. Moreover, anisometric particles generally have a preferred orientation near a wall or surface. Therefore confinement, e.g. by using slit-pore cells, can be used to influence the LC formation [11].

Several experimental techniques are used to characterize and give insight in colloidal LC structures. Frequently used are small angle x-ray scattering (SAXS) [12, 13], polarized light microscopy (PLM) [14, 15], and to a lower extent transmission and scanning electron microscopy (cryo-TEM/SEM) [16]. As discussed in several other chapters in this thesis, SAXS is an excellent technique to characterize *average* bulk liquid crystalline structures. However various studies, like confinement studies, require characterization of the local crystal structure. PLM can be used to analyse smaller domains, but cannot access the structure on the single-particle level and mainly gives information about average particle orientations. PLM is therefore predominantly suited to visualise the particle director field in, e.g., nematic liquid crystals. Cryo-electron microscopy does give information at the particle level, but the required elaborate sample preparation, which includes freezing and cutting of the sample, is challenging and can have an influence on the structures.

Techniques to study liquid crystals in real-time and direct space at the single particle level are rare. The recently developed technique of full-field transmission x-ray microscopy (TXM) enables taking real-space images of even opaque liquid crystals [17]. With this technique, which uses hard x-rays (> 10 keV), the smectic phase in a system of colloidal silica rods was visualized. However, TXM visualizes the entire sample thickness in one image. Therefore, highly ordered, single LC domains are required. Resolution limits and imaging contrast could be significantly improved by using softer x-rays in vicinity of the adsorption edge of a particular element present in the sample. This, however, severely limits the sample thickness to a few microns [18-21].

Confocal laser scanning microscopy (CLSM) is a technique that is able to image one spot of a 3D sample at a time. CLSM is intensively used to study crystallization of spherical particles [22, 23]. Also anisotropic colloids are on the verge of becoming accessible with CLSM. With e.g. CLSM it was revealed that the director field of nematic liquid crystals of fd-virus in wedge-structured channels depends on the wedge angle [24]. Another example is described in the work by Lettinga and Grelet who directly visualized single particle transport between *S* layers of fd-virus [25].

All these examples deal with rod-like particles. In this chapter we, to our knowledge, characterize for the first time the liquid crystal structure of plate-like particles in real-time and space using CLSM. We chose colloidal gibbsite as a model system. Regular gibbsite platelets have dimensions, a diameter (D) of typically ~160 nm and a thickness (L) of ~15 nm [26], which are below the resolution of a confocal microscope. Additionally, CLSM requires fluorescent particles. Gibbsite is not fluorescent. We therefore adapted the gibbsite system. Platelets were grown to larger sizes [27] and were fluorescently labelled via two different methods. These syntheses as well as the sample preparation are described in section 7.2. Dispersions of the resulting systems were studied with CLSM, supported by SAXS. The results are described in section 7.3. Due to the large particle size the formation of (long-range) positionally ordered phases turned out to be challenging. We therefore end with recommendations for further research and conclusions in section 7.4.

7.2 Experimental

The gibbsite platelets were grown to larger sizes via two different methods, either via the seeded growth method [27] or via a one-step synthesis [28]. This is described in section 7.2.1. We labelled the particles via two different methods. In method 1 we first sterically stabilize the particles and subsequently attach a fluorescent dye to the stabilizing pol ymers. In method 2 a fluorescent silica shell is grown around the particles. These synthesis steps are described in section 7.2.2. In section 7.2.3 and section 7.2.4 the sample preparation and equipment used are described, respectively.

7.2.1 Gibbsite synthesis

Seeded growth method

The seed particles were synthesized by hydrothermal treatment of aluminium alkoxides, according to the procedure described by Wierenga *et al*. [26] An acidic solution containing 1.0 L hydrochloric acid (0.09 M, 37 %, Merck), 15.2 g aluminium-iso-propoxide (> 97 % Fluka) and 20.0 g aluminium-sec-butoxide (97 %, Aldrich) was mechanically stirred for 10 days. The mixture was subsequently heated in a glass reaction vessel in a 85 ˚C thermostatted water bath for 72 h. The resulting colloidal dispersion was centrifuged at 1000*g* (overnight) in order to remove the

smallest particles and to decrease the polydispersity. The resulting dispersion was dialyzed against demineralized (dd) water in tubes of regenerated cellulose (Visking, MWCO 12000 – 14000) until the conductivity dropped to 20 mS cm^{-1}. According to the seeded growth method described by Wijnhoven [27] the seed particles were dispersed in a fresh batch of the acidic alkoxide solution described above. The mixture was again heated at 85 ˚C for 72 h under constant mechanical stirring to perform a seeded growth step. After growth the particles were treated as described above: dialysis against dd water and centrifugation. This seeded growth step was repeated 5 times. Centrifugation and stirring speeds were adjusted for the larger particles. The resulting platelets were stored in dd water.

Direct-growth method
Large gibbsite platelets were also synthesized via a one-step method. According to this direct-growth method described by Shen *et al*. [28] 10.11 g aluminium-nitrate-nonahydrate (p.a. Sigma-Aldrich) was dissolved in 200 mL Millipore (mp) water under continuous magnetic stirring to obtain a homogeneous solution. Ammonia (10 wt%, 28-30 % in H_2O, Sigma-Aldrich) was added dropwise until the pH of the mixture was 5. Subsequently, the mixture was vigorously stirred for 10 min to obtain a homogeneous gel. The gel was transferred to a glass bottle and heated in an electrical oven at 100 ˚C for 10 days. The white precipitate that formed was recovered via three cycles of centrifugation (3 h, 500*g*) and redispersion in mp water.

7.2.2 Fluorescent labelling

Sterically stabilized fluorescent gibbsite
The large gibbsite particles synthesized were sterically stabilized with amino-modified polyisobutylene chains (PIB) by the method described by Mourad *et al*. [29, 30]. 5.0 g PIB (SAP230TP, Infineum U.K. Ltd.) was added to 40 mL 1-propanol (> 99%, Acros Organics). The mixture was magnetically stirred for ~20 h until the polymer looked well dispersed. 25 mL of aqueous gibbsite solution (40 g/l) was added dropwise to the mixture. The solvents were removed using a rotational vacuum evaporator, followed by a freeze-drying step. The resulting mixture of particles and PIB polymer was redispersed in toluene (technical grade, Interchema). Some particles aggregated. These aggregates sediment within minutes and were removed by allowing the dispersion to sediment for ~30 min and removing the supernatant (which now only contains stabilized particles). The supernatant was washed to remove excess PIB through multiple cycles of centrifugation (500*g* for 3 h) until the supernatant remained colourless. The sterically stabilized particles obtained were transferred to tetralin (99%, Sigma-Aldrich) through two cycles of centrifugation and redispersion.

19 mg fluorescein isothiocyanate isomer 1 dye (FITC, 90%, Sigma) was dissolved in 2.00 mL toluene by magnetically stirring overnight, to obtain a solution with a concentration of 0.025 M. Part of the sterically stabilized gibbsite was fluo-

rescently labelled by adding 100 μL of the dye solution to 1 mL of the gibbsite (370 g/L) dispersion under continuous stirring for ~20 h. The resulting yellow mixture was washed by centrifugation and redispersion in tetralin until the supernatant remained colourless.

Gibbsite coverage with a (fluorescent) silica shell

The gibbsite particles were covered with a (fluorescent) silica layer grown via the hydrolysis of the silica precursor tetra-ethylortho-silicate (TEOS) in a Stöber mixture consisting of ethanol, water and ammonia [31], based on the methods described by Vonk *et al*. [32, 33] and Wijnhoven [33].

To enhance the stability of the gibbsite particles in ethanol first a polymer, polyvinyl pyrrolidone (PVP), is grafted onto the surface of the platelets. 100 g PVP (MW = 40.000 g/mol, Aldrich) was dissolved in 1L dd water by magnetically stirring for ~3 h. Aqueous gibbsite dispersion was added such that the resulting dispersion had a gibbsite concentration of ~1 g/L. This dispersion was stirred vigorously for ~24 h. Subsequently, the dispersion was centrifuged (300*g* for 3h) and redispersed in ethanol (p.a. Merck).

A dye solution was prepared by dissolving 0.018 g FITC and 107 μL amino-propyltriethoxy-silane (APS, > 98%, Sigma-Aldrich) in 700 μL ethanol (technical grade, Interchema) by continuous stirring for ~24 h.

The Stöber mixture was created by adding, consecutively, ethanol and ammonia under continuous stirring to the gibbsite-PVP dispersion such that the resulting mixture had a gibbsite concentration of 1 g/L and an ammonia (25 wt% in H2O, Contain) concentration of 6.8 v/v%. The resulting mixture was equally divided over two closed glass flasks. To one of the flasks 81 μL of the APS-dye solution was added under the surface of the mixture, directly followed by the addition of 50 μL of TEOS (> 99%, Aldrich). The mixture was stirred at 150 rpm [34] overnight. Then another 250 mL of TEOS was added under continuous stirring (150 rpm) to grow a non-fluorescent outer silica-shell around the fluorescent silica-shell. Simultaneously the same steps were performed for the dispersion in the other flask, except the addition of the dye solution. This was done in order to obtain both non-fluorescent and fluorescent gibbsite particles with a comparable silica shell thickness. Both mixtures were stirred overnight and were subsequently washed with ethanol by two cycles of centrifugation (300*g*, 3h) and redispersion. The gibbsite-silica platelets were transferred to dimethyl formamide (DMF). 50:50 v/v% ethanol/DMF (> 99%, Sigma-Aldrich) was added to the gibbsite-ethanol dispersion such that the total v/v% of DMF was ~5%. After centrifugation (300*g*,3 h) the particles were redispersed in DMF. Finally the dispersion was washed by three subsequent cycles of centrifugation and redispersion in DMF.

7.2.3 Sample preparation

Dispersions series were made with gibbsite volume fractions (ϕ_g) ranging from 0.4

to 19%. For the gibbsite-PIB system (**gp**), dispersions of non-fluorescent particles were mixed with dispersions of fluorescent particles. In the resulting dispersions 0, 5, 10, 20, 50 or 100% of the particles were fluorescently labelled, respectively (indicated as **gpf-5%** etc). Additionally, a sample was prepared in which the solvent was fluorescently labelled as well. To this end, part of a **gpf-5%** dispersion was centrifuged and the particles were redispersed in a solution of 0.01 M DANS (4-dimethylamino-4'-nitrostilbene, > 99%, Sigma) in tetralin.

For the gibbsite-silica system (**gs**), dispersions either contained only dyed particles (**gsf**) or only non-fluorescent particles (**gsn**).

For PLM and SAXS measurements, the dispersions were stored in rectangular glass capillaries with internal dimensions of 4.0 x 0.2 x 100 mm^3 (#W3520-100, VitroCom Inc.) which were flame-sealed and stored in upright position to ensure the formation of a density gradient. For CLSM measurements dispersions were stored in home-made sample cells. These sample cells were prepared by gluing round capillaries with an internal diameter of 2.0 mm (#CV2024-100, VitroCom Inc.) on rectangular microscope slides (Menzel Gläzer, 24 x 60 mm, nr. 1). For the **gp** samples an epoxy glue (Araldite AW2101) was used with a hardener (HW2951). In the **gs** samples particles were dispersed in DMF, which dissolves epoxy glue. Therefore glue from a Reka glue applicator was used. Since this glue adheres poorly to the glass slide a second layer of glue (Araldite AW2101/HW2951) was applied to fixate the Reka-glue layer on the microscope slide.

7.2.4 Equipment

Confocal microscopy

A Nikon Eclipse TE2000U inverted microscopy equipped with a Nikon C1 scanning head and an oil immersion lens (100 Nikon Plan Apc, NA 1.4) was used to image the gibbsite particles. For illumination, a Spectra Physics 163C air cooled Ar-ion laser with a wavelength of 488 nm was used. The microscope has a maximum radial and axial resolution of ~212 and ~750 nm for the solvents used, respectively.

Polarized light microscopy

The samples were studied using the same set up as described in section 2.2.2.

SAXS

Small angle x-ray scattering patterns were collected using the microradian diffraction set up[35] at the BM26 DUBBLE beamline [36] of the European Synchrotron Radiation Facility (ESRF, Grenoble, France). A photon energy of 12 keV was used, with a sample-detector distance of 7 m. Patterns were collected using a two-dimensional x-ray CCD-based detector with a pixel size of 9 μm (Photonic Science). Patterns were collected in the middle of the capillary at different heights using a motorized remotely-controlled translational stage.

TEM
The synthesized particles were characterized using a Technai 10 (FEI company) transmission electron microscope (TEM). Particle size distributions were determined using iTEM imaging software.

AFM
The particle thickness was determined using atomic force microscopy (AFM) utilizing a multimode scanning probe microscope (Digital Instruments). AFM measurements were performed in tapping mode with a standard TESP silicon tip.

7.3 Results and Discussion

7.3.1 Large platelets

Transmission electron microscopy images of the large gibbsite platelets synthesized by the seeded and direct growth method are shown in Fig. 7.1. The particles have a well-defined pseudo-hexagonal shape characteristic of gibbsite [26] and appear to be single particles, aggregates were not observed. The diameter D and thickness L were determined using TEM and AFM, respectively, and are shown in Table 7.3. D was determined from measuring the surface area of the platelet (A) and is defined by

$$D \equiv \sqrt{\frac{4A}{\pi}}. \tag{7.1}$$

D was calculated and averaged for well over 300 particles. L was measured and averaged for approximately 90 particles. Both synthesis methods resulted in particles with a similar size and aspect ratio. The particles synthesized according to the seeded growth method have a lower polydispersity, as is expected from a seeded growth method [27].

Table 7.3 Dimensions of the gibbsite particles with their corresponding polydispersities (σ) as obtained from TEM and AFM.

Growth method	$<D>$ (nm)	σ_D (%)	$<L>$ (nm)	σ_L (%)	L/D
Seeded	662	9	33	12	0.05
Direct	690	14	33	32	0.05

Remarkable observations were made for the particles obtained via the direct-growth method. Whereas the seeded-growth particles have a smooth surface, the surface of the direct-growth particles appears to be covered with thin fibre-like structures (Fig. 7.1(c)). The fibres appear to be irreversibly attached; several wash-

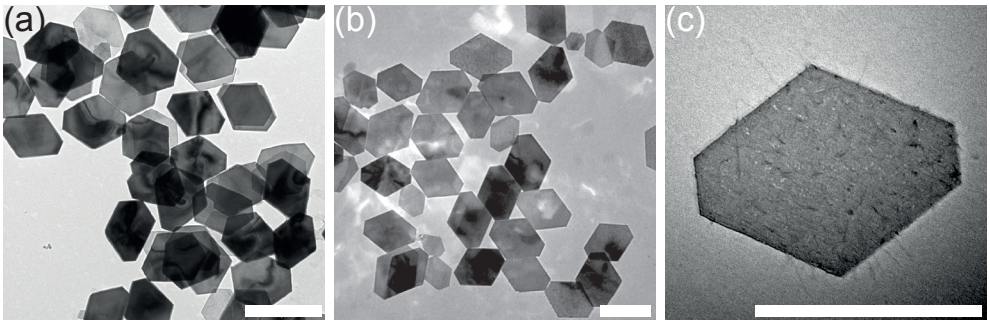

Fig. 7.1 TEM pictures of large gibbsite particles synthesized by (a) the seeded growth method and (b), (c) the direct growth method. The white bars denote 1 μm.

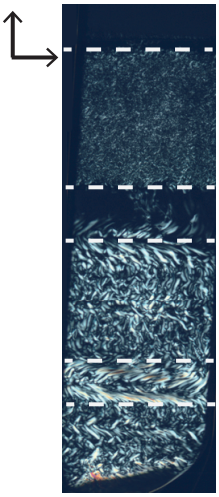

Fig. 7.2 Polarized light microscopy image of PIB-stabilized gibbsite particles obtained from the direct growth synthesis, dispersed in tetralin (ϕ_g = 8.5%) taken 2 months after sample preparation. The solid arrows indicate the direction of the polarizers.

ing steps and ultrasonication did not significantly reduce the number of fibres. The fibres most likely consist of boehmite (γ-AlOOH), which is a known side product of the regular aluminium-alkoxide based gibbsite synthesis [26]. Colloidal boehmite consists of stiff fibrils with a length of typically 100 - 400 nm and high aspect ratio [37, 38] and typically forms at temperatures T > 150 ˚C. They are generally not attached to the surface of the platelets and can easily be removed by centrifugation. The paper of Shen *et al*., in which the direct growth method is described, reports the formation of boehmite for syntheses performed at pH = 10 (at 100 ˚C). They do not report boehmite formation for the synthesis executed at pH = 5, which is the synthesis we performed. A careful study of the microscopy images and XRD diffractograms in their paper however, indeed shows that the particles do not consist

purely of gibbsite. Some fibril-like material similar to our results can be observed in their TEM pictures. It is not clear though whether these are, like in our study, irreversibly attached to the surface of the gibbsite platelets.

To check whether this surface roughness inhibits the liquid crystal formation process, part of the direct-growth platelets were sterically stabilized and dispersed in tetralin. Samples of these dispersions were studied with PLM which revealed (Fig. 7.2) a birefringent sediment indicating liquid crystal formation. The white dashed lines in (Fig. 7.2) indicate that different regions can be observed along the vertical direction of the capillary. This typically indicates phase separation. However optical Bragg reflections, indicating a positionally ordered phase, were not observed on a timescale of 1.5 years, meaning that all domains are nematic. It appears that these fibres inhibit the formation of a positionally ordered (columnar) phase. Since the dimensions of our particles are already challenging for CLSM, positionally ordered phases are preferred. The seeded-growth particles did phase-separate into a *N* and a *C* phase when sterically stabilized and dispersed in tetralin. We therefore selected the seeded-growth platelets for further (fluorescence) measurements.

7.3.2 Fluorescent sterically stabilized gibbsite

Stability of the particles and dispersions

In this system the dye is attached to the polymers on the particle surface, which can have a negative influence on the stability of the particles. Therefore samples were prepared with different fractions -100, 50, 20, 10 and 5%- of labelled particles. Fig. 7.3 shows pictures of the samples one day after sample preparation. The dispersions, with ϕ_g = 19%, are coloured yellow by the FITC-dye. In the samples with the lower fractions of labelled particles, **gpf-20%** (not shown here) **gpf-10%** and **gpf-5%**, a sedimentation profile, characteristic of a stable dispersion, can be observed (Fig. 7.3(c, d)). The sediments were found to be birefringent. After 10 days iridescence could be observed upon illumination with white light, both when the light was transmitted (Fig. 7.4(a)) or reflected (Fig. 7.4(b)) by the sample. This indicates that a positionally order phase has formed and we can conclude that these samples are stable.

In contrast, the particles in the systems with a higher fraction of labelled particles, **gpf-50%** and **gpf-100%**, completely sedimented within one day forming a gel-like structure with pure solvent on top (Fig. 7.3(a, b)). These gels were found to be, apart from a very small layer at the bottom of the capillary, non-birefringent. From these systems we can therefore conclude that the dye destabilizes the particles and inhibits liquid crystal formation at higher fraction of labelled particles.

Phase behaviour

Even though the particles were grown to substantially larger sizes, imaging of single particles remains challenging as the thickness *L* of the platelets is below the resolution of the microscope. Apart from stability issues, labelling only part of the

Fig. 7.3 Pictures of capillaries filled with gpf-dispersions with ϕ_g = 19% in which (a) 100, (b) 50, (c) 10 and (d) 5 % of the particles are fluorescently labelled. The pictures were taken one day after sample preparation.

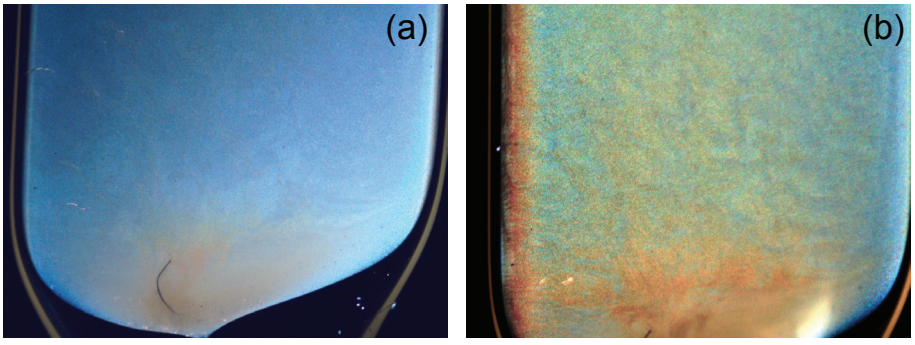

Fig. 7.4 Pictures of sample **gpf-5%** with ϕ_g = 19% under illumination with white light, where the light is (a) transmitted and (b) reflected. Pictures were taken 10 days after sample preparation.

particles can be advantageous: it increases the distance between two fluorescent particles which is expected to improve the visibility. Fig. 7.5 shows typical confocal images taken in samples in which respectively 5, 10, 20 or 50% of the particles

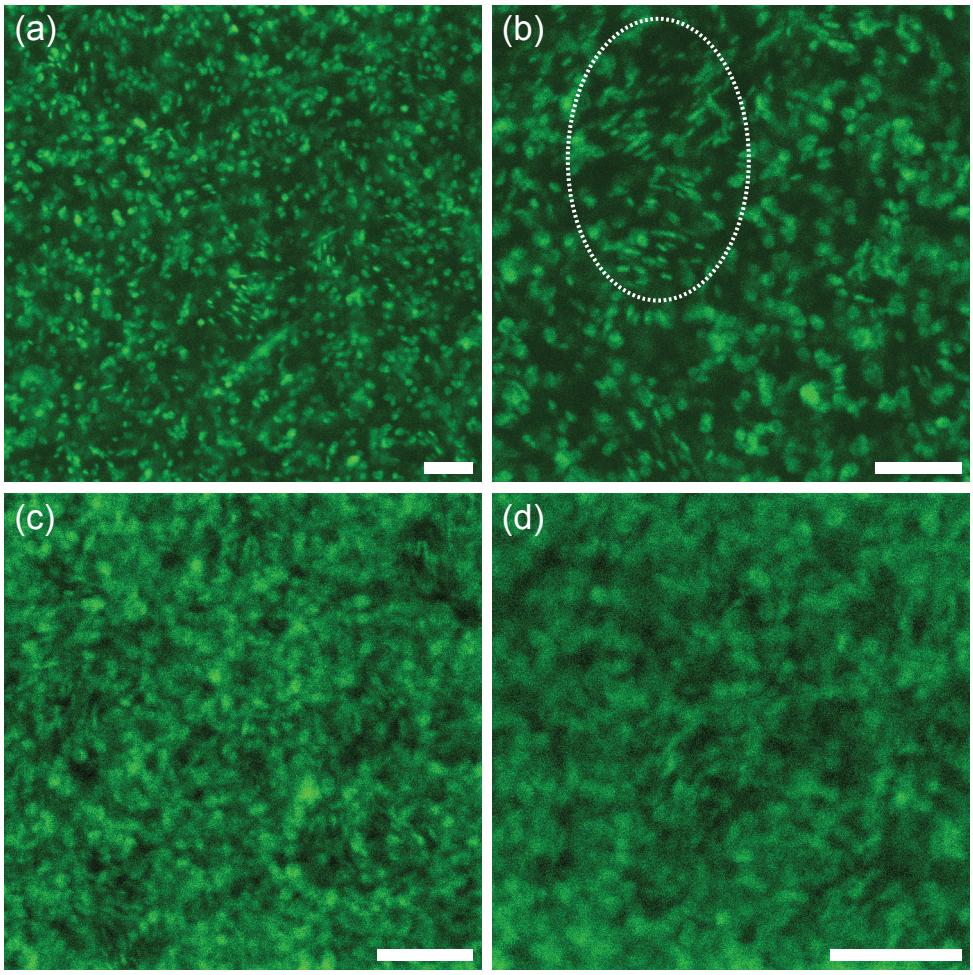

Fig. 7.5 Confocal microscopy images of **gpf**-dispersions in which respectively (a) 5, (b) 10, (c) 20 and (d) 50% of the platelets were fluorescently labelled. The pictures were taken ~3 μm from the bottom of the sample and ~15 days after sample preparation. ϕ_g = 19% for (a), (b), (d) and 9% for (c). The white bar denotes 5 μm.

were labelled. The samples were allowed to sediment for ~15 days. In all four images shown in Fig. 7.5 individual particles can be observed. The particles in the samples with 5, 10 or 20% labelled particles were found to exhibit Brownian motion. Their random walk appears to be confined to a small volume in the order of the particle size indicating that the particles are 'caged', which is characteristic for dense positionally ordered phases. The particles in the system **gpf-50%** did not exhibit Brownian motion, confirming the gel-like structure of the system. Fig. 7.5 reveals the presence of different domains in which the particles are orientation-

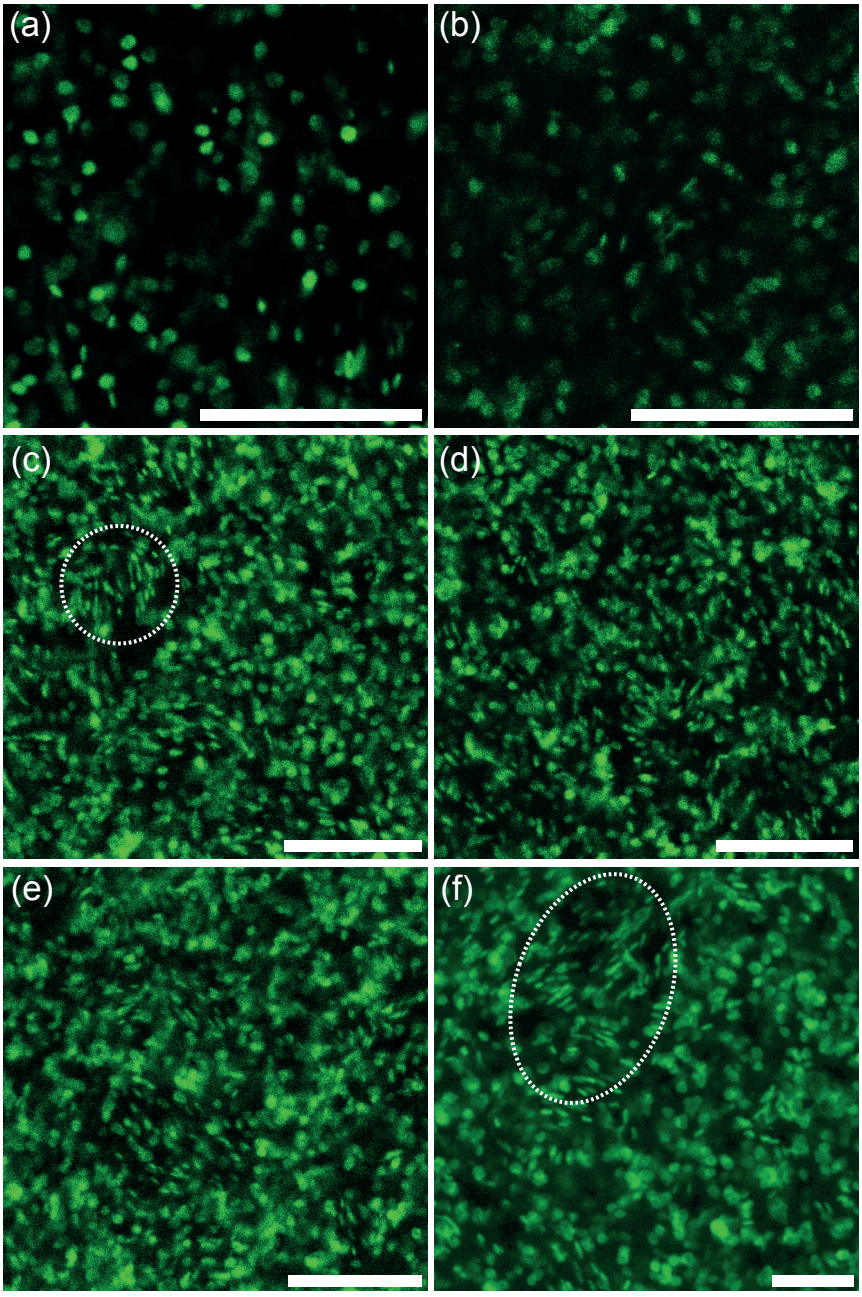

Fig. 7.6 Confocal microscopy images of **gpf-10%** dispersion with ϕ_g = 19%. The pictures were taken 5 μm from the bottom of the sample after sedimentation for (a) 3 hours, (b) 3 days, (c) 6 days (d) 13 days, (e) 1 month and (f) 2.5 months. The white bar denotes 10 μm.

ally ordered. This is emphasized by the white ellipse in Fig. 7.5(b), which denotes a domain in which the majority of the visible particles appears to be perpendicular to the focal plane.

Fig. 7.5 shows that there is a marked improvement in visibility upon decreasing the fraction of labelled particles from 20 to 10%. The development of the liquid crystal phases in time was therefore studied in a sample containing a dispersion in which 10% of the particles carried a fluorescent label (**gpf-10%**, ϕ_g = 19%). In Fig. 7.6 we present typical confocal microscopy images taken after different sedimentation times at different positions in the focal plane but at a fixed height of 5 μm from the bottom of the sample. Fig. 7.6(a) shows a typical image taken 3 hours after sample preparation. Although only 10% of the particles are visible, it is clear that the density of particles is low. The particles are in the *I* phase: orientationally ordered domains were not observed. After 3 days of sedimentation (Fig. 7.6(b)) the particle volume fraction appears to be higher, but is still below the $I - N$ volume fraction as the particles have random orientations. After sedimentation for approximately a week (Fig. 7.6(c)) the image is different: the apparent volume fraction is significantly higher and domains in which particles are orientationally ordered can be observed. The white ellipse indicates a μm-sized domain in which the particle orientation is perpendicular to the focal plane. Fig. 7.6(d, e, f) are taken after respectively 13, 30 and 70 days of sedimentation. There are no significant differences compared to the image taken after ~ 1 week of sedimentation; the dynamics of liquid crystal phase formation has slowed down. However, the particles exhibit Brownian motion and therefore the ordering can still improve [39]. It e.g. appears that the domain size of differently oriented particles increases with increasing sedimentation time, as is illustrated by the domain in Fig. 7.6(f) which appears to be twice as large as the domain in Fig. 7.6(c). However, more quantitative research is required to draw proper conclusions.

Determining the liquid crystal phase purely from these confocal microscopy images is challenging. It is clear that the neighbouring particles possess some orientational order. Upon careful studying various confocal pictures, it appears that the particles locally possess positional order as well. This is illustrated in Fig. 7.7, which displays a typical confocal microscopy image taken in a sample containing dispersion **gpf-10%** with ϕ_g = 19%. The sample was 1 month old at the moment of measuring. In the images small columns of particles can be observed in the domains in which the particles are oriented perpendicular to the focal plane. Additionally, the stacks of particles that are in close proximity of each other appear to be aligned. However, long range positional order is not observed. These small stacks of particles are characteristic of the columnar nematic (N_C) phase (Chapter 6). This phase is often formed on relative short time scales in systems of particles with high sedimentation speeds, or in systems consisting of highly polydisperse particles. Both polydispersity and fast formation inhibit the formation of long range positional order. The particles in our system are large and sediment on relatively short time-

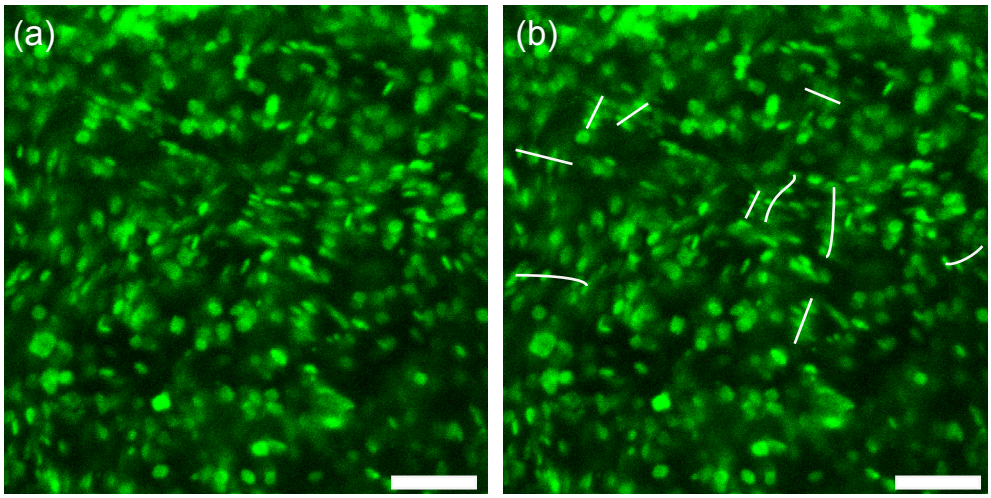

Fig. 7.7 Typical confocal microscopy image of **gpf-10%** dispersion with ϕ_g = 19%. The image was taken after sedimentation for $\sim$ 1 month. The white lines in (b) indicate small columns of particles. The white bars denote 10 μm.

scales. It is therefore likely, especially in the bottom part of the sample, that these large particles form a N_C phase. It is however hard to be conclusive since only 10% of the particles can be observed.

Since a higher percentage of fluorescently labelled particles was found to inhibit liquid crystal phase formation (Fig. 7.3) and to reduce the visibility (Fig. 7.5), we additionally dyed the solvent to enable imaging of all the gibbsite platelets. We studied the phase behaviour of a sample of sterically stabilized gibbsite platelets, of which 5% are fluorescently labelled, dispersed in solution of 0.01 M DANS in tetralin. DANS and FITC emit at different wavelengths of respectively 518 and 600 nm, which can be detected separately.

In Fig. 7.8(a, c, e) we present typical confocal microscopy images taken $\sim$ 1.5 month after sample preparation at three different positions in the sample. In these images the particles are either green (labelled) or black (unlabelled) and the solvent is orange. For a complete picture we additionally present in Fig. 7.8(b, d, f) the same images in which now only the solvent is visible (green for an improved contrast), all the particles are black. Fig. 7.8(a, b) are taken 3 μm above the sample bottom. Again domains with different particle orientations can be observed. The white dashed lines indicate a domain with particles perpendicular to the focal plane enclosed between two domains with particles parallel to the focal plane. In this enclosed domain again small stacks of particles can be observed. They are aligned, but the columns are undulating and long range positional order is not present. Similar conclusions can be drawn from the domains in which the stacks are perpendicular to the focal plane. Several stacks are hexagonally packed, as illustrated by the white

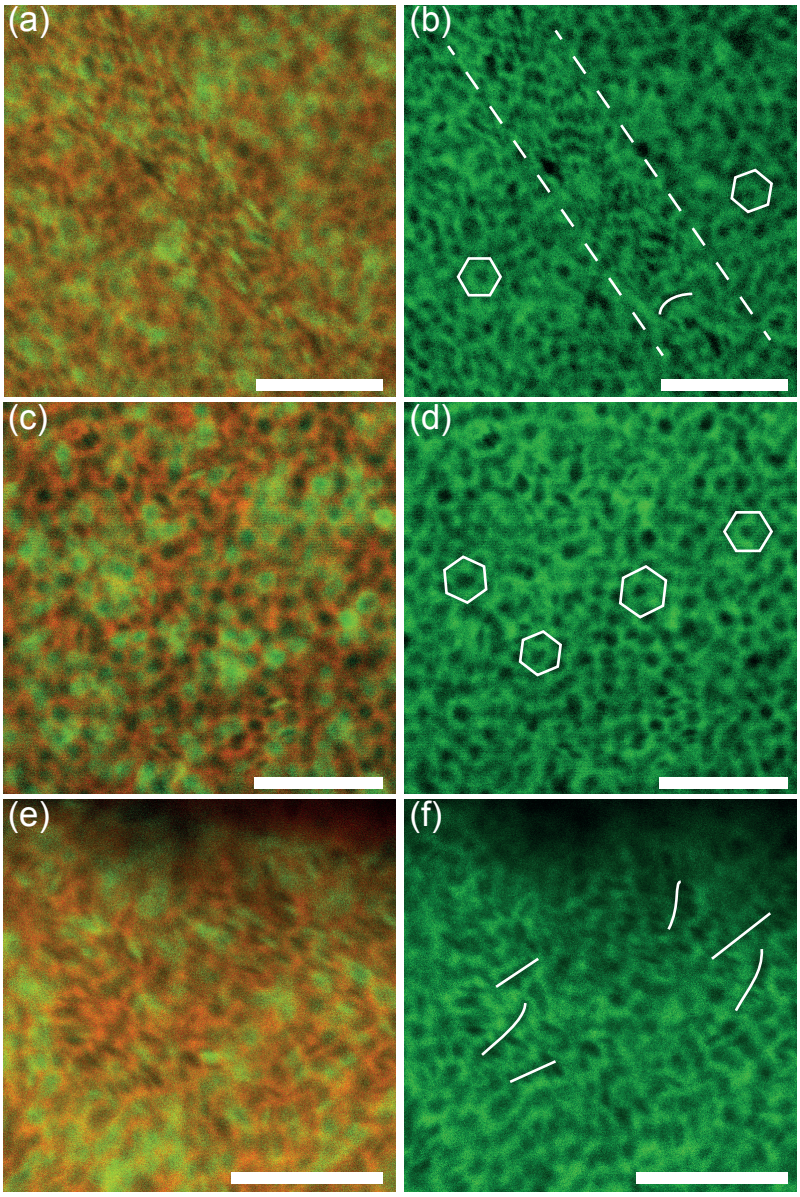

Fig. 7.8 Typical confocal microscopy images taken in sample **gpf-5%-DANS**, ϕ_g = 4.5%. The sample was allowed to sediment for 1.5 months before the images were taken. (a) en (b) are taken 3 μm from the bottom and in the middle of the capillary. (c - f) are taken 0.5 μm from the bottom of the capillary, (c, d) in the middle and (e, f) near the edge of the capillary, respectively. In (a, c, e) the particles are either green (labelled) or black (non-labelled), the solvent is orange. In (b, d, f), although confusing, the solvent is green and all particles are black, to improve the visibility. The white bars denote 5 μm.

hexagons. However, this order is only local and is not evident for all particles.

Fig. 7.8(c, d) are taken at a height of 0.5 μm, significantly closer to the bottom of the sample. The particles have a preferential orientation near the bottom; they prefer to align parallel to the surface. Indeed only few particles are perpendicular to the focal plane; the majority of the particles is parallel to the bottom of the sample. Domains of particles with a perpendicular orientation, like those observed at a height of 3 μm (Fig. 7.8(a, b)), are not observed at this height and a larger number of particles have neighbours in a (distorted) hexagonal surrounding. There is however, no true long-range positional order. The microscopy images shown in Fig. 7.8(e, f) are taken at the same height, but close to the capillary wall. Also here the effect of the wall can clearly be observed. The majority of the particles is, in contrast to what is observed far away from the wall, perpendicular to the focal plane. Various stacks of particles can be observed.

The results of the confocal studies indicate that the particles have formed a N_C phase. To support these results we additionally used small-angle x-ray scattering to characterize the liquid crystal phase. SAXS patterns were taken at various positions in a rectangular capillary containing dispersions **gpf-10%** (ϕ_g = 4.5%). The phase behaviour in these capillaries is expected to be similar to the behaviour in the confocal sample cells. Fig. 7.9(a, b) show images of the capillaries upon illumination with white light. Bragg reflections, indicating positional order, can clearly be observed. They are most pronounced in the top part of the sample. SAXS patterns taken at the positions denoted by O and X are shown in Fig. 7.9(c) and Fig. 7.9(d), respectively. In the pattern taken higher in the capillary (d) an intense, but rather broad, reflection can be observed at Q = 0.009 nm^{-1} combined with a weak and diffuse reflection at Q = 0.06 nm^{-1} (Fig. 7.9(f)). These reflections indeed originate from the (multi-domain) N_C phase [29] (see also Chapter 6 in this thesis). The intense peak at low Q corresponds to a repetition distance of 698 nm, which is slightly larger than the particle diameter (~662 nm). This peak originates from the positional correlation between the stacks. Since the characteristic 10, 11, 20 and 21 reflections of a hexagonal columnar crystal lattice are absent, it is highly unlikely that the phase present is hexagonal columnar. The weak and diffuse reflection observed at high Q originates from the liquid-like correlations between the particles within the stacks. This peak corresponds to a real space value of ~100 nm, which is significantly larger than the particle thickness (~33 nm). Although the particles are dispersed in an organic solvent, some charges are always present, which leads to large double layers surrounding the particles. The resulting electrostatic repulsion is stronger between the particles within the stacks, which are oriented face-to-face, than between particles in different stacks, which are oriented edge-to-edge. This might explain the increased spacing between the particles within the stacks.

The positional peak at low Q corresponding to the side-to-side correlations of the stacks can be observed as well in the pattern taken lower in the capillary (Fig.

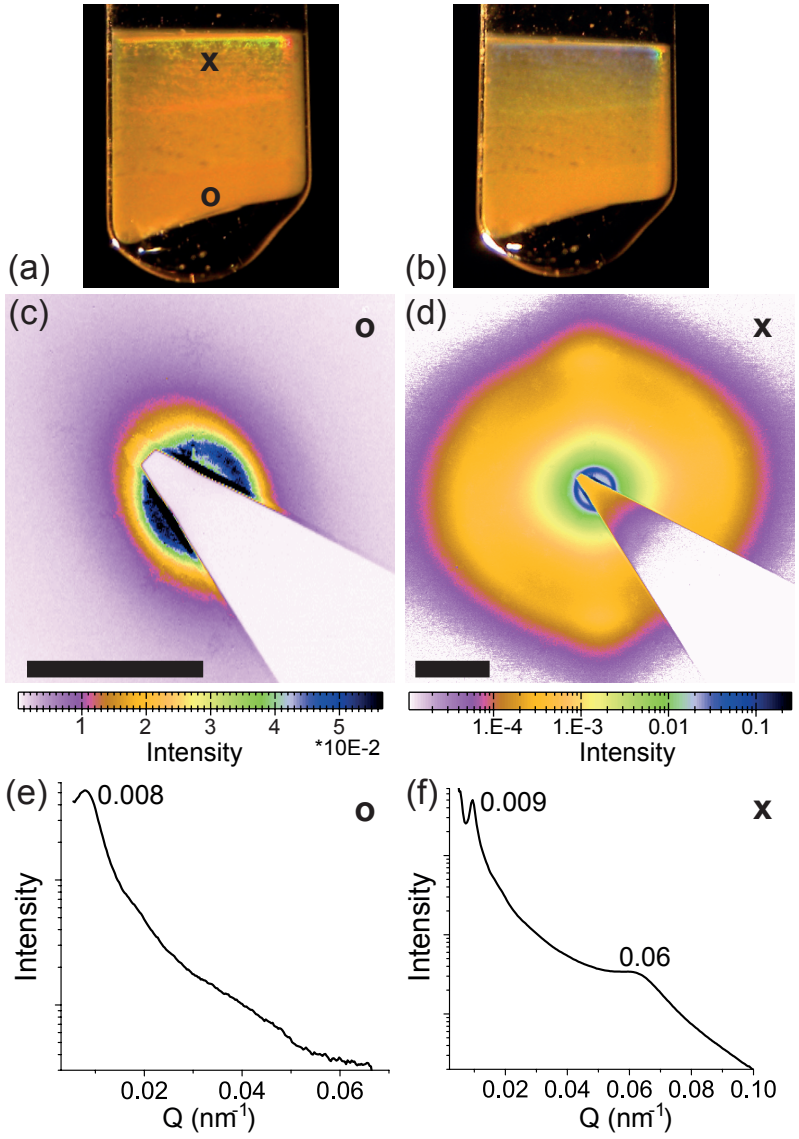

Fig. 7.9 Photographs (a, b) taken under illumination, under different angles, with white light taken of sample **gpf-10%** (ϕ_g = 4.5). The sample was 3 months old. X and O denote where the SAXS patterns shown in (c), (d), respectively, were taken. (e, f) show the I(Q) profiles averaged over all angles corresponding to the SAXS patterns shown in (c, d), respectively. Q-values (in nm^{-1}) corresponding to the peak positions are indicated. The black bars denote 0.03 nm^{-1}.

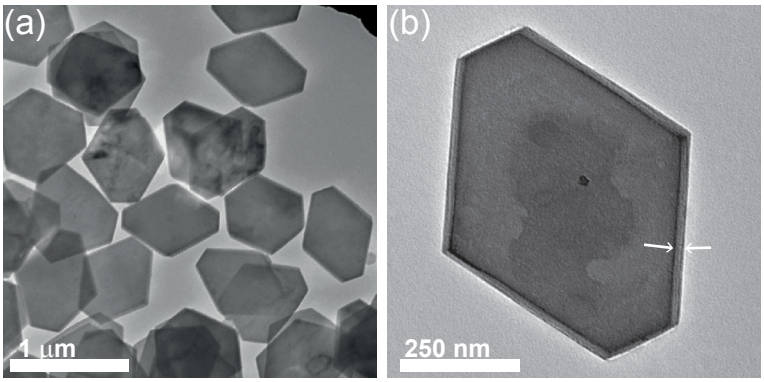

Fig. 7.10 TEM pictures of gibbsite particles covered with a non-fluorescent (a) and fluorescent (b) silica shell. The white arrows in (b) point to the silica layer.

7.9(c)). This peak is broader, weaker and found at a slightly lower Q-value. The liquid reflection of the particles within the stacks was too weak to observe with normal exposure times. This indicates that the N_C phase present in the lower part of the capillary is less well ordered than the N_C phase higher in the sample. In the lower parts of the capillary the phase is formed on short time scales and at a higher osmotic pressure than higher in the capillary, which frustrates (long-range) ordering.

The SAXS results confirm the formation of the N_C liquid crystal phase. Also the distances found for the side-to-side correlations of the stacks agrees well with the confocal results. Measuring stack distances in the confocal pictures, like in e.g. Fig. 7.8, reveals values of roughly 730 nm. SAXS results revealed that the N_C phase is less well ordered further down in the samples. Due to the maximum focal depth of the confocal microscope (~200 μm) this region is unfortunately the only region that can be studied with CLSM. However, CLSM definitely complements SAXS measurements. With CLSM local ordering, at the particle level, can be studied quite well while the smallest area that can be investigated by SAXS is at least 500 x 500 μm.

7.3.3 Fluorescent silica coated gibbsite

The technique of covering gibbsite particles with first a layer of fluorescent silica, followed by a layer of non-fluorescent silica is promising for confocal microscopy studies. The addition of the non-fluorescent layer is expected to shield the interactions of the dye, and is additionally expected to improve the visibility.

TEM images of the particles as obtained from the synthesis are shown in Fig. 7.10. The particles appear to be stable; after washing aggregates were not observed. The arrows in Fig. 7.10(b) indicate the silica shell. The thickness of the silica shell was determined from the increase in the average particle diameter *D*. The thickness of the silica layer was found to be 15 nm for the fluorescent particles and 17 nm for the non-fluorescent particles.

The samples containing the particles dispersed in DMF sedimented within one

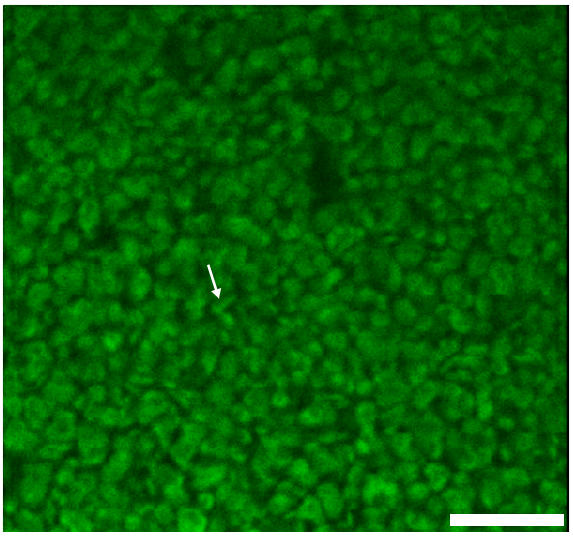

Fig. 7.11 Typical confocal microscopy image taken in a sample containing dispersion **gsf**, with a goethite volume fraction of 2.1% taken 1 day after sample preparation. The white arrow points to a particle which is perpendicular to the focal plane. The white bar denotes 2 μm.

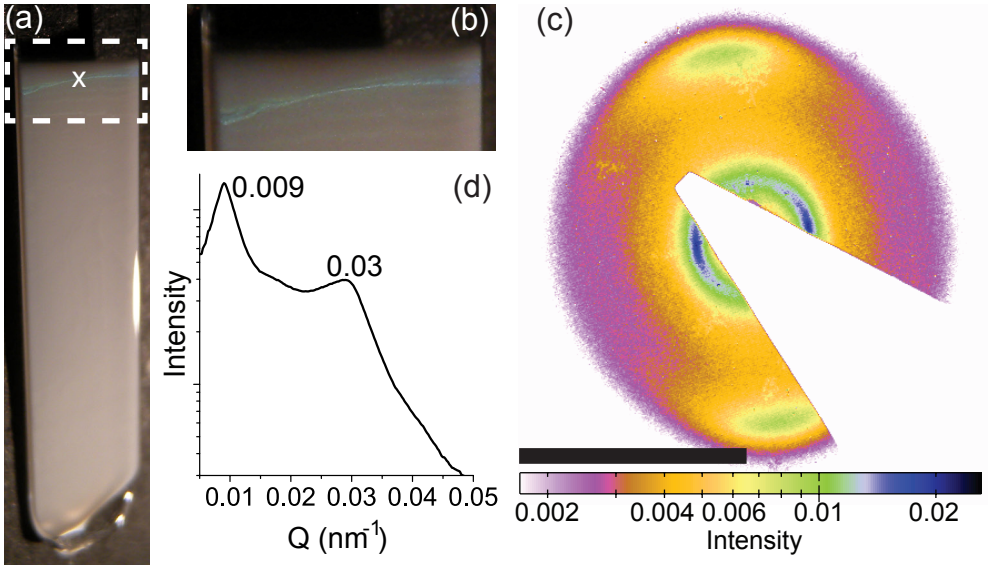

Fig. 7.12 (a) Picture of a capillary containing dispersion **gsn** with a ϕ_g = 13% under illumination with white light. The sample was allowed to sediment for ~ 1 year. A zoom of the area in which Bragg reflections were observed (white dashed box) is given in (b). The SAXS pattern shown in (c) is taken at the place denoted by X (a). The black bar denotes 0.025 nm^{-1}. The accompanying I(Q) profile averaged over all angles is shown in (d).

day, independent of the gibbsite volume fraction and presence of fluorescent particles. The density difference between DMF and gibbsite is even smaller than for gibbsite and tetralin and it is therefore expected that their gravitational length (Eq. (1.1) is larger. The observed increase in sedimentation speed therefore indicates a reduced particle stability.

A typical confocal microscopy image, taken in a sample containing dispersion gsf with a gibbsite volume fraction of 2.1%, is shown in Fig. 7.11. The visibility of the particles is quite good, single particles and their orientation can clearly be resolved. Unfortunately, it appears that the particles do not possess either orientational or positional order, independent of the volume fraction, sedimentation time and height in the capillary.

A sample containing a dispersion consisting of only unlabelled particles (**gsn**) was studied to investigate if the fluorescent dye inhibits liquid crystal phase formation. Also in this sample birefringence or Bragg reflections were not observed on a timescale of months. After sedimentation for approximately a year, Bragg reflections were observed, but only in the very top part of the sediment (Fig. 7.12(a, b)). SAXS revealed, like for the **gpf**-system, an intense and sharp reflection at low Q combined with a diffuse and weak reflection at higher Q, characteristic of the N_C phase. Unfortunately SAXS revealed isotropic patterns for the remainder of the capillary indicating that these particles are not ordered.

These results indicate that it is highly challenging to form liquid crystals from the silica covered particles. As practically no order is observed in the non-fluorescent particles as well, it is assumed that the fast sedimentation speed of the particles is inhibiting the particles from ordering. Several methods were tried to decrease the gravitational length. It was tried to obtain hollow particles by removing the gibbsite core through etching using concentrated HCl. Unfortunately, we found that for a silica layer thickness < ~20 nm, the silica shells break or collapse. Increasing the solvent viscosity by dispersing particles in a mixture of water and glycerol, also decreases the dynamics of particles reorienting and did therefore not lead to the formation of LCs. Like in the work described by Kuijk *et al*. [8, 40] and Murray *et al*. [40], we tried sterically stabilizing the surface of the silica particles with OTMOS (octadecyltrimethoxysilane), but unfortunately these syntheses resulted in particles aggregating.

7.4 Conclusions and Recommendations

We have developed two different systems of fluorescent plate-like gibbsite particles suitable for CLSM and we have studied the liquid crystal phase behaviour of these systems in real-time and space using CLSM.

One system consists of submicrometer-sized sterically stabilized gibbsite platelets dispersed in an organic solvent. Since the dye, which was attached to the steric stabilizer, destabilizes the particles only part of the platelets in the dispersion could

be labelled. With CLSM single particles as well as their orientation could be observed. By additionally dying the solvent, all particles could be visualized. The particles were found to form a multi-domain columnar nematic liquid crystal phase: domains of stacks of particles with different orientations could be observed but long-range positional order was not present.

The second system consists of large gibbsite particles around which a (non-) fluorescent silica layer was grown. Also for this system single particles could be imaged with CLSM. Unfortunately, the particles did not possess orientational or positional order.

Additional SAXS-measurements on vertically stored capillaries revealed that only the particles in the very top layer of the sediment possessed order. The particles have a short gravitational length (Eq. (1.1). This leads to high sedimentation speeds which inhibit LC phase formation. This effect is most pronounced near the bottom of the sample, which is exactly the region that can be studied by CLSM.

The fluorescent particles do have a good visibility and are therefore promising for CLSM experiments. Several methods were tried to reduce the sedimentation speed but this has not led to the formation of well-ordered liquid crystals, yet. For future research we believe the most promising method to decrease the high sedimentation speed is to grow a thick (> 20 nm) silica layer around the particles, followed by etching out the gibbsite core. Increasing the amount of silica precursor during the Stöber synthesis often leads to the formation of secondary growth and irreversible cluster formation. We therefore recommend to execute the synthesis in an ultrasonic bath and to add the silica precursor gradually using a peristaltic pump, as described by for example Rossi *et al*. [41]

In summary our results show that CLSM is a promising technique supplementary to the techniques generally used to study liquid crystal formation. Whereas the strength of other techniques, like SAXS, is in characterizing the average structure of bulk liquid crystal phases, CLSM enables studying liquid crystalline order locally and at the single particle level. This allows studies of e.g. nucleation and growth, and of transitions between different (domains of) liquid crystalline phases. We were able to observe wall-induced alignment in a system of gibbsite platelets, which indicates that CLSM is a promising technique for confinement studies as well. The methods we applied to make the gibbsite platelets suitable for CLSM are quite general and could be applied to various other (anisotropic) metal-oxide particles.

Acknowledgements

Elleke van Harten is thanked for performing the experiments and acquiring the data for the figures shown in this chapter. We would like to thank Fiona Yarrow for her help with the AFM measurements and Sonja Castillo for her help with the EM measurements. Additionally we would like to thank the staff of the BM26 beamline

"DUBBLE" at the ESRF, as well as Vera Meester and Antara Pal for their support during the synchrotron experiments.

References

[1] L. Onsager, *Ann. N. Y. Acad. Sci.*, 1949, **51**, 627-659.
[2] J. A. C. Veerman and D. Frenkel, *Phys. Rev. A*, 1992, **45**, 5632-5648.
[3] D. Frenkel, H. N. W. Lekkerkerker and A. Stroobants, *Nature*, 1988, **332**, 822-823.
[4] A. Stroobants, H. N. W. Lekkerkerker and D. Frenkel, *Phys. Rev. Lett.*, 1986, **57**, 1452-1455.
[5] P. Davidson and J. C. P. Gabriel, *Curr. Opin. Colloid In.*, 2005, **9**, 377-383.
[6] H. N. W. Lekkerkerker and G. J. Vroege, *Philos. T. R. Soc. A*, 2013, **371**, 20120263.
[7] A. Kuijk, A. van Blaaderen and A. Imhof, *J. Am. Chem. Soc.*, 2011, **133**, 2346-2349.
[8] A. Kuijk, *Fluorescent colloidal silica rods - synthesis and phase behavior*, 2012.
[9] F. van der Kooij, K. Kassapidou and H. Lekkerkerker, *Nature*, 2000, **406**, 868-871.
[10] A. B. G. M. Leferink op Reinink, E. van den Pol, A. V. Petukhov and G. J. Vroege, *Eur. Phys. J. Spec. Top*., 2013, **222**, 3053-3069
[11] D. de las Heras, E. Velasco and L. Mederos, *Phys. Rev. Lett.*, 2005, **94**, 017801.
[12] D. van der Beek, A. V. Petukhov, S. M. Oversteegen, G. J. Vroege and H. N. W. Lekkerkerker, *Eur. Phys. J. E*, 2005, **16**, 253-258.
[13] J. Kim, A. de la Cotte, R. Deloncle, S. Archambeau, C. Biver, J. Cano, K. Lahlil, J. Boilot, E. Grelet and T. Gacoin, *Adv. Funct. Mater.*, 2012, **22**, 4949-4956.
[14] A. A. Verhoeff, I. A. Bakelaar, R. H. J. Otten, P. van der Schoot and H. N. W. Lekkerkerker, *Langmuir*, 2011, **27**, 116-125.
[15] A. A. Verhoeff and H. N. W. Lekkerkerker, *Soft Matter*, 2012, **8**, 4865-4868.
[16] M. C. D. Mourad, D. V. Byelov, A. V. Petukhov, D. A. M. de Winter, A. J. Verkleij and H. N. W. Lekkerkerker, *J. Phys. Chem. B*, 2009, **113**, 11604-11613.
[17] D. V. Byelov, J. Meijer, I. Snigireva, A. Snigirev, L. Rossi, E. van den Pol, A. Kuijk, A. Philipse, A. Imhof, A. van Blaaderen, G. J. Vroege and A. V. Petukhov, *Rsc Advances*, 2013, **3**, 15670-15677.
[18] M. M. van Schooneveld, J. Hilhorst, A. V. Petukhov, T. Tyliszczak, J. Wang, B. M. Weckhuysen, F. M. F. de Groot and E. de Smit, *Small*, 2011, **7**, 804-811.
[19] J. Hilhorst, M. M. van Schooneveld, J. Wang, E. de Smit, T. Tyliszczak, J. Raabe, A. P. Hitchcock, M. Obst, F. M. F. de Groot and A. V. Petukhov, *Langmuir*, 2012, 28, 3614-3620.
[20] S. Brisard, R. S. Chae, I. Bihannic, L. Michot, P. Guttmann, J. Thieme, G. Schneider, P. J. M. Monteiro and P. Levitz, *Am. Mineral.*, 2012, **97**, 480-483.
[21] L. J. Michot, I. Bihannic, F. Thomas, B. S. Lartiges, Y. Waldvogel, C. Caillet, J. Thieme, S. S. Funari and P. Levitz, *Langmuir*, 2013, **29**, 3500-3510.

[22] W. Kegel and A. van Blaaderen, *Science*, 2000, **287**, 290-293.
[23] A. Yethiraj and A. van Blaaderen, *Nature*, 2003, **421**, 513-517.
[24] O. J. Dammone, I. Zacharoudiou, R. P. A. Dullens, J. M. Yeomans, M. P. Lettinga and D. G. A. L. Aarts, *Phys. Rev. Lett.*, 2012, **109**, 108303.
[25] M. P. Lettinga and E. Grelet, *Phys. Rev. Lett.*, 2007, **99**, 197802.
[26] A. M. Wierenga, T. A. J. Lenstra and A. P. Philipse, *Colloid. Surface. A*, 1998, **134**, 359-371.
[27] J. Wijnhoven, *J. Colloid Interf. Sci.*, 2005, **292**, 403-409.
[28] S. Shen, P. S. Chow, F. Chen, S. Feng and R. B. H. Tan, *J. Cryst. Growth*, 2006, **292**, 136-142.
[29] M. C. D. Mourad, E. J. Devid, M. M. van Schooneveld, C. Vonk and H. N. W. Lekkerkerker, *J. Phys. Chem. B*, 2008, **112**, 10142-10152.
[30] M. C. D. Mourad, A. V. Petukhov, G. J. Vroege and H. N. W. Lekkerkerker, *Langmuir*, 2010, **26**, 14182-14187.
[31] W. Stober, A. Fink and E. Bohn, *J. Colloid Interf. Sci.*, 1968, **26**, 62.
[32] C. Vonk, S. Oversteegen and J. Wijnhoven, *J. Colloid Interf. Sci.*, 2005, **287**, 521-525.
[33] J. Wijnhoven, *Chem. Mat.*, 2004, **16**, 3821-3828.
[34] C. Graf, D. Vossen, A. Imhof and A. van Blaaderen, *Langmuir*, 2003, **19**, 6693-6700.
[35] A. Petukhov, J. Thijssen, D. t Hart, A. Imhof, A. van Blaaderen, I. Dolbnya, A. Snigirev, A. Moussaid and I. Snigireva, *J. Appl. Crystallogr.*, 2006, **39**, 137-144.
[36] W. Bras, I. Dolbnya, D. Detollenaere, R. van Tol, M. Malfois, G. Greaves, A. Ryan and E. Heeley, *J. Appl. Crystallogr.*, 2003, **36**, 791-794.
[37] A. Wierenga, A. P. Philipse, H. N. W. Lekkerkerker and D. V. Boger, *Langmuir*, 1998, **14**, 55-65.
[38] P. A. Buining, C. Pathmamanoharan, J. B. H. Jansen and H. N. W. Lekkerkerker, *J. Am. Ceram. Soc.*, 1991, **74**, 1303-1307.
[39] A. B. G. M. Leferink op Reinink, E. van den Pol, D. V. Byelov, A. V. Petukhov and G. J. Vroege, *J. Phys.: Condens. Matter*, 2012, 24, 464127.
[40] E. Murray, P. Born, A. Weber and T. Kraus, *Adv. Eng. Mat.*, 2010, **12**, 374-378.
[41] L. Rossi, S. Sacanna, W. T. M. Irvine, P. M. Chaikin, D. J. Pine and A. P. Philipse, *Soft Matter*, 2011, **7**, 4139-4142.

Summary

This thesis discusses lyotropic liquid crystals of anisometric colloidal mineral particles. While lyotropic liquid crystals generally form spontaneously, the focus in this thesis is on manipulating the formation of liquid crystals and tuning the (spontaneously) formed liquid crystalline structures. Small angle x-ray scattering (SAXS) is an excellent technique to characterize liquid crystalline structures and is therefore the technique that is predominantly used throughout this thesis.

This thesis is split in two parts. **Part 1** describes various approaches to influence the liquid crystal phase behaviour of board-like *goethite* (α-FeOOH) particles. In **Chapter 2** the phase behaviour of a dispersion of polydisperse chromium-modified goethite colloids slowly sedimenting in the earth gravitational field is studied over a time span of five years. Despite the high particle polydispersity (30%) the dispersion displays rich phase behaviour; the colloids spontaneously form isotropic, nematic, smectic as well as two types of columnar phases. We found that, under the influence of the gravitational field, the nematic phase grows at the expense of a better ordered smectic phase, by absorbing particles that do not fit the smectic periodicity. We additionally found that the system displays fractionated crystallization in both the smectic and the columnar phase. Furthermore, it was found that the two columnar phases spontaneously transform into each other.

In **Chapter 3** we influence the phase behaviour by changing the inter-particle interactions by introducing a depletant into the suspension. We find that the depletant-induced attraction between the particles leads to the formation of a smectic phase superseding the nematic phase. Careful analysis of the scattering patterns suggests that the particles within the layers are biaxially ordered.

In the final two chapters of **Part 1**, **Chapter 4** and **Chapter 5**, we utilize an external magnetic field to tune the liquid crystalline phases. In **Chapter 4** the influence of an external magnetic field on the *biaxiality* of nematic phases is studied both experimentally and theoretically. It is found that applying a weak field to the biaxial nematic phase can (at sufficiently high field strength) completely suppress the biaxiality, causing the biaxial nematic phase to transform into a regular prolate uniaxial nematic phase. Our theoretical results confirm these findings. Additionally, they predict that applying a magnetic field to an oblate uniaxial nematic phase induces the formation of the rare biaxial nematic phase. This opens up novel possibilities of tuning biaxiality in nematic liquid crystals.

In **Chapter 5** a strong external magnetic field is used to study the reorientation behaviour of the goethite columnar phase. Dynamics are slow in this dense and viscous phase, enabling the characterization of the transient structures by small angle x-ray scattering. The transient scattering patterns show typical deformed Bragg reflections which reveal the reorientation pathway. It appears that realignment

proceeds via collective rotations of domains inducing nanoshear between the layers. These results support the martensitic transition pathway that was proposed in Chapter 2 for the reversible transition between the two different columnar phases.

Part 2 of this thesis describes the plate-like *gibbsite* (γ-$Al(OH)_3$) system. Gibbsite is, compared to goethite, less susceptible to external magnetic fields. However, the particles have a strong preferential orientation near a wall or surface. It is therefore predicted that spatial confinement can have a strong influence on gibbsite liquid crystal phase formation. Experimental confinement studies are rare, especially of positionally ordered liquid crystals. The challenge lies in the characterization techniques. In this thesis we therefore focus on large (> 500 nm) gibbsite platelets, which are advantageous as they can be made visible with optical microscopy. Their SAXS studies are, however, more challenging since the formed structures are less ordered. In **Chapter 6** we develop a 3D-SAXS method, in which the measurements are performed with various sample orientations. We observe that Bragg reflections of the side-to-side correlations of particles in the columnar nematic phase shift to larger Q-values upon sample rotation. In contrast, observable Bragg reflections of particles in the columnar phase stay at constant Q for all angles. This method gives more insight in 3D liquid crystal structures and helps unambiguous identification of the liquid crystal phase.

In the final chapter (**Chapter 7**) of this thesis we take steps towards enabling real time and space studies of liquid crystals by adapting the gibbsite system such that the particles can be studied with confocal laser scanning microscopy. We describe two synthesis routes to obtain large and fluorescently labelled platelets. Additionally, the results of a preliminary confocal microscopy study of the formed (liquid crystal) structures are discussed. Although particle stability remains an issue -due to dye-dye interactions- we were able to observe single particles, resolve their (local) ordering and determine the liquid crystal phase.

Samenvatting in het Nederlands (ook voor leken)

De titel van dit proefschrift, 'Colloidal mineral liquid crystals, *Formation & manipulation'*, zal de meeste mensen zeer weinig tot helemaal niets zeggen. De Nederlandse titel: 'Vloeibare kristallen van minerale colloïden, *Formatie & manipulatie*' maakt het eigenlijk ook niet veel beter. In de afgelopen jaren hebben veel mensen interesse getoond in en vragen gesteld over wat ik nou eigenlijk precies doe op mijn werk. Ondanks mijn pogingen om het uit te leggen blijft het voor veel mensen moeilijk te bevatten. Over bijvoorbeeld het begrip 'vloeibare kristallen', hoor ik regelmatig: "daar heb ik nog nooit van gehoord". Dit is opmerkelijk, aangezien bijna iedereen er vrijwel elke dag mee te maken heeft. Tv's, laptops en smartphones bevatten heel vaak een LCD – oftewel *Liquid Crystal Display* – scherm.
In deze samenvatting probeer ik daarom op een begrijpelijke manier uit te leggen wat ik gedaan heb. Ik zal daartoe eerst de vaktermen uitleggen om vervolgens de diepte in te gaan door per hoofdstuk te omschrijven wat de resultaten van mijn onderzoek zijn.

Vloeibare kristallen

Bij het woord '*kristal*' zullen mensen wellicht denken aan edelstenen, zoals opalen. Of bergkristallen en ijskristallen. Al deze voorbeelden hebben één gezamenlijke eigenschap die ze typeert als kristal: de moleculen of atomen waaruit ze bestaan zijn ruimtelijk geordend in alle 3 de dimensies. Oftewel: ze zijn gerangschikt in een geordend patroon. Dit is te zien in Figuur S1(a); de atomen/moleculen (grijze bolletjes) lijken op een rooster te liggen. Bovenstaande kristal voorbeelden zijn van bolvormige (sferische) atomen/moleculen. Ze zijn alleen positioneel geordend en het kristal is een vaste stof.

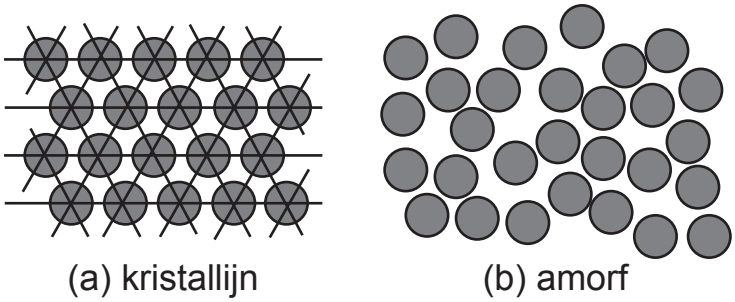

Figuur S1. Schematische tekeningen van atomen/moleculen die (a) kristallijn, oftewel ruimtelijk geordend en (b) amorf, oftewel ongeordend zijn.

Tegenovergesteld daaraan zijn vaste stoffen waarin de atomen/moleculen ongeordend zijn, dit noemen we *amorf* (Figuur S1(b)). Een voorbeeld daarvan zijn de silicium atomen in glas ('kristallen' glazen zijn volgens de wetenschappelijke definitie dus geen kristallen!).

Sferische moleculen en atomen in een *vloeistof* zijn net als in een amorfe vaste stof *ongeordend*. Maar in tegenstelling tot vaste stoffen is een vloeistof *vloeibaar*. Waar moleculen/atomen in een vaste stof alleen op hun eigen plek een heel klein beetje kunnen bewegen, kunnen moleculen/atomen in een vloeistof vrij langs elkaar heen bewegen.

Vloeibare kristallen zijn, zoals de naam al zegt, kristallen, oftewel geordende structuren, die nog vloeien als een vloeistof. Dit is mogelijk omdat vloeibare kristallen gevormd worden door anisotrope moleculen. Anisotroop betekent 'niet gelijk in alle richtingen' en betekent in dit geval niet-bolvormig. Een voorbeeld hiervan zijn staaf-, balk- of schijfvormige moleculen. Hierdoor ontstaan er nieuwe mogelijkheden: deze moleculen kunnen behalve positionele ordening (zoals in een regulier kristal), ook oriëntatie-ordening hebben. Dit is bijvoorbeeld wanneer alle deeltjes dezelfde kant uitwijzen, oftewel allemaal dezelfde oriëntatie hebben (zoals Mikado stokjes in hun verpakking). Wanneer de deeltjes wel dezelfde oriëntatie hebben, maar geen positie-ordening, dan wordt dit een *nematisch* vloeibaar kristal genoemd. Dit is in Figuur S2 geïllustreerd voor zowel staafvormige moleculen, die hun lange as uitlijnen, als voor schijfvormige moleculen, die hun korte as uitlijnen (pijltjes in Figuur S2). Wanneer de moleculen vervolgens ook in één richting positioneel geordend zijn, noemen we dit een *smectisch* vloeibaar kristal. De moleculen hebben dan lagen gevormd, waarin ze vrij kunnen bewegen. Dit is weergegeven in Figuur S2 voor staafvormige deeltjes, schijfvormige deeltjes vormen doorgaans geen smectisch vloeibaar kristal. Een andere vloeibaar kristalfase is de *columnaire* fase. Hierin vormen de deeltjes kolommen. Deze kolommen ordenen zich dan (positioneel) in twee richtingen (2D), zoals te zien is in Figuur S2. Behalve deze (deels) geordende fasen is er nog de isotrope fase (in alle richtingen gelijk), waarin de deeltjes niet geordend zijn (zoals Mikado stokjes in spelsituatie).

Vloeibare kristallen hebben meerdere toepassingen, waarvan de LCD-schermen veruit de meest voorkomende zijn. Vloeibare kristallen hebben de eigenschap dubbelbrekend te zijn. Dit betekent dat de brekingsindex van het materiaal afhangt van de invalrichting en polarisatie van het licht. Verschillen in brekingsindex spelen ook een rol bij een rietje in een glas water: doordat water een andere brekingsindex heeft dan de lucht lijkt de positie van het rietje in het water te zijn versprongen ten opzichte van de positie in de lucht. Het is precies deze eigenschap die vloeibare kristallen geschikt maakt voor LCD's. De oriëntatie van de moleculen is aan te passen met een elektrische spanning. Elektrische spanning wordt in beeldschermen dan ook gebruikt om pixels (kleine kamertjes vloeibaar kristal) aan en uit te zetten.

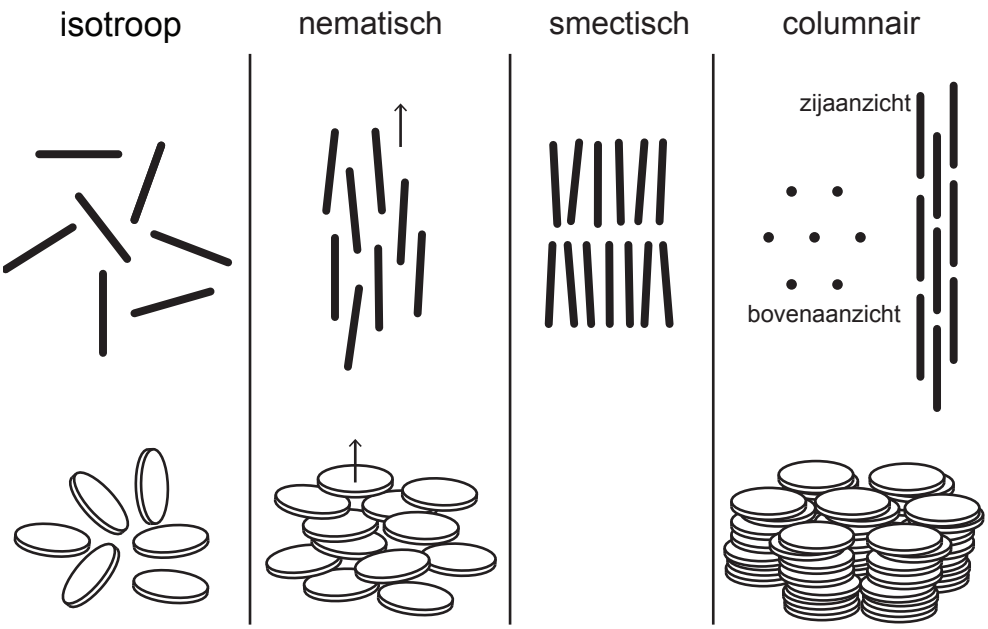

Figuur S2. Schematische illustraties van de verschillende vloeibaar kristalfasen. Van links naar rechts: isotroop, nematisch, smectisch en columnair, hier weergegeven voor zowel staaf- als schijfvormige moleculen.

Colloïden

Colloïden zijn deeltjes met een afmeting tussen de pakweg 1 en 1000 nanometer. Een nanometer is een miljard keer zo klein als een meter. Om het je beter voor te kunnen stellen: een colloïd van 500 nanometer groot is ongeveer 100 keer kleiner dan de dikte van een hoofdhaar. Ondanks dat dit zeer klein is, is dit nog altijd grofweg 1000 keer zo groot als een atoom of een klein molecuul, zoals een watermolecuul (H_2O). Ter vergelijking: een olympisch zwembad is ongeveer 1000 keer zo groot als een glas water. Het is precies deze colloïdale afmeting, die deze deeltjes zo interessant maakt. Omdat ze zeer klein zijn gedragen ze zich net als moleculen en atomen, maar doordat ze toch veel groter zijn dan dat zijn ze makkelijker te bestuderen (met bijvoorbeeld microscopen). Colloïden worden daarom regelmatig gebruikt als 'modelsysteem' voor atomaire en moleculaire systemen.

Vanwege hun kleine afmeting kunnen colloïden net als opgeloste moleculen door een vloeistof heen zweven, zonder dat ze direct naar de bodem zinken (zoals de al vele malen grotere zandkorrels). Wanneer colloïden in een vloeistof zijn gebracht noemen we het een colloïdale dispersie, of kortweg: *dispersie*. Colloïdale dispersies zijn veelvoorkomend in het dagelijks leven. Voorbeelden zijn onder andere latexverf, melk, mayonaise en inkt.

Colloïdale vloeibare kristallen

Colloïdale vloeibare kristallen bestaan dus uit anisotrope (niet-bolvormige) colloïden. Er bestaat een grote verscheidenheid aan anisotrope colloïdale deeltjes zoals virus en klei deeltjes. Veel van deze colloïden vormen inderdaad vloeibare kristallen.

Behalve de grootte van de deeltjes is er een ander groot verschil tussen colloïdale en moleculaire vloeibare kristallen: de wijze waarop de kristallen gevormd worden. Bij moleculaire vloeibare kristallen is het de temperatuur die bepaalt of de moleculen isotroop geordend zijn, of een vloeibaar kristal vormen. Dit noemen we daarom *thermotrope* vloeibare kristallen.

Vloeibare kristallen van colloïden zijn zogeheten *lyotrope* vloeibare kristallen. Dit betekent dat de vloeibaar kristal fase (isotroop, nemaat, smectisch, columnair) die gevormd wordt alleen afhangt van de vorm van de colloïden, en van hun concentratie (hoeveelheid colloïden per volume vloeistof). Als de concentratie colloïden laag is, is er genoeg ruimte voor de deeltjes om vrijuit te kunnen bewegen en de deeltjes zijn dus in de isotrope fase (Figuur S2). Als de deeltjesconcentratie toeneemt wordt deze ruimte beperkter. Het wordt dan gunstiger voor de colloïden om zich op te lijnen, en dus allemaal dezelfde oriëntatie aan te nemen. Ze verliezen weliswaar hun vrijheid van oriëntatie, maar krijgen in ruil daarvoor meer 'persoonlijke' ruimte waarin ze kunnen bewegen. Bij hogere concentraties vormen de deeltjes dus spontaan een nematische (opgelijnde) fase. Bij nog hogere concentraties zullen de colloïden zich ook positioneel gaan ordenen en ontstaan er smectische en/of columnaire fasen.

Voor netjes geordende fasen is het van belang dat de vloeibare kristallen zich langzaam vormen; de deeltjes hebben tijd nodig om hun ideale oriëntatie aan te nemen. Deeltjes direct in een heel hoge concentratie in een vloeistof brengen, leidt doorgaans dus niet tot mooie vloeibare kristallen. Daarom is het gebruikelijk om een dispersie te maken met een relatief lage concentratie colloïden. Langwerpige smalle glazen buisjes worden vervolgens gevuld met deze dispersie. Deze buisjes zullen dan verticaal (dus rechtop) bewaard worden. Onder de invloed van de zwaartekracht zullen de colloïden heel langzaam bezinken, waardoor de concentratie colloïden toe neemt in het onderste deel van het buisje. Daardoor ontstaat er in het sample een *gradiënt* in de colloïd concentratie, waarbij de concentratie hoger wordt naarmate men lager in het buisje komt. Op den duur (dit kan maanden en soms zelfs jaren duren) zullen zich dan vloeibare kristallen vormen in de delen van het buisje waar de concentratie hoog genoeg is. Omdat er meerdere concentraties voorkomen in hetzelfde buisje kunnen meerdere vloeibaar kristalfasen voorkomen. Doorgaans bevinden zich onderin het buisje de positioneel geordende fasen (smectisch en/of columnair), met direct daarboven een nematische fase, en daar weer boven de isotrope fase. Dit is in Figuur S3 schematisch weergegeven voor staafvormige colloïden.

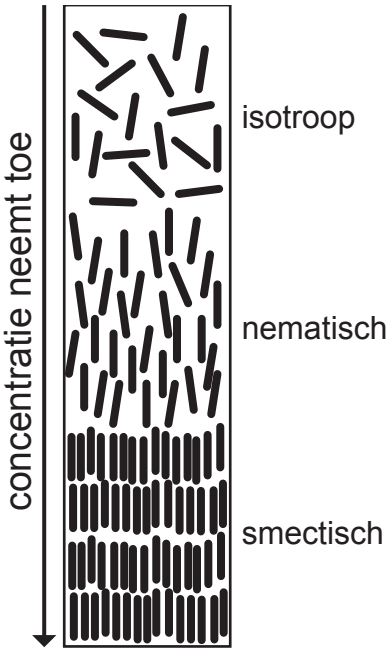

Figuur S3. Schematische tekening van een rechtop bewaard buisje met een colloïdale dispersie van een staafjes, die heel langzaam bezinken waardoor de concentratie colloïden toeneemt naarmate men lager in het buisje komt.

Momenteel zijn er weinig toepassingen voor colloïdale vloeibare kristallen. Echter, ook in dit geval kunnen ze fungeren als modelsystemen. De ontdekkingen die gedaan worden aan dit soort vloeibare kristallen kunnen vaak toegepast worden op moleculaire vloeibare kristallen, die wel toepassing vinden. Colloïden zijn vaak makkelijk te sturen met een elektrische spanning of een magneetveld. Daarom kunnen ook lyotrope vloeibare kristallen beïnvloed worden met bijvoorbeeld elektrische en/of magnetische velden.

In het onderzoek beschreven in dit proefschrift is de rode draad dan ook het uitzoeken op welke manieren we de formatie van vloeibare kristallen kunnen *beïnvloeden* en *sturen*, en daarmee samenhangend hoe we al gevormde vloeibare kristallen kunnen aanpassen. Het gecontroleerd kunnen bepalen welke vloeibaar kristal gevormd wordt, en in staat zijn om zeer goed geordende vloeibare kristallen te maken is belangrijk is voor toepassingen.

In dit proefschrift zijn vloeibare kristallen van twee verschillende colloïden bestudeerd: *goethiet* en *gibbsiet*. Beiden zijn mineralen: niet-organische verbindingen (d.w.z. dat ze geen koolstofatomen bevatten) die in de natuur voorkomen. In de volgende twee hoofdstukjes zal ik zowel goethiet als gibbsiet beschrijven.

Goethiet

Goethiet is een ijzeroxide met de molecuulformule FeOOH, en is dus in feite in soort roest. Het is een ijzererts dat over de hele wereld voorkomt. Het heeft een geeloranje kleur en werd daarom eeuwen geleden al gebruikt als pigment. In bijvoorbeeld prehistorische grotschilderingen in Frankrijk is goethiet aangetroffen. Meer recentelijk, in 2004, werd goethiet zelfs aangetroffen op de planeet Mars door Nasa's Mars Rover Opportunity.[1] Omdat goethiet alleen ontstaat als er water aanwezig is, levert goethiet hierdoor zelfs indirect bewijs dat er water was op Mars.

Ondanks dat goethiet ruimschoots voorkomt in de natuur, maken wij colloïdaal goethiet zelf in het lab via een chemische reactie. Daardoor hebben we meer controle over de grootte van de deeltjes. Colloïdaal goethiet heeft de vorm van een balk/baksteen, zoals te zien is op de foto die is genomen met een elektronenmicroscoop in Figuur S4 en op de schematische tekening in Figuur S5(a). De vorm en grootte van een goethiet deeltje wordt dan gedefinieerd door de lengte, breedte en dikte. Door deze heel specifieke vorm kan goethiet speciale vloeibaar kristal fasen vormen, namelijk *biaxiale* fasen. Biaxiaal betekent 'beide assen volgend', en dit beschrijft meteen wat een biaxiale fase is. In een normale nematische fase zijn de deeltjes uitgelijnd langs 1 as (Figuur S2). In het geval van schijfjes is dit de korte as. Voor staafjes en vaak ook goethiet is dit hun lange as (lengte) en kunnen ze om deze as vrij roteren, zoals te zien is in Figuur S5(b). Balkvormige deeltjes hebben een vorm die eigenlijk tussen staaf- en schijfvormig in zit. Daarom zullen de deeltjes in sommige gevallen niet alleen hun lange, of alleen hun korte as uitlijnen, maar *beide* assen. Dit noemen we een biaxiale (nematische) fase. Doordat beide assen zijn opgelijnd zijn de deeltjes dus meteen in alle drie de richtingen orientationeel geordend, zoals is weergegeven in Figuur S5(c t/m e). Behalve biaxiaal nematische fasen bestaan er ook biaxiaal smectische fasen. In dit geval zijn de deeltjes dan ook in de lagen in twee richtingen uitgelijnd.

Behalve isotroop, nematisch, biaxiaal nematisch, smectisch en biaxiaal smectisch vormt goethiet ook nog twee verschillende columnaire fasen.

Ook heeft colloïdaal goethiet erg interessante magnetische eigenschappen. De deeltjes zijn van zichzelf zwak magnetisch. Daarnaast kan een magnetisch veld eenvoudig een magnetisch moment induceren in de deeltjes (hetzelfde principe als het tijdelijk magnetisch maken van een spijker door er met een magneet langs te wrijven). Goethiet deeltjes zijn daardoor eenvoudig te sturen met een magneetveld.

Gibbsiet

Gibbsiet is een mineraal met molecuulformule $Al(OH)_3$. Zoals je misschien aan de molecuulformule kan zien, is gibbsiet een aluminiumhydroxide. Gibbsiet is dan ook

1. *http://www.nasa.gov/vision/universe/solarsystem/mer-121304b.html*

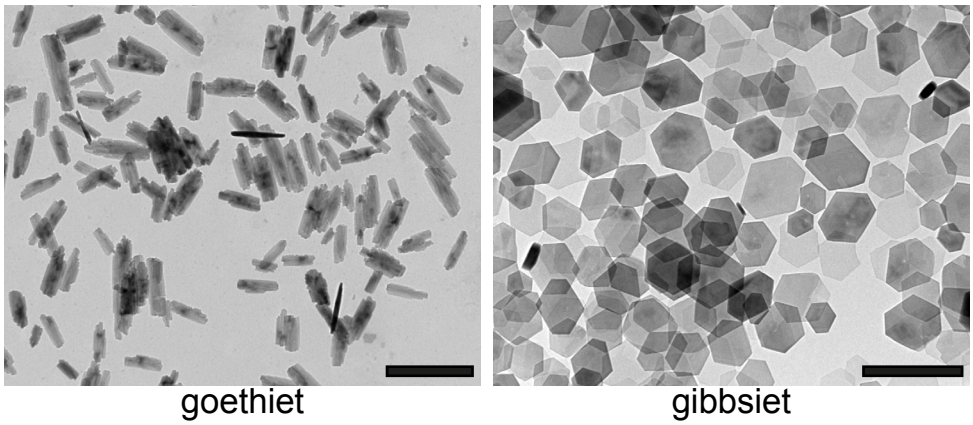

Figuur S4. Foto's van goethiet (links) en gibbsiet (rechts) colloïden genomen met een elektronenmicroscoop. De zwarte balkjes geven een lengte van 500 nm aan.

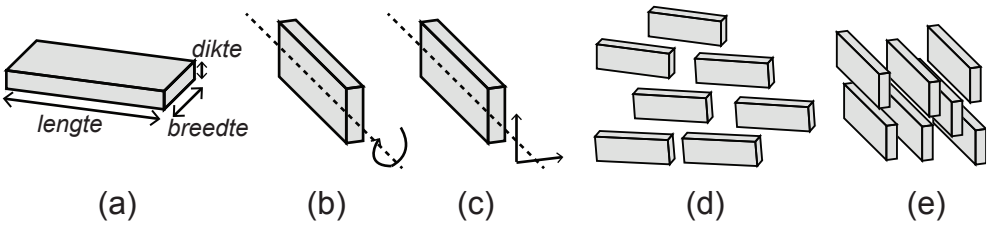

Figuur S5. Schematische tekeningen van (a) een goethiet colloïd, die zich in een normale nematische (b) en in een biaxiaal nematische (c) fase bevindt. In een normale nemaat kunnen de deeltjes nog draaien om hun lange as, terwijl ze in de biaxiaal nematische fase in drie richtingen uitgelijnd zijn, zoals te zien is in (d) en (e).

een belangrijke component van het erts bauxiet, dat de grondstof is voor de aluminiumproductie. Gibbsiet is een kleiachtig materiaal, en bestaat uit schijfvormige deeltjes. Net als goethiet is het veelvoorkomend, maar maken we colloïdaal gibbsiet voor vloeibaar kristalonderzoek zelf in het lab. Een (elektronenmicroscopie) foto van de hexagonale schijfjes is te zien in Figuur S4. Wanneer de gibbsiet deeltjes in dispersie worden gebracht, kunnen naast de isotrope fase zowel nematische als columnaire vloeibare kristallen ontstaan, zoals schematisch weergegeven in Figuur S2. Net als andere schijfvormige deeltjes vormt ook gibbsiet doorgaans geen smectische vloeibare kristallen.

In dit proefschrift

Dit proefschrift bestaat uit 7 hoofdstukken en gaat over het bestuderen en beïnvloeden van het vloeibaar kristalfasegedrag van goethiet en gibbsiet. Het bestuderen en vaststellen van de vloeibare kristalfasen is in dit proefschrift voornamelijk

gedaan met de techniek 'SAXS', wat staat voor small-angle X-ray scattering, oftewel: kleine-hoek Röntgen verstrooiing. Ondanks dat colloïden stukken groter zijn atomen en moleculen, zijn goethiet en gibbsiet moeilijk te bestuderen met optische microscopie. Dit komt door hun anisotropie: hun kleinste afmeting is kleiner dan de resolutie van een optische microscoop. Elektronenmicroscopie heeft een veel betere resolutie (kleiner dan een nanometer), maar voor deze techniek zijn droge samples nodig, en we willen juist *vloeibare* kristallen onderzoeken. SAXS is wel een heel geschikte techniek. Bij SAXS wordt het sample in een röntgenbundel geplaatst. De colloïden verstrooien deze röntgenstraling. De verstrooide röntgenstralen worden opgevangen door een detector, die er een plaatje van maakt. Een voorbeeld van een SAXS patroon is weergegeven in Figuur S6. De pieken die te zien zijn (zwart) geven informatie over de (vloeibaar) kristalstructuur. Zo kan uit de afstand vanaf het midden (zwarte kruis) tot de pieken worden afgeleid hoe groot de afstand tussen de colloïden in het kristal is, terwijl de breedte van de pieken aangeeft hoe goed geordend het (vloeibaar) kristal is.
Voordat in dit proefschrift eigen onderzoeksresultaten beschreven worden geeft Hoofdstuk 1 eerst een uitgebreide introductie in lyotrope vloeibare kristallen en hoe externe velden - onder andere het zwaartekrachtveld van de aarde en een extern magneetveld - gebruikt kunnen worden om invloed uit te oefenen op (de formatie van) vloeibare kristallen. Daarna is het proefschrift opgesplitst in twee delen. Deel 1 (Hoofdstukken 2 t/m 5) gaat over goethiet. Deel 2 (Hoofdstukken 6 en 7) gaat vervolgens over gibbsiet.

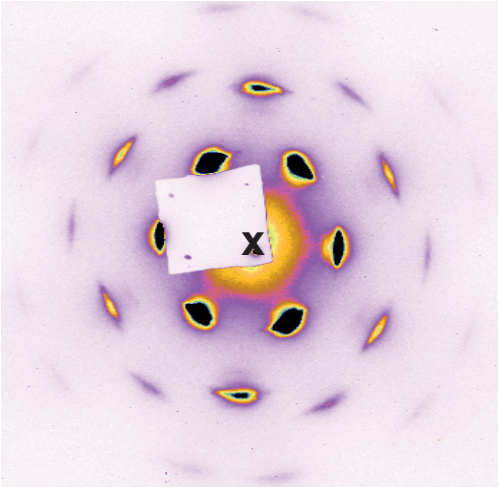

Figuur S6. Typisch SAXS-patroon, in dit geval van de gibbsiet columnaire fase.

Deel 1 – Goethiet

In dit deel van het proefschrift ligt de focus volledig op het beïnvloeden en sturen van goethiet vloeibare kristallen.

In Hoofdstuk 2 kijken we naar de invloeden van het zwaartekrachtsveld van de aarde. Zoals boven uitgelegd maken we samples door goethiet dispersies met lage concentraties te laten bezinken (sedimenteren) in het zwaartekrachtsveld van de aarde. Behalve het creëren van een concentratiegradiënt is dit ook noodzakelijk omdat goethiet colloïden, net als veel andere colloïden, *polydispers* zijn. Dit houdt in dat niet alle deeltjes even groot zijn. De dispersie beschreven in dit hoofdstuk bestaat uit goethiet deeltjes met een lengte van 227 nanometer en een polydispersiteit van 30%. Dit houdt in dat de deeltjes gemiddeld 227 nanometer lang zijn, maar dat er ook deeltjes voorkomen van 160 en 290 nanometer lang, en van alles daartussenin. Dit is ook te zien op de foto in Figuur S4. Voor het vormen van bijvoorbeeld de nematische fase maakt dit niet uit. Echter, voor de smectische fase is het problematisch. Sommige deeltjes zijn dan te lang of te kort om fatsoenlijk in de lagen te passen. Als de polydispersiteit te hoog is (hoger dan ongeveer 17%) kan er daarom geen smectische fase gevormd worden. Echter, in het zwaartekrachtsveld zullen grotere deeltjes sneller sedimenteren dan de kleinere. Daardoor zal de polydispersiteit afnemen; de grotere deeltjes bevinden zich voornamelijk onderin het buisje, terwijl de kleineren nog hoger zijn.

In dit hoofdstuk is een goethiet sample bestudeerd gedurende 5 jaar. In het sample vinden we, van boven naar beneden, een isotrope, een nematische, een smectische en een mengsel van een smectische en columnaire fase. We ontdekten dat de deeltjes blijven bewegen, zelfs tot 5 jaar nadat het sample gemaakt was. Daardoor kunnen zich zeer goed geordende vloeibare kristallen vormen. Ondanks dat de deeltjes een polydispersiteit hebben van 30% vinden we een smectisch fase, die naarmate het sample ouder wordt beter geordend is. Dit komt doordat de deeltjes die te klein zijn uit de smectische fase gedreven worden, en opgenomen worden in de nematische fase. Verder vinden we 'gefractioneerde kristallisatie'. Dit betekent dat er op dezelfde hoogte in het buisje verschillende kleine kristalletjes naast elkaar zijn waar het ene kristalletje bestaat uit de wat kleinere, en het andere kristalletje uit de wat grotere deeltjes. Tenslotte vinden we dat de twee columnaire fasen spontaan in elkaar overgaan, waarvoor we een verklaring geven.

In Hoofdstuk 3 en Hoofdstuk 4 focussen we op biaxiale kristallen. Biaxiale kristallen zijn erg interessant vanuit een fundamenteel oogpunt. Daarnaast zijn biaxiaal nematische vloeibare kristallen veelbelovend voor snellere en betere LCD-schermen. Helaas zijn biaxiale fasen zeer zeldzaam. Goethiet is één van de zeer weinige systemen die biaxiale fasen kunnen vormen, en zelfs goethiet vormt alleen een biaxiale fase als de deeltjes een vorm hebben die voldoet aan een heel specifieke eis: de lengte-breedte verhouding moet gelijk zijn aan de breedte-dikte verhouding (dus precies tussen staaf- en schijfvormig in). De colloïden die wij zelf maken in het

lab voldoen slechts af en toe aan die eis. Doorgaans zijn de balkjes wat langwerpiger en lijnen daarom slechts hun lange as op, waar om ze vrij kunnen roteren. In Hoofdstuk 3 proberen we daarom een biaxiaal nematische fase te induceren in een dispersie die spontaan geen biaxiaal, maar een normale nematische fase vormt. Dit willen we te bereiken door kleine silicabolletjes toe te voegen aan de dispersie. Deze bolletjes zorgen ervoor dat de goethiet colloïden elkaar licht gaan aantrekken. Theoretische berekeningen voorspellen dan de formatie van een biaxiaal nematische fase. Onze experimenten echter, tonen aan dat het toevoegen van de silicabolletjes de smectische fase induceert, en het vormen van de nematische fase compleet onderdrukt. Wel vinden we dat de goethiet colloïden in de smectische lagen biaxiaal geordend zijn. We berekenen dat de geïnduceerde aantrekkingskracht vrij sterk is, wat verklaart waarom we geen nematische fase vinden. Deze resultaten geven ons veel informatie, en suggereren dat als de experimenten herhaald zullen worden met een lagere concentratie silicabolletjes (equivalent aan een kleinere aantrekkingskracht), er waarschijnlijk wel een biaxiaal nematische fase gevormd zal worden.

In Hoofdstuk 4 onderzoeken we vervolgens de invloed van een magneetveld op de biaxiaal nematisch fase. Hiertoe legden we een magneetveld aan op een goethiet sample met een biaxiaal nematische fase. Terwijl we stapsgewijs de sterkte van het magneetveld verhoogden deden we SAXS-metingen. De SAXS-patronen lieten zien dat in een sterk genoeg magneet veld, de biaxiale nematische fase overging in een reguliere nematische fase. Behalve experimenteel onderzochten we dit ook theoretisch. Deze resultaten onderbouwen wat we experimenteel observeren. Daarnaast hebben we theoretisch ook gekeken naar balkjes met net iets andere afmetingen. Kortere balkvormige deeltjes, dus met een iets kleinere lengte-breedte verhouding dan de breedte-dikte verhouding, vormen normaal een nematische fase waarin hun kortste as is opgelijnd (zoals bij schijfjes). Onze theorie voorspelt dat wanneer een magnetisch veld wordt aangebracht op zo'n nematische fase, de biaxiaal nematische fase geïnduceerd wordt. Dit is een erg belangrijke bevinding die niet alleen geldt voor goethiet, maar ook voor een verscheidenheid aan andere relatief korte balkvormige deeltjes. In systemen daarvan zou dus eenvoudig de zeldzame biaxiaal nematische fase geïnduceerd kunnen worden.

In Hoofdstuk 5 gebruiken we ook een magnetisch veld, maar nu om te bestuderen hoe de columnaire fase zich heroriënteert in een magneetveld. Zoals eerder beschreven lijnen de deeltjes zich makkelijk op in een magneetveld. Hier leggen we een magneetveld aan over een columnair vloeibaar kristal. Deze fase ontstaat bij heel hoge concentraties goethiet en de deeltjes zitten dan erg dicht op elkaar. Hierdoor is er voor de deeltjes niet genoeg ruimte om zich stuk voor stuk op te lijnen in het veld, maar zullen grote delen van het vloeibaar kristal tegelijk moeten draaien. Tijdens dit proces hebben we SAXS-metingen gedaan die dat bevestigen. Verder waren er in deze SAXS-patronen vervormde pieken te zien. Daaruit kunnen we af-

leiden wat er op nanometer schaal gebeurt: het reoriënteren van erg veel colloïden tegelijk zorgt ervoor dat de kolommen met deeltjes langs elkaar gaan glijden. Dit onderzoek laat ook zien dat SAXS een bruikbare techniek is om de bewegingen van colloïden op nanometer schaal te onderzoeken, wat toepassing zou kunnen vinden in verscheidene andere onderzoeken.

Deel 2 – Gibbsiet

In de laatste 2 hoofdstukken van dit proefschrift onderzoeken we gibbsiet. In deze twee hoofdstukken is de studie van het beïnvloeden en manipuleren van gibbsiet vloeibare kristallen wat minder direct aanwezig. Gibbsiet is niet zo gevoelig voor externe (magneet)velden, zoals goethiet. Echter, gibbsiet plaatjes hebben wel een heel duidelijke voorkeur voor een oriëntatie wanneer ze in de buurt van een glaswand of een oppervlak zijn: ze willen graag plat tegen een wand of een oppervlak liggen. Er is daarom voorspeld dat 'confinement', oftewel het beperken van gibbsiet deeltjes in hun ruimte, een grote invloed kan hebben op de vloeibaar kristalvorming van gibbsiet. Een voorbeeld van confinement is wanneer de dispersies in heel dunne, micrometers grote, platte buisjes worden gebracht. De afstand tussen de glaswanden is dan zo klein dat er niet zo veel deeltjes tussen passen. Theorie voorspelt dat er dan zeer goed geordende vloeibaar kristal fasen zouden kunnen ontstaan. Dit soort samples zijn echter moeilijk te maken, en moeilijk te analyseren. Daarom focussen we in deel 2 van dit proefschrift op *grotere* gibbsiet plaatjes (groter dan 500 nm), omdat deze potentie hebben om met optische microscopie bestudeerd te worden.

SAXS-studies aan grote gibbsiet deeltjes zijn echter moeilijker. In Hoofdstuk 6 gebruiken we daarom een '3D'-SAXS methode. In deze methode roteren we de buisjes zodat van alle kanten SAXS-patronen gemeten kunnen worden. Dit helpt om meer inzicht te krijgen in de 3D-structuur van het vloeibaar kristal.

In Hoofdstuk 7 proberen we vloeibare kristallen te bestuderen met een speciaal soort microscoop: de confocale laser scannende microscoop (CLSM). In tegenstelling tot SAXS, waarbij in één meting het hele sample meegenomen wordt, kan met CLSM heel lokaal de structuur bestudeerd worden. De deeltjes moeten echter wel groot genoeg zijn. Daarnaast moeten ze ook een fluorescente kleurstof bevatten. Gibbsiet deeltjes zijn normaal ongeveer 180 nm groot (in diameter), en ~15 nm dik. Voor microscopie willen we deeltjes die minstens 500 nm groot zijn én kleurstof bevatten. In het eerste deel van dit hoofdstuk beschrijven we dan ook twee verschillende manieren om zulk soort deeltjes te maken. In deel 2 bestuderen we dispersies van deze deeltjes met de microscoop. Ondanks dat het moeilijk is om stabiele dispersies te maken van deze deeltjes, waren we in staat om de deeltjes te observeren met de microscoop, hun ordening te zien en te bepalen in welke vloeibaar kristalfase de deeltjes zich bevonden.

De methodes die we toepassen in zowel Hoofdstuk 6 en 7, zijn wederom niet alleen voor gibbsiet interessant, maar voor een verscheidenheid aan systemen.

Uit de resultaten beschreven in dit proefschrift kunnen we concluderen dat de onderzochte methodes zicht bieden op het gecontroleerd vormen van de gewenste vloeibaar kristalfase. Met name voor de zo interessante biaxiaal nematische fase is er flinke vooruitgang geboekt. De resultaten van dit onderzoek suggereren dat deze fase gecontroleerd gevormd zou kunnen worden in systemen van langere of juist kortere balkvormige deeltjes die niet spontaan biaxiale fasen vormen. Daarnaast zijn er flinke stappen gezet om onderzoek aan vloeibare kristallen met microscopie mogelijk te maken.

Fundamenteel onderzoek – waarom?

Het onderzoek beschreven in dit proefschrift valt in de categorie 'fundamenteel onderzoek'. Dit houdt in dat de motivatie achter dit onderzoek voornamelijk nieuwsgierigheid is, het willen weten waarom. Fundamenteel onderzoek is doorgaans dan ook niet direct gericht op een specifieke toepassing. Het levert echter wel belangrijke informatie die noodzakelijk is om vooruitgang te boeken in de ontwikkeling van nieuwe toepassingen, en is daarom erg nuttig.

Dit geldt ook voor de resultaten beschreven in dit proefschrift. Deze colloïdale systemen zullen niet direct toepassing vinden. Maar zoals eerder beschreven in deze samenvatting worden colloïden vaak gebruikt als modelsystemen. De resultaten in dit poefschrift zijn dus wel interessant en nuttig voor onderzoekers die wel toepassingsgericht onderzoek doen.

Dankwoord

Dit proefschrift is het resultaat van 4 jaar onderzoek doen als PhD-student: meer dan 7000 uur werken, 20 nachten doorhalen bij de deeltjesversneller in Grenoble, 14 buitenlandtripjes, talloze besprekingen, vreugdemomenten, dipjes en tientallen borrels. Veel mensen hebben bijgedragen aan het tot stand komen van dit proefschrift, zowel direct als indirect. Deze mensen wil ik daarom graag bedanken.

Als allereerste wil ik graag mijn co-promotor Andrei bedanken. Als mijn dagelijkse begeleider was jij mijn eerste aanspreekpunt. Hoe druk je zelf ook was, je maakte altijd tijd voor me vrij en was altijd enthousiast om mijn vragen te beantwoorden. Je hebt me veel vrijheid gegeven om mijn eigen pad te kiezen, maar stond altijd klaar met ideeën en advies. Ook heb je me geïntroduceerd in de wonderlijke wereld van small-angle X-ray scattering. Hier heb je me bovendien ook erg enthousiast voor hebt gemaakt. Ik heb erg genoten van de synchrotron tripjes en ik ben blij dat ik in februari nog een laatste keer mee mag. Ook wil ik graag mijn tweede co-promotor, Gert Jan, bedanken. Je was hier slechts één dag per week, maar na mijn wekelijkse meeting met jou zat ik altijd vol nieuwe ideeën en was ik altijd extra enthousiast om weer aan het werk te gaan. Ook was jij de persoon die rust en orde aanbracht in de chaos die onderzoek doen soms kan zijn. Mijn promotor Henk ben ik ook dank verschuldigd. Als (bijna) gepensioneerde professor was je minder direct betrokken bij mijn onderzoek, maar toch is menig manuscript van mij verbeterd door jouw encyclopedische kennis van de literatuur. Ook ben ik dankbaar voor de vele uitnodigingen voor dinertjes en de gezellige tripjes naar Frankrijk (UNO-meeting) en de conferentie op het prachtige landgoed van de Royal Society in Chicheley.

Ook ben ik dank verschuldigd aan mijn voorgangers in het vloeibaar kristal onderzoek. Esther van den Pol, Maurice Mourad en Lia Verhoeff, jullie 'erfenis' was een kick-start voor mijn onderzoek. I also would like to thank Simone Belli. Our pleasant collaboration has lead to Chapter 4 of this thesis, as well as to a beautiful publication.

Ook mijn directe collega's ben ik dank verschuldigd. Bonny, Emile en Stefan, dank voor alle ICT-gerelateerde dingen en Bonny daarnaast ook voor de polarisatie-, magneet- en elektrische meetopstellingen. Dominique en Kanvaly wil ik bedanken voor het in goede banen leiden van het lab en Marina voor haar hulp met allerlei administratieve dingen, met name omtrent mijn verdediging.

Tijdens mijn PhD heb ik met meerdere collega's een kantoor gedeeld. Thanks to Sandra, Dima and Dzina. You were wonderful office mates! The greater part of my PhD however, I shared my office with Ping en Sonja. I would like to thank you for all

the nice conversations and especially for all the fun we had. Ook mijn andere collega's van het Van 't Hoff Laboratorium hebben er voor gezorgd dat ik hier een heel fijne tijd heb gehad. Ben, Albert, Willem, Jan, Hans, Remco, Joost, Chris, Roel, Bas, Antara, Nina, Yong, Mark, Rocio, Laura, Julius, Bob, Jos, Rob, Mikal en Jan. Jos en Rob, ook bedankt voor het beantwoorden voor mijn paniekerige vragen omtrent mijn promotie. Jan en Mikal bedankt voor de introductie tot (zelf gebrouwen) speciaalbier en Jan daarnaast ook nog voor de grote hoeveelheden snoep, hulp en gezelligheid tijdens de ESRF-tripjes.

Ook de collega's van de Soft Condensed Matter group, the Condensed Matter and Interfaces group and the Institute for Theoretical Physics, bedankt voor de gezelligheid tijdens conferenties en de summer-, spring- and winterschools.

Tijdens mijn PhD heb ik meerdere studenten mogen begeleiden, die allemaal direct of indirect hebben bijgedragen aan dit proefschrift. Als eerste mijn enige masterstudent: Elleke van Harten. Elleke, bedankt! Je was een erg fijne student, zowel op wetenschappelijk als op sociaal/gezellig gebied. Je bent ondanks meerdere tegenslagen door blijven zetten en jouw resultaten vormen Hoofdstuk 7 van dit proefschrift. Verder mijn bachelor studenten Anne en Wingjohn, en 2e- en 1e-jaarsstudenten Ilse, Stephan, Katinka, Wouter, Tineke, Maartje, Koen en Thomas, bedankt!

Mijn vrienden wil ik graag bedanken voor de leuke tijd die ik heb (gehad) buiten werktijd. Veel plezier heb ik gehad van mijn volleybalvrienden, zowel bij de vereniging Van Slag als bij vv Boni. Met name wil ik dan Daniela, Marieke, Nikkie, Maarten en Hester bedanken. Hes, jij bent altijd mijn rustpunt in het veld, en vaak ook daarbuiten! Bedankt voor alle goede en fijne gesprekken. Via volleybal heb ik ook Liesbeth en Annerie leren kennen. Met jullie gaat de vriendschap veel verder dan het volleybalveld en de kantine. Bedankt voor veel gezellige avondjes met slechte series en films, etentjes en borrel/stapavondjes met cocktails, wijn, wodka en soms nog meer wijn. Ook de Azië-reis met Annerie, en de citytrips naar Rome en Moskou met z'n 3-en (en Marga!), waren onvergetelijk. Ik hoop dat er nog veel zullen komen in de toekomst.

Daarnaast wil ik ook graag mijn vriendinnen uit Twente bedanken. Bijna 10 jaar in Utrecht wonen betekent gelukkig niet dat die vriendschappen er niet meer zijn. Loes en Els, al vriendinnen sinds de basisschool. Mijn middelbare school vriendinnen Judith, Heleen, Miranda, Jony, Anne en Carolien, ondanks dat iedereen verspreid door het land woont blijven we elkaar zien, en onze jaarlijkse weekendjes/nachtjes weg zijn al bijna een traditie.

Ook dank aan mijn oud-huisgenootjes van de Ina Boudier-Bakkerlaan 175 voor de leuke tijd, zowel toen ik bij jullie woonde als daarna.

Daarnaast wil ik ook graag mijn scheikunde vrienden bedanken. Anoeska, Arjan, Piter, Sander, Koen en Marleen, maar voornamelijk Susanne en Janne-Mieke. Janne-Mieke, jij bent behalve een vriendin ook de collega met wie ik het meest

samengewerkt hebt, in Utrecht, maar ook tijdens de 'werk'reisjes naar Grenoble, Bombannes, Wenen en Sydney. Suuz, eigenlijk zijn we al sinds praktisch mijn allereerste seconde in Utrecht vriendinnen. Niet alleen hebben we zo'n beetje onze hele bachelor, master en PhD-opleiding samen gedaan, ook heb je me leren koken, me geïntroduceerd in de wereld van de tv-series en hebben we vele avondjes samen gekookt, gekletst, wijntjes gedronken en wat minder avondjes samen gesport. Ook zijn we al meerdere keren samen op vakantie geweest: wintersport en Rome & Perugia, waren onwijs tof. Net als mijn bezoek aan Coïmbra. Zodra jij klaar bent gaan we die citytrip naar Spanje maken!

Janne-Mieke en Susanne, ik ben heel blij dat jullie straks mijn paranimfen zullen zijn!

Als laatste wil ik dan graag mijn familie bedanken. Mijn ooms, tantes, neefjes en nichtjes van de Leferink op Reinink kant: bedankt voor de gezellige familiefeestjes, etentjes en de stapavondjes! Van de Mensink kant: bedankt voor alle interesse in wat ik doe en de gezellige familie-etentjes en de wintersportvakanties, zowel in Oostenrijk als in Winterberg. Met name de ladies bedankt, Brigit, Leonie, Willemijn, Elke en Karin, super fijn dat jullie elk jaar naar Utrecht komen voor ons shopdagje en ook voor de onvergetelijke reis naar Istanbul.

Karin, je was trots op en geïnteresseerd in wat ik deed. Je had erg graag bij mijn promotie willen zijn, het is verschrikkelijk dat dat niet zo heeft mogen zijn.

Elke, je voelt al helemaal als familie en ik kan me geen leuker, gezelliger en fijner schoonzusje wensen!

Rick, bedankt voor de laatste loodjes.

Als allerlaatst wil ik dan graag de voor mij allerbelangrijkste mensen bedanken: mijn broertjes Joost & Wim en Papa & Mama. Jullie zijn er al mijn hele leven voor me geweest en hebben me altijd vrij gelaten om mijn eigen keuzes te maken. Ik woon al een hele tijd in Utrecht, maar naar jullie toe gaan in Twente voelt altijd als thuiskomen. Bedankt voor alles.

Resume

Anke Brigitta Geertruida Maria Leferink op Reinink was born on December 27th 1985 in Weerselo, the Netherlands. In 2004 she graduated from secondary school at the Thij College in Oldenzaal. She continued her education with the study 'Chemistry' at Utrecht University. She received her Bachelor's degree in August 2007 with a Bachelor's thesis titled "In-plane stacking disorder and partial dislocations in hard sphere colloidal crystals". She performed this research at the Van 't Hoff Laboratory for Physical and Colloid Chemistry under the supervision of Volkert the Villeneuve and dr. Andrei Petukhov.

In that same year she started with the Master study 'Nanomaterials: Chemistry & Physics'. She performed her Master's thesis in the Condensed Matter and Interfaces group under the supervision of Aleksander Zych and prof. dr. Andries Meijerink. Her thesis was titled: "Cerium, praseodymium and neodymium doped alkaline earth chlorides as scintillators for PET-scanners". After this, in 2009, she spent six months at Philips Research in Eindhoven doing an internship under the supervision of dr. Johan Klootwijk and prof. dr. Erik Bakkers. The topic of her internship was nanowire field effect transistors (NW-FETs) for use as DNA sensor. She received her Master's degree in November 2009.

In that same month she was employed by the 'Stichting voor Fundamenteel Onderzoek der Materie' (FOM) and started working as a Ph.D. student in the Van 't Hoff Laboratory for Physical and Colloid Chemistry under dr. Gert Jan Vroege, dr. Andrei Petukhov and prof. dr. Henk Lekkerkerker. This thesis comprises the results of her Ph.D. research on the formation and manipulation of colloidal mineral liquid crystals.